Meiosis-Specific Regulation of Centromeric Chromatin and Chromosome Segregation by a Transposase-Derived Protein

Author: Lauren Francis Meyer

Boston College

The Graduate School of Arts and Sciences

Department of Biology

MEIOSIS-SPECIFIC REGULATION OF CENTROMERIC CHROMATIN AND CHROMOSOME SEGREGATION BY A TRANSPOSASE-DERIVED PROTEIN

a dissertation

by

LAUREN MEYER

submitted in partial fulfillment of the requirements

for the degree of

Doctor of Philosophy

Abstract: Meiosis-specific regulation of centromeric chromatin and chromosome segregation by a transposase-derived protein. Lauren Meyer. Advisor: Hugh P. Cam, PhD

Faithful chromosome segregation is necessary for the successful completion of mitosis and meiosis. The centromere is the site of kinetochore and microtubule attachment during chromosome segregation, and it is critical that the centromere is properly formed and maintained. Many proteins contribute to centromere formation, and this process has been extensively studied during the mitotic cell cycle. However, the roles of the centromere and its associated proteins during meiosis and their contribution to the fidelity of chromosome segregation process are not as well understood. Here, I aim to elucidate a mechanism that may contribute to aneuploidy in gametes, which is a major contributing factor in human infertility. In this study, I investigate the role of Abp1, the most prominent member of the transposase-derived protein family homologous to mammalian CENP-B in the assembly of centromeric chromatin during meiosis in the fission yeast *Schizosaccharomyces pombe*. I reveal that in contrast to its known role as a major regulator of *LTR* retrotransposons during the mitotic and meiotic cell cycles, Abp1 has a specialized role at the centromere during meiosis. My results indicate that Abp1 displays dynamic localization to the centromeres during meiosis compared to the vegetative cell cycle. I show that loss of *abp1* impairs pericentromeric heterochromatin and the localization of Cnp1, a CENP-A ortholog, to the centromere central cores during meiosis.

Moreover, Abp1 appears to suppress formation of meiotic neocentromeres by restricting deposition of Cnp1 at certain heterochromatin loci. Loss of *abp1* has a drastic effect on chromosome segregation, resulting in dramatic frequency of aneuploidy. Furthermore, the genome surveillance role for retrotransposons by Abp1 appears to encompass centromeres as the mere insertion of an *LTR* sequence within the centromere central cores further exacerbates incidence of meiotic aneuploidy in *abp1* null cells. This study provides intriguing insights into factors controlling the assembly of centromeric chromatin and its impact on the fidelity of chromosome segregation process during meiosis with important implications for advancing our understanding of the evolutionary forces driving the evolution of eukaryotic centromeres.

Dedication

This dissertation is dedicated to my mother, Marianne Meyer for providing nothing but support throughout all of my endeavors. Thank you for always believing that my hard work would pay off. To anyone who is having a difficult time while pursuing his or her dreams, do not give up because it is all worth it in the end.

Acknowledgements

I would like to thank my advisor, Dr. Hugh Cam, for his endless guidance, knowledge, and patience during the production of this dissertation. You have helped me achieve more than I thought possible. I would also like to thank my committee members, Dr. Anthony Annunziato, Dr. Charles Hoffman, Dr. Michele Meyer, and Dr. Rebecca Dunn. I appreciate all of you helping me prioritize and focus on the important projects of this dissertation. You all are amazing scientists, and I strive to reach that level of expertise.

Thank you to the members of the Cam lab for all of your support and assistance through the years. I would especially like to thank my fellow graduate students David Layman, Pat Grady, and Peter Johansen. It was truly helpful having all of you be part of this experience. I would also like to thank our former postdoctoral fellow, Dr. David Lorenz, and former technician, Irina Mikheyeva, for their assistance with many experiments, especially ChIP-chip and qPCR. Thank you to all of the undergraduates for their assistance with experiments and lab maintenance, and to everyone else at Boston College for all of their technical, experimental, and academic support. A special thank you to Peter Marino and Colette McLaughlin for assisting me with anything I needed outside of the lab.

Finally, I would like to thank all of my family and friends who believed in and supported me, especially when I found it difficult to believe in myself. A special thank you to my fiancée, Jay Brothers, and best friend, Jess Krause, for their love, support, encouragement, and humor throughout this journey.

Table of Contents

Dedication i

Acknowledgements ii

Table of Contents iii

List of Figures v

Abbreviations Used vii

Chapter I: Introduction 1

- **Chromosomes as carriers of genetic information- a brief history** 2
- **Centromere function and chromosome segregation** 3
- **Meiotic defects in human diseases** 3
- **Centromere proteins in various eukaryotes** 4
- **The kinetochore** 7
- **Mitotic CENP-A deposition at the centromere** 7
- **Maintenance of CENP-A at the centromere** 10
- **Centromere DNA structure** 11
- **Chromatin organization at regional centromeres** 11
- **Overview of meiosis** 12
- **Nondisjunction and aneuploidy during meiosis** 14
- ***S. pombe* as a model for studying centromere functions** 15
- **Chromatin organization of *S. pombe* centromeres** 17
- **Centromere proteins of *S. pombe*** 18
- **Regulation of transposable elements in *S. pombe*** 19
- **Mitotic Cnp1 deposition in *S. pombe*** 20
- **CENP-A deposition during meiosis** 22
- **Important centromere proteins and regulators** 23
- **Abp1 and pericentromeric heterochromatin** 25
- **Summary of results by chapter** 26
- **Figures** 29

Chapter II: Materials and Methods 36

- **Strain Construction** 37
- **Strain growth conditions** 37
- **Meiotic synchronization** 37
- **Mitotic synchronization** 38
- **Calcofluor staining** 39
- **Chromatin Immunoprecipitation (ChIP)** 39
- **Quantitative real-time PCR (qPCR)** 40
- **Fluorescence microscopy analyses of WT, *abp1*Δ, and *rdp1*Δ asci** 40
- **Western blot analysis of Cnp1** 41

Chapter III: Genome-wide analysis of Abp1 localization during the mitotic cell cycle and meiosis 42

- **Summary** 43
- **Constitutive low enrichment of Abp1 at the pericentromeres across the mitotic cell cycle** 43
- **Abp1 is dynamically enriched at the centromere central cores upon meiotic entry** 45

Figures 48

Chapter IV: Investigating the effects of *abp1* loss on the localization of Cnp1, Scm3 and H3K9 methylation at centromeres in mitotic and meiotic cells. 69

A loss of *abp1* impairs the deposition of Cnp1 at centromeric chromatin in meiosis 70

A loss of *abp1* does not impact Scm3 localization to the centromere 72

Cnp1 localizes to novel sites in meiotic cells deficient in *abp1* 72

H3K9me2 levels at the *dg/dh* repeats are decreased in meiotic *abp1*Δ cells 74

Figures 76

Chapter V: Meiotic progression and fidelity of chromosome segregation in the presence and absence of Abp1 93

Abp1 and RNAi are important for proper meiotic progression and chromosome segregation 94

***LTR* insertion into centromere central core negatively affects meiotic chromosome segregation in *abp1*Δ strains.** 96

Figures 99

Chapter VI: Discussion 104

A novel role for a *S. pombe* CENP-B homolog in meiosis 105

The paradox of CENP-B functions: from *S. pombe* to mice, monkeys, and humans 105

Abp1-mediated localization of Cnp1 at meiotic centromeres 108

The role of Abp1 in the suppression of meiotic neocentromeres 110

The nature of meiotic chromosome segregation defects in *abp1Δ* cells 111

Potential forces driving the domestication of CENP-Bs within the *Schizosaccharomyces* lineage 112

Appendix: 114

Table 1: Strains used in this study 115

Table 2: *t*-test analysis of Cnp1-FLAG ChIP qPCR at the centromere 116

Table 3: *t*-test analysis of Scm3-FLAG ChIP qPCR at the centromere 117

Table 4: *t*-test analysis of Cnp1-FLAG ChIP qPCR at the mating type region 118

Table 5: *t*-test analysis of Cnp1-FLAG ChIP qPCR at the mating type region 119

Table 6: *t*-test analysis of H3K9me2 ChIP qPCR at the centromere 120

Table 7: *t*-test analysis of heterozygous DAPI-stained asci assay 121

Table 8: *t*-test analysis of DAPI-stained asci assay 122

Table 9: *t*-test analysis of homozygous DAPI-stained asci assay 123

Bibliography 124

List of Figures

Figure 1. Model of nucleosome positioning on the eukaryotic chromosome……..…...33
Figure 2. Model of Centromere Protein (CENP) binding at the human centromere……..……..34
Figure 3. Model of eukaryotic centromeres…….…..35
Figure 4. Light microscopy image of diploid *S. pombe* cells after being allowed to sporulate……36
Figure 5. Model comparing mammalian CENP-B with its homologous proteins in *S. pombe*……..……...37
Figure 6. Light microscopy image of haploid *S. pombe* cells……..….38
Figure 7. Schematic of the LTR-containing *Tf2* retrotransposon of *S. pombe*……..39
Figure 8. Mitotic synchrony of *S. pombe* using the *cdc25-22* temperature sensitive mutant……....49
Figure 9. Abp1 displays minimal binding to the centromere during the synchronized mitotic cell cycle……..…….50
Figure 10. Abp1 remains enriched at *Tf2-1* throughout the mitotic cell cycle……..……... 51
Figure 11. Abp1 displays genome-wide binding on chromosome I in vegetative and meiotic cells using ChIP-chip……....52
Figure 12. Abp1 displays genome-wide binding on chromosome II in vegetative and meiotic cells using ChIP-chip. ……..53
Figure 13. Abp1 displays genome-wide binding on chromosome III in vegetative and meiotic cells using ChIP-chip……54
Figure 14. Abp1 displays genome-wide binding on chromosome I in vegetative and meiotic cells using ChIP-chip. ……..55
Figure 15. Abp1 displays genome-wide binding on chromosome II in vegetative and meiotic cells using ChIP-chip……....56
Figure 16. Abp1 displays genome-wide binding on chromosome III in vegetative and meiotic cells using ChIP-chip……....57
Figure 17. Abp1 enrichment at *Tf2*s is similar between vegetative and meiotic cells……..……58
Figure 18. Abp1 enrichment at example solo *LTR* loci is similar between vegetative and meiotic cells…..59
Figure 19. Abp1 enrichment at the autonomously replicating sequence (*ars*) locus is similar between vegetative and meiotic cells.…….……..…….…..60
Figure 20. Abp1 enrichment at the mating type locus is similar between vegetative and meiotic cells . ……..61
Figure 21. Reduced Abp1 binding at certain gene promoters during meiosis……...62
Figure 22. Abp1 displays increased binding at centromere I upon meiotic entry relative to vegetative cells. …….……63
Figure 23. Abp1 displays increased binding at centromere II upon meiotic entry relative to vegetative cells……..….64
Figure 24. Abp1 displays increased binding at centromere III upon meiotic entry relative to vegetative cells…….……..65
Figure 25. Abp1 displays increased binding at centromere I during meiosis relative to vegetative cells……...66
Figure 26. Abp1 displays increased binding at centromere II during meiosis relative to vegetative cells……...67
Figure 27. Abp1 displays increased binding at centromere III during meiosis relative to vegetative cells……....68
Figure 28. Abp1 remains enriched at the *cnt* region at 8 hours post-meiotic induction……69
Figure 29. Cnp1 localization to the centromere during the vegetative cell cycle is similar between wild type and *abp1*Δ cells……..……..74
Figure 30. Cnp1 localization to the centromere upon meiotic entry is decreased in *abp1*Δ cells……75
Figure 31. Cnp1 localization to the centromere during early meiosis is decreased in *abp1*Δ……...76
Figure 32. Scm3 localization remains similar during the vegetative cell cycle between WT and *abp1*Δ cells. ……..…….……77
Figure 33. Scm3 localization remains similar upon meiotic entry between WT and *abp1*Δcells……78
Figure 34. Scm3 localization remains similar upon meiotic entry between WT and *abp1*Δ cells……79

Figure 35. Cnp1 protein levels remain similar between vegetative and meiotic WT and *abp1*Δ cells…...80
Figure 36. The loss of *abp1* leads to decreased localization of Cnp1 to centromere I upon meiotic entry……81
Figure 37. The loss of *abp1* leads to decreased localization of Cnp1 to centromere II upon meiotic entry. ……..…82
Figure 38. The loss of *abp1* leads to decreased localization of Cnp1 to centromere III upon meiotic entry……83
Figure 39. Cnp1 localizes to the silent mat locus in *abp1*Δ cells during meiosis……..…84
Figure 40. Cnp1 enrichment at the silent mat locus is increased in *abp1*Δ meiotic cells……..85
Figure 41. Cnp1 enrichment at the silent mat locus is similar in WT and *abp1*Δ vegetative cells. ……86
Figure 42. H3K9me2 enrichment remains similar at the centromere between vegetative WT and *abp1*Δ cells……87
Figure 43. H3K9me2 enrichment is decreased at the *dg/dh* pericentromeric repeats in *abp1*Δ cells upon meiotic entry……88
Figure 44. H3K9me2 enrichment is decreased at the *dg/dh* pericentromeric repeats in *abp1*Δ cells during meiosis. ……..89
Figure 45. H3K9me2 enrichment at the mating type is similar between vegetative and meiotic WT and *abp1*Δ cells…….....90
Figure 46. *abp1*Δ cells display a delay and loss of synchrony during meiosis……..…95
Figure 47. *abp1*Δ cells display an increased incidence of abnormal meiotic chromosome segregation……..96
Figure 48. *abp1*Δ cells display increased defects in Meiosis I chromosome segregation……..97
Figure 49. Chromosome segregation defects in meiotic *abp1*Δ cells……98
Figure 50. *rdp1*Δ cells display an increased incidence of abnormal meiotic chromosome segregation…...99

Abbreviations Used

ChIP	Chromatin immunoprecipitation
ChIP-chip	Chromatin immunoprecipitation combined with microarray
PCR	Polymerase chain reaction
qPCR	Quantitative polymerase chain reaction
HDAC	Histone deacetylase
SHREC	Snf2/HDAC-containing repressor complex
CENP-A	Centromere protein A
CENP-B	Centromere protein B
CENP-C	Centromere protein C
Abp1	ARS-binding protein 1
imr	inner most region
otr	outer most region
cnt	central core
DNA	Deoxyribose nucleic acid
CAC	CENP-A C-terminus
CATD	CENP-A targeting domain
H2A	Histone 2 A
H2B	Histone 2 B
H3	Histone 3
H4	Histone 4
HJURP	Holliday junction recognition protein
RNAi	RNA interference
H3K9	Lysine residue 9 of histone 3
H3K9me	Methylation of H3K9
H3K9me2	Dimethylation of H3K9
H3K9me3	Trimethylation of H3K9
H3K4me2	Dimethylation of lysine residue 4 of histone 3
H3K14	Lysine residue 14 of histone 3
ARS	Autonomously replicating sequence
LTR	Long terminal repeat
MI	Meiosis I
MII	Meiosis II

Chapter I: Introduction

Chromosomes as carriers of genetic information- a brief history

The inheritance of genetic information of all known cellular life relies on the faithful chromosome segregation during cellular division. In eukaryotes, there are two types of cellular division: mitosis and meiosis. The mitotic cell cycle is the process by which a mother cell creates two, genetically identical daughter cells through chromosome duplication, which is followed by one round of chromosome segregation, and cell division. During meiosis, each chromosome is replicated once, and this is followed by two rounds of chromosome segregation, once during meiosis I (MI) and once during meiosis II (MII). This results in the production of four haploid gametes from one parent cell [1].

The methods by which chromosomes are accurately inherited during cellular division have long been studied. In the late 1800s, the American geneticist and physician Walter Sutton and German biologist Theodor Boveri were both investigating the processes that are involved in genetic inheritance. Boveri had previously shown that, throughout the process of cell division, chromosomes remain as organized units and contain the "factors"—as Mendel called the genes. He also demonstrated that sperm and egg cells both contribute the same number of chromosomes during fertilization. Sutton had also become familiar with the process of "reduction division" (later called meiosis), during which the number of chromosomes is reduced by half in sperm and egg cells. The original number is restored in the zygote, or fertilized egg, during reproduction. This process was in agreement with the idea of segregation proposed by Mendel [2].

In 1902, Boveri and Sutton independently developed the chromosome theory of inheritance, also known as the Boveri-Sutton chromosome theory. The theory states that

chromosomes are the carriers of genetic material and are linear structures with genes located at specific sites called loci along them. This theory helped explain the mechanism underlying the laws of Mendelian inheritance [2,3].

Centromere function and chromosome segregation

Segregation of chromosomes is mediated by attachment of microtubules to kinetochores assembled at a specific site on chromosome called the centromere. During cell division, the chromosomal DNA coils up and condenses into a more compact structure, forming highly compacted chromosomes. After the chromosomes condense, mitotic or meiotic spindles attach to the centromere of each duplicated chromosome via the kinetochore protein complex. This attachment allows one copy of each chromosome to be segregated to each daughter cell [4].

The eukaryotic centromere is a highly specialized region of the chromosome that holds sister chromatids together in mitotic metaphase and throughout the first meiotic division. This ensures accurate segregation of chromosomes to daughter cells during cell division [5-7]. Proper kinetochore assembly on the centromere requires the cooperation of many proteins, and is crucial for normal chromosome segregation during mitosis and meiosis [8-10].

Meiotic defects in human diseases

Aneuploidy is a chromosomal abnormality that results in the gain or loss of chromosomes from the normal ploidy of the organism due to errors in chromosome

segregation. Defects of the centromere (via DNA or protein), kinetochore, or spindle checkpoint, as well as abnormal centrosome duplication [11,12] can cause aneuploidy. Aneuploidy is the most common genetic cause of developmental and intellectual deficiencies in humans, and occurs in 0.3% of newborns, 4% of stillbirths, and more than 35% of all human spontaneous abortions [13]. Aneuploidy is also strongly associated with reproductive failure, cancer, and mental deficiencies [14-16]. Meiosis in human oocytes is more susceptible to chromosome segregation defects than mitosis [17,18], meiosis during spermatogenesis [13,19], and female meiosis in other organisms [13,20]. Therefore, it is extremely important that the centromere and its associated proteins are constructed and functioning properly.

Centromere proteins in various eukaryotes

Many proteins are involved in ensuring that chromosomes are correctly segregated during cellular division. Proteins associated with the centromere are especially important for maintaining the fidelity of genetic inheritance. Studies in humans have discovered the role of an evolutionarily conserved 17-kDa protein, CENP-A (CENtromere Protein-A), as an essential centromere-specific histone (cenH3) that replaces the canonical H3 **(Figure 1)** [21]. CENP-A is known as CID in *Drosophila melanogaster*, Cnp1 in *Schizosaccharomyces pombe*, and Cse4 in *Saccharomyces cerevisiae* [22]. It is believed that CENP-A is the epigenetic mark that identifies all active centromeres [21,23-27]. The structure of CENP-A is similar to H3 in that two thirds of the amino acid sequences of the carboxylic-acid terminal region are identical to those of histone H3, while one-third of the amino-terminal is highly variable [28].

CENP-A has been found at active centromeres along with the centromere proteins CENP-B and CENP-C [29] **(Figure 2)**. The recruitment of centromere-kinetochore proteins to the centromere appears to be a unique function of CENP-A, as other centromere components were not adequate for assembly of the same complex [30]. Additionally, CENP-A has been demonstrated to be the epigenetic mark that functions through a two-step mechanism to identify, maintain and propagate centromere function indefinitely [31-34]. It is believed that this function of CENP-A is mediated at least partially through the recruitment and maintenance of CENP-B and CENP-C at the centromere [34]. The N-terminus of CENP-A is required for recruiting the DNA-binding protein CENP-B to the centromere, while the C-terminus is required for recruiting CENP-C to the centromere [34]. Data suggest that CENP-B and CENP-C recruit other CENPs involved in kinetochore assembly to the centromere, including CENP-N, creating a physical link between centromeric DNA sequences containing CENP-A and the kinetochore [34].

In humans, the 80-kDa CENP-B protein has been found to bind to a specific 17-bp region of alpha satellite DNA at the centromere, called the "CENP-B box", through its amino-terminal region, and it is the only centromere sequence-specific DNA-binding protein found in mammals [35-38]. Studies show that CENP-B is not essential, as *CENP-B* knockout mice are viable, appear to undergo normal development, and are fertile [39,40]. However, it has been found that *CENP-B* null mice do display lower body and testis weights, along with lower sperm counts [40]. CENP-B binding near the CENP-A nucleosome has been shown to markedly stabilize the CENP-A nucleosome on human alphoid DNA, which is a type of centromeric, repetitive DNA sequence containing tandem arrays of 170 base pair segments [38]. Additionally, the loss of CENP-B has been

found to lead to chromosome mis-segregation, an increased rate of micronuclei formation, and a decrease in CENP-C localization at the centromere in mice [41]. A micronucleus forms when a full chromosome or a fragment of a chromosome is not incorporated into one of the daughter nuclei during cell division. CENP-B is neither sufficient nor essential for centromere formation and function [40,42], and functionally redundant protein(s) may be present that make up for the loss of CENP-B [43]. Recent findings propose that CENP-B is an important contributor to centromere strength and the frequency of faithful chromosome segregation through stabilization of binding of other centromere and/or kinetochore proteins, such as CENP-C [41].

CENP-C is a 107-kDa human centromeric protein that localizes to the inner kinetochore plate [44]. CENP-C is believed to play an important role in establishing and/or maintaining proper kinetochore size and stabilizing microtubule attachments [45]. More recent studies by Falk *et al* (2015) have elucidated additional roles of CENP-C at the human centromere [46]. First, CENP-C was found to affect CENP-A-containing nucleosome shape and dynamics in a way that promotes CENP-A nucleosome incorporation at the centromere, while CENP-C depletion leads to rapid elimination of CENP-A from centromeres, suggesting collaboration between CENP-A and CENP-C in maintaining centromere identity [46]. Second, studies indicate that CENP-C aids in the initiation of kinetochore assembly and in the spatial organization during localization of all other constitutive centromere-associated network (CCAN) subunits downstream of CENP-A [46]. CCAN is a 16-subunit complex that is comprised of CENPs, and creates the centromere-kinetochore boundary [47].

The kinetochore

The kinetochore and its associated proteins have significant roles in chromosome segregation, as the kinetochore is the site of microtubule attachment at the centromere during mitosis and meiosis [48-50]. The assembly of the kinetochore on the centromere is a complex, dynamic process that has long been studied. Findings suggest that a properly assembled and functioning centromere is required for kinetochore assembly and function [51]. Hooser *et al* (2001) reveal at least two distinct steps in kinetochore assembly [30]. Step one is the specific targeting of CENP-A to the centromeric DNA at the inner kinetochore during S phase, which is sufficient to assemble components of a centromere-prekinetochore scaffold. Step two is localization of kinetochore microtubule-associated proteins by an additional mechanism located only at active centromeres. The outer kinetochore assembles or dissembles rapidly as cells enter or exit mitosis or meiosis, respectively [52].

Mitotic CENP-A deposition at the centromere

Identifying the factors that specify a chromosomal site as a centromere, and not just another part of the chromosome, has been a long and difficult process. This research is important, however, for elucidating the formation and function of the centromere, as well as how centromere abnormalities and aneuploidy can occur. It is believed that the centromere is epigenetically marked, and that the DNA sequence of the centromere is not the defining aspect. While CENP-A is highly conserved, centromeric DNA sequences vary greatly between organisms [53,54].

Many studies have proposed that the centromere-specific histone, CENP-A, acts as an epigenetic marker for centromere identity [28,55]. Therefore, CENP-A deposition at the centromere is an important process needed for centromere formation and function. Targeting of CENP-A to the centromere is believed to be influenced either by some aspect of DNA structure other than DNA sequence, or by the interaction of CENP-A with one or more kinetochore protein components [56]. Shelby *et al* (1997) demonstrate that CENP-A expression occurs later in the cell cycle than histone H3 expression, peaking during G2, and that this timing is important for proper targeting of CENP-A to the centromere [57].

Recent progress has yielded considerable insights into the mechanisms that control the deposition of CENP-A during the vegetative cell cycle [58]. A conserved histone chaperone, Scm3, helps shepherd CENP-A to the centromeres in *S. cerevisiae* [59,60] and *S. pombe* [22,61]. In humans, the CENP-A chaperone is called HJURP [63]. Deposition of new CENP-A occurs during S and G2 phases in *S. pombe* [64,65], G1 in humans [66], G2 in *A. thaliana* [67], and during anaphase in *Drosophila* embryos [68]. The C-terminus of CENP-A has been found to be sufficient for centromere targeting in humans [69], *Drosophila* [70], and *A. thaliana* [67], while the CENP-A targeting domain (CATD) and N-terminus are required for *S. pombe* [34]. The function of the CATD, which is comprised of loop 1 and the α2 helix within the histone fold of CENP-A, is conserved from fungi to mammals [55].

Deposition of CENP-A has been found to take place during G1 of the cell cycle in humans, and its localization at the centromere is maintained throughout mitotic divisions. CENP-A is distributed equally among daughter cells during cell division, and is

replenished during the following G1 [66]. Centromere defects and chromosome segregation errors can occur if CENP-A nucleosomes are not properly replenished during each cell cycle [34,71].

In humans, the cell cycle regulated chaperone for CENP-A loading into nucleosomes at replicated centromeres is HJURP (Holliday junction recognizing protein). Reduction of HJURP results in a decrease of CENP-A loading at the centromere [63]. HJURP recognizes the CATD motif of CENP-A, and CATD can facilitate CENP-A assembly at neocentromeres that lack alpha-satellite DNA sequence [71,72]. The CATD motif has been found to induce a conformational change in CENP-A nucleosomes that promotes assembly and maintenance of these nucleosomes at the centromere. CATD-containing H3 histones can be targeted to the centromere and rescue the lethal phenotype of CENP-A depleted in human and yeast cells [73].

The targeting of CENP-A and HJURP to the centromere is dependent on the Mis18 complex, comprised of Mis18-α, Mis18-β and M18BP1 in humans [74]. Centromere recruitment of newly synthesized CENP-A is quickly abolished if any of these three Mis18 proteins is depleted. Mis18 depletion results in mitotic defects such as misaligned chromosomes, chromosome mis-segregation and interphase micronuclei formation [74].

The centromeres have been found to be sensitive to changes in CENP-A loading. CENP-A reduction or mutation results in centromere dysfunction [73-76], while forced loading of CENP-A to specific DNA loci has created partial ectopic centromere formation at the subtelomere region and nuclear periphery [77-80]. Such ectopic centromere can acquire a fully functional kinetochore after deletion of the native centromere [81], suggesting that CENP-A plays an important role in centromere identity. It has been found

that CENP-A is overexpressed and localized at non-centromeric chromatin in primary colorectal cancer tissues of humans, suggesting that CENP-A overexpression can lead to aneuploidy and cancer [82]. Several studies have proposed that an ubiquitin-mediated proteasome degradation process is responsible for removing non-centromeric CENP-A. The CATD of CENP-A is believed to aid in the identification of CENP-A for degradation by distinguishing it from H3. This process is conserved from yeast to humans [83-85].

Maintenance of CENP-A at the centromere

Once CENP-A has been stably incorporated into the centromere, it must remain there to maintain its role as the marker of the centromere. Incorporation of CENP-A at the centromere persists through cell division [66], and is distributed among sister chromatids during S phase [86]. Many studies have focused on how CENP-A is steadily retained at the centromere. Perpelescu *et al* (2009) suggest that the ATP-dependent chromatin remodeling and spacing factor RSF promotes maintenance of newly assembled CENP-A [87]. It has been proposed that a small GTPase switch is also involved in this function, as a depletion of either of these elements results in a decrease of centromere-associated CENP-A [88].

It has also been suggested that intrinsic characteristics of CENP-A promote its maintenance at the centromere. For instance, the CATD motif of CENP-A mediates the assembly and stabilization of CENP-A/H4–containing nucleosomes at centromeres compared to general chromatin, through multiple cell divisions. This allows for long-term stability and epigenetic maintenance of centromere position, as dictated by the presence

of CENP-A [71]. It is not believed that the CENP-A chaperone, HJURP, plays a role in the maintenance of previously incorporated CENP-A [71].

Centromere DNA structure

All eukaryotes contain and rely on the centromere for proper chromosome segregation, but the level of centromere complexity and the actual DNA sequence of the centromere can vary greatly among eukaryotes [89]. For instance, the budding yeast *Saccharomyces cerevisiae* contains small, 125bp non-repetitive centromeres, called "point centromeres". Although these centromeres function comparably to those of higher eukaryotes, they share very little structural similarities [89]. We use *Schizosaccharomyces pombe* as a model organism for centromere studies because it shares many functional and structural similarities to centromeres of higher eukaryotes **(Figure 3)**. Centromeres of *S. pombe* and higher eukaryotes, known as "regional centromeres", are larger and more complex than point centromeres. These centromeres are also characterized by the presence of highly repetitive DNA sequences. *S. pombe* centromeres range from 40-100kb, and contain a central core (*cnt*) region of 4-7kb that is flanked by repetitive heterochromatin. Human centromeres range from 0.3Mb to 5Mb, and contain several thousand tandem repeats of a 171bp sequence termed α-satellite DNA [15,89].

Chromatin organization at regional centromeres

Regional centromeres contain neighboring blocks of heterochromatin that contribute to the establishment of CENP-A chromatin [90]. In humans and flies, canonical

histone H3 in pericentromeric chromatin is epigenetically marked by methylation at lysine 9 (H3K9me). This modification distinguishes it from canonical H3 at the centromere, which is marked by dimethylation at lysine 4 (H3K4me2). It is believed that this methylation pattern contributes to the unique domain organization and three-dimensional structure of centromeric regions, and possibly to the epigenetic information that establishes centromere identity [33]. In human chromosomes, CENP-A is localized to alpha-satellite DNA (alphoid DNA), located in between the pericentromeric chromatin. Within alphoid DNA are multiple CENP-B boxes, a 17-bp motif that specifically binds CENP-B [35,36].

Overview of meiosis

Meiosis is the process by which gametes, such as egg, sperm, and spores, are produced for the purpose of passing down their genome to the subsequent generation during reproduction [92]. In the unicellular organism, *S. pombe*, the prominent life cycle is haploid, and these haploid cells are the direct result of meiosis. When nitrogen-starved, haploid *S. pombe* cells of opposite mating type will mate with each other to form a diploid cell. This diploid cell can then proceed with meiosis, creating four haploid spores upon completion of meiosis II. Once the four spores break free from the ascus, they become individual, viable haploid cells that are able to reproduce vegetatively. They also may proceed with meiosis under the necessary conditions, such as nutrient deprivation [93].

Reproduction of a sexually reproducing organism is complex, especially in multicellular organisms, such as mammals, that spend the majority of their life cycle as a diploid. Many developmental steps are required for an organism to fully form. The

specialized initial cell that the diploid organism develops from is created from the union of two haploid gametes originating from two separate individuals, or parents. Gametes are created from germ-line cells within the parental organisms by the process of meiosis. The fusion of two haploid gametes and their genomes creates a genetically distinct diploid cell, or zygote, containing both parental genomes [4].

Meiosis occurs when diploid germ cells undergo one round of DNA replication followed by two rounds of cell division, resulting in four haploid gametes. The exception to this is oogenesis, when one germ cell creates one mature egg cell and three polar bodies [94]. The first step of meiosis involves the DNA replication of all of the chromosomes within the germ cell. The resulting copies, or sister chromatids, remain closely attached as they would during mitosis. Following DNA replication is a step that is unique to meiosis: each duplicated paternal chromosome locates and attaches itself to the corresponding duplicated maternal homolog. This process is called pairing, and it allows for homologous recombination between maternal and paternal chromosomes, as well as proper homolog segregation during the two following cell divisions. Homologous recombination is the process by which two identical or nearly identical nucleotide sequences exchange genetic information with each other [95]. The physical process of the genetic exchange between maternal and paternal homologs is called crossing-over. Each chromatid of one duplicated homolog can form a crossover with one or both of the chromatids from the other duplicated homolog. Crossing over during meiosis facilitates genetic variation in the species by making the resulting gametes genetically distinct from the parental germ cells [1].

During meiosis I (MI), maternal and paternal homolog pairs are separated from each other after the cohesin that was maintaining their attachment has been degraded and the meiotic spindle pulls the duplicated homologs in opposite directions towards the poles through attachment at the kinetochore [96]. Cytokinesis occurs, resulting in two diploid cells containing a random combination of the maternal or paternal homologs. After the first meiotic division, a second meiotic division, meiosis II (MII), occurs. In most animals, oocytes are arrested at meiotic prophase I until ovulation. Upon ovulation, the increase in ovulatory luteinizing hormone (LH) stimulates the continuation of meiosis of the arrested oocytes and their progression through the second meiotic cycle. The oocytes are then arrested again at metaphase II until fertilization [96]. Again, a meiotic spindle forms, attaches to the kinetochores of each sister chromatid, and pulls them apart towards the poles of the cell. Cytokinesis then occurs, resulting in four haploid gametes, each containing one of each sister chromatid that has likely undergone homologous recombination [4].

Nondisjunction and aneuploidy during meiosis

Like mitosis, meiosis is not always a perfect process. Nondisjunction, the failure of chromosomes to accurately separate, can occur if homologous chromosomes or sister chromatids do not segregate properly during MI or MII, respectively [97]. Aneuploidy, the condition in which cells do not contain the correct number of chromosomes, can result from nondisjunction. If nondisjunction occurs during MI, two of the resulting gametes will contain an extra chromosome while the other two gametes will lack a chromosome. If nondisjunction occurs during MII, two of the resulting gametes will be normal, while

the other two will have either one too many or few chromosomes. If these abnormal gametes are viable and contribute to fertilization, an abnormal embryo will form. While many embryos do not survive aneuploidy, some can result in a live birth with negative genetic consequences [98].

A common human example of viable aneuploidy is when an embryo contains an extra copy of chromosome 21 due to nondisjunction in MI, resulting in Trisomy 21, or Down syndrome. Other examples of viable aneuploidy conditions include Patau's syndrome (trisomy 13) and Edward's syndrome (trisomy 18) [99]. These conditions display a wide range of symptoms depending on the exact genetic abnormality, including neurological and developmental disorders [99]. It is estimated that aneuploidy occurs at a rate of at least 10% during meiosis of human oocytes likely due to the long duration of meiotic arrests experienced by oocytes, while spermatogenesis has a lower rate of aneuploidy (<5%) [14]. It is believed that this lower rate is due to a more rigorous cell cycle checkpoint control in sperm compared to eggs. Aneuploidies originating in egg or sperm comprise approximately 80% of all chromosomal abnormalities observed in miscarriages [100].

S. pombe **as a model for studying centromere functions**

S. pombe, also known as fission yeast, serves as a model organism for studying centromeric function of higher eukaryotes for many reasons [101]. *S. pombe*, although unicellular, undergoes mitosis and meiosis in a similar manner as higher eukaryotes [102]. The mitotic cell cycle in *S. pombe* occurs within 2-4 hours, allowing for rapid growth and analysis of strains. A fission forms in the middle of a dividing cell, while the diameter of

S. pombe remains constant throughout growth and division. *S. pombe* and higher eukaryotes contain regional centromeres that participate in chromosome segregation during cell division, as opposed to point centromeres that are found in *S. cerevisiae.* Many centromere proteins in *S. pombe* have homologs in higher eukaryotes, and the chromosome structure of *S. pombe* has similar features to those of higher eukaryotes [103,104].

S. pombe has a standard mitotic cell cycle, which contains both G1 and G2 phases, with G2 taking up about 70% of the division time [105]. Reorganization of microtubules and mitotic spindle formation take place during G2. There are several checkpoints that ensure proper transition between G2 and M, and will activate causing cell arrest if these checkpoints are not satisfied [105]. During M phase, chromosomes condense, line up in the center of the nucleus, and segregate to the poles. This segregation is achieved through the attachment of mitotic spindles to the kinetochore complex at the centromere and subsequent pulling of the chromosomes to the poles. Cytokinesis then takes place, resulting in two, genetically identical daughter cells through septation and medial fission. Unlike higher eukaryotes, cytokinesis of fission yeast cells occurs at the end of S phase. This causes cells in G1 and S phase to be binuclear, with each nucleus containing a haploid genome (1C) [106].

The mitotic cell cycle will continue in *S. pombe* until nutrients are no longer available. At this point, the cells may arrest in G1 or G2, and enter stationary phase. Alternatively, if both mating types (*p* and *m*) of *S. pombe* are present, mating between haploid cells can occur. Non-switchable heterothallic cells need the opposite mating type present in order to mate, while homothallic cells capable of switching between *m* and *p*

types can mate with themselves [107]. Mating types are determined by information expressed at the mating type locus [108]. Mating results in the formation of a diploid cell, which will immediately proceed to meiosis, as this diploid state is unstable in *S. pombe*. However, genetic manipulations can force *S. pombe* cells into a vegetative diploid state [105]. The result of meiosis in *S. pombe* is a tetrad ascus containing four haploid spores, or gametes **(Figure 4)**. The packaging of the four haploid spores by the ascus is beneficial for meiotic studies, as it allows researchers to analyze the products of a single meiotic event.

Chromatin organization of *S. pombe* centromeres

In *S. pombe*, pericentromeric heterochromatin spans the outer (*dg* and *dh*) repeats and a portion of the inner (*imr*) repeats [109-112]. The DNA sequence of all *dg* and *dh* repeats is very similar, but the amount and organization of these elements vary among the three centromeres [113]. tRNA genes embedded within the *imr* repeats act as boundary elements [114,115] that partition the flanking heterochromatin from the *cnt* central cores enriched for Cnp1 [116]. The *cnt* regions appear to contain a small fraction of canonical histone H3 [114,116]. However, while the surrounding pericentromeric heterochromatin domains are highly enriched for histone H3 lysine 9 methylation (H3K9me), the central cores are modestly enriched for histone H3 lysine 4 methylation (H3K4me) [114,117]. Despite the absence of heterochromatin marks at the central cores, the regions are transcriptionally repressed and maintained in part by histone deacetylases (HDACs) [118,119].

Centromere proteins of *S. pombe*

Several centromere proteins found in *S. pombe* are conserved in higher eukaryotes, including mice and humans. In *S. pombe*, Abp1, Cbh1, and Cbh2 are partially redundant homologs of human CENP-B. Abp1 and Cbh1 localize to the pericentromeres [120,121]. Specifically, in relation to the human CENP-B amino acid sequence, Abp1 is 50% similar and 25% identical, Cbh1 is 46% similar and 25% identical, and Cbh2 is 40% similar and 31% identical [43]. CENP-B and its homologs in *S. pombe* are believed to have developed from independent domestication of *pogo*-like transposons, supporting their structural and functional similarities [122] **(Figure 5)**.

Abp1 was first discovered as a 60-kDa protein that binds to autonomously replicating sequences (ARS) elements in *S. pombe* and has significant sequence homology to human CENP-B [123]. ARS elements are DNA sequences that can act as origins of replication in yeast. They contain several copies of the consensus sequence reported by Maundrel [124], and can be found at the centromere [123]. Of the CENP-B homologs, Abp1 appears to be the most prominent member. A loss of Abp1 results in a slow-growth phenotype, with the majority of cells being branched, elongated, or multiseptated **(Figure 6)**. A loss of Abp1 also results in minichromosome loss, aneuploidy, and meiotic defects [42,125]. All of these defects are exacerbated by the additional loss of either Cbh1 or Cbh2, suggesting partial compensation of Abp1 functions by Cbh1 and Cbh2 [42]. Abp1 has also been found to be important for recruiting certain proteins, including HDACs Clr3 and Clr6 [120] to transposable elements to be silenced.

Regulation of transposable elements in *S. pombe*

Mobile, or transposable, elements and their remnants often constitute a significant fraction of eukaryotic genomes, including up to half of the genome of humans and nearly 90% of the genome of some plant species [126,127]. These elements are found scattered throughout the genome, and can impact gene expression, development, and evolution of organisms if located near promoters, enhancers, or within genes [128,129]. Strategies such as DNA methylation, heterochromatin formation, and RNA interference (RNAi) have been developed by host cells to control the activity of transposable elements [130-133]. Occasionally, host cells can "domesticate" transposable elements so that they perform cellular functions [134-136]. Human CENP-B, JRK, and TIGGER supergene family, as well as CENP-B homologs in *S. pombe* are believed to have derived from transposases of pogo DNA transposons [43,122,137,138].

Most laboratory strains of *S. pombe,* including those used in the experiments described in this thesis, contain 13 full-length *Tf2* long terminal repeat (*LTR*) retrotransposons, which are capable of replicating and mobilizing themselves throughout the genome, as well as hundreds of *Tf* remnants, or solo *LTR*s [113,139]. The genome structure of a *Tf2 LTR* retrotransposon is highly similar to those of retroviruses such as HIV, containing an *LTR* sequence flanking each side of the coding sequences for *Gag* and *Pol* genes that encode for capsid proteins and enzymes (protease, reverse transcriptase, and integrase), respectively [139] **(Figure 7)**. The *S. pombe* CENP-B homologs mediate *Tf2* suppression by binding to the *LTR*s of *Tf2s* and recruiting HDACs Clr3 and Clr6 [140-142]. In addition, by binding to solo *LTR*s located near gene promoters, CENP-B homologs are able to regulate expression of nearby genes, likely due to their

ability to recruit histone modifiers [120]. Research has shown that CENP-B homologs, particularly Abp1, aid in the clustering of *Tf2s* scattered across the genome into, in general, 1-2 *Tf* bodies that can be visualized as discrete foci using FISH analysis. Additionally, Abp1 has been found to be crucial for preventing expression of *Tf2s*, solo *LTR*s and *LTR*-associated genes [120]. Other silencing mechanisms of *Tf2s* include an exosome-based pathway and an RNA interference-dependent pathway that results in the heterochromatization of the elements during nutrient deficiency [143,144]. It is hypothesized that only a fraction of the total full-length *Tf2* elements contribute to the majority of *Tf2* expression [145].

Mitotic Cnp1 deposition in *S. pombe*

Like in humans, Cnp1 localization to the centromere in *S. pombe* is believed to be dependent on the context of DNA sequence, rather than the DNA sequence itself. This is supported by research that shows that Cnp1 can localize to DNA of neocentromeres that were artificially created on chromosomes [146]. An overexpression of histone H3 can compete with Cnp1 deposition, leading to a decrease in Cnp1 localization and gene silencing in the central core region of the centromere, as well as kinetochore dysfunction [31].

In fission yeast, Scm3 is part of the Mis16-Mis18 complex that, unlike Cnp1, is not a constitutive component of the centromeres and temporarily dissociates from centromeres during the cell cycle [22,61]. The homologs of Mis16 and Mis18 in humans are RbAp46/RbAp48 and hMis18 (α and β isoforms), respectively [74,147]. These proteins are necessary for CENP-A localization at centromeres in humans. In *Drosophila,* RbAp48

has been detected in a complex with CenH3 and histone H4 [148]. It is been shown that Scm3 depends on the Mis16-Mis18 complex for localization at the centromeres, while centromeric deposition of Cnp1 is dependent on Scm3. Scm3 or Mis18 deactivation decreases Cnp1 localization at the centromere, while increasing centromere localization of histones H3 and H2A/H2B, which are largely absent from centromeres in wild type cells [22].

In *S. pombe*, the CATD domain of Cnp1 has been found to be necessary and sufficient for Cnp1 localization to centromeres. However, the N-terminus of Cnp1 is required for long-term Cnp1 maintenance and centromere function [34]. Data regarding the importance of the N-terminus in Cnp1 loading is supported by further experiments performed in *S. pombe* using strains that contain a GFP tag at the N-terminus of Cnp1. It was found that these tagged Cnp1 molecules displayed reduced localization at the centromere, presumably due the presence of GFP interfering with the normal function of Cnp1 N-terminus [65].

In *S. pombe*, it is believed that Cnp1 deposition during the G2 phase is a compensatory mechanism that can make up for an insufficient amount of Cnp1 loading during S phase. S phase deposition appears to be dependent on the Ams2 GATA factor, which promotes histone gene activation. In *ams2*Δ, Cnp1 is not retained at the centromere in S phase, but it localizes again onto centromeres via the G2 deposition pathway. Decreasing the length of the G2 phase in *ams2*Δ leads to the failure of Cnp1 accumulation at the centromere, resulting in chromosome missegregation [65].

An overexpression of Cnp1 in *S. pombe* has been found to lead to ectopic deposition of Cnp1 at non-centromeric chromatin during the mitotic and meiotic cell

cycles [149,150]. Ectopic deposition of Cnp1 predominately took place at other heterochromatic loci, such as the telomere. This resulted in the accumulation of kinetochore proteins and microtubule attachment at the ectopic Cnp1 loci, leading to severe chromosome segregation defects, spindle microtubule disorganization, and aneuploidy. This mislocalization of overexpressed Cnp1 was found to persist for several generations, but could be alleviated by overexpression of histone H3 or H4 [151].

CENP-A deposition during meiosis

While not as well understood, CENP-A deposition during meiosis appears to differ from the mitotic cell cycle. During spermatogenesis in *Drosophila*, imaging analysis reveals two phases of CENP-A^{CID} deposition with the first phase during the extended prophase of meiosis I that requires CAL1 (HJURP ortholog) and CENP-C and the second phase after exit from meiosis II during the formation of spermatids [86]. CENP-A^{CID} was retained on mature sperm despite total chromatin remodeling that happens during protamine exchange of histones late into the haploid stage of spermatogenesis. During female meiosis, CENP-A^{CID} deposition during prophase I was found to be conserved [86].

In pollen mother cells of *Arabidopsis thaliana*, which are the result of meiosis, CENP-A^{CENH3} histones with a disrupted N-terminus were found to display reduced localization to the centromere during meiosis. However, the localization of CENP-A^{CENH3} to the centromere in vegetative cells was not impaired. In addition to this, these studies demonstrated that a CENP-A^{CENH3} RNAi mutant has a slower mitotic rate, resulting in dwarfism. The consequences of proceeding with meiosis under these conditions were

severe, leading to reduced fertility due to chromosome segregation defects and the formation of micronuclei [153-155].

Important centromere proteins and regulators

In eukaryotes, the organization of chromatin at the centromere is important for centromere structure and function [156]. The formation of the higher order chromatin structure, heterochromatin, is essential for chromosome segregation, genome stability, and epigenetic gene silencing [157]. Several critical proteins and protein complexes contribute to the silencing of the centromere. In *S. pombe,* the methyltransferase Clr4 catalyzes H3K9me, which acts as a marker that recruits the heterochromatin protein Swi6 (HP1 in humans) for heterochromatin assembly and gene silencing [158,159].

It has been found that the Clr4 H3K9 methyltransferase and intact *otr* heterochromatin containing H3K9me2 are both necessary to establish, but not maintain, Cnp1 chromatin at the *cnt* [160], though H3K9me2 is barely detectable at the *cnt* itself [159]. The *cnt* DNA sequence alone is not sufficient for de novo Cnp1 binding, as incorporation of this sequence into cells without flanking heterochromatin does not result in Cnp1 localization [160,161].

RNA interference (RNAi) promotes the assembly of heterochromatin at the pericentromeric *dg/dh* repeats. It does so through the targeting and silencing of *dg/dh* repeats transcribed by RNA polymerase II (RNAPII) during S phase [162,163] and the following recruitment of the RNAi and RITS (RNA-induced initiation of transcriptional gene silencing) machinery [163-165,167,168]. The components of RITS include Ago1 (the fission yeast Argonaute homolog), Chp1 (a heterochromatin-associated chromodomain

protein), and Tas3 (a novel protein that is required for cis spreading of RITS in centromeric DNA regions) [169]. The complex also contains small RNAs that require the RNA-dependent RNA polymerase complex (RDRC) encoded by *rdp1*, and Dicer ribonuclease for their production [170]. These small RNAs that are homologous to centromeric *dg/dh* repeats, as well as H3K9me, are necessary for the localization of RITS to heterochromatic domains [168].

Set1 is the methyltransferase that adds methyl tags to histone 3 at lysine 4 [171]. Usually, H3K4me is associated with highly expressed euchromatin, but this epigenetic modification can also be found at silenced heterochromatin, such as the central core of the centromere [172]. It has been found that the loss of Set1, or its chaperone Atf1, results in a decrease of H3K4me at the central core of the centromere [117]. It is believed that Set1 and the histone deacetylase (HDAC) Clr3 also work together to assemble H3K9me-associated heterochromatin, contributing to the silencing of heterochromatic repeats of the centromere [117]. HDACs remove acetyl tags from chromatin that is to be silenced, allowing for methylation and silencing [156,173].

Transcriptional gene silencing (TGS) is the mechanism believed to effect silencing at heterochromatin. The complex that has been found to mediate TGS in *S. pombe* is SHREC (Snf2/HDAC-containing Repressor Complex). SHREC consists of four proteins, Clr1, Clr2, Clr3, and Mit1. These proteins distribute throughout all major heterochromatin domains, including the centromere. Swi6/HP1 provide a platform for stable binding and spreading of SHREC across heterochromatic domains [142]. The centromeric association of Swi6 is diminished after removal of the CENP-B homologs Abp1 or Cbh1, resulting in a decrease in silencing of the region [152].

The binding profile of the SHREC components resembles those of H3K9me3 and Swi6. The exception to this is Clr2, which is found primarily at the central core (*cnt*) of the centromere, which does not contain H3K9me or Swi6 [114]. However, the SHREC components also localize to euchromatin independent of Swi6. SHREC promotes TGS through specific enzymatic activities associated with the HDAC Clr3 and the SNF2 chromatin-remodeling factor homolog Mit1. Clr3 and Mit1 are crucial for proper positioning of nucleosomes at heterochromatin and for TGS function of SHREC [142]. SHREC also restricts RNA polymerase II (Pol II) occupancy at heterochromatic repeats. Each component of SHREC is necessary for TGS, as derepression of reporter genes inserted at major heterochromatin domains including pericentromeric repeats, the silent *mat* locus, telomeres, and rDNA loci occurred in strains lacking any individual component of SHREC [142].

Abp1 and pericentromeric heterochromatin

The structure and organization of the centromere is important for centromere function in both *S. pombe* and higher eukaryotes. In *S. pombe*, heterochromatin is present at the pericentromeric repeats that flank the *cnt* of each centromere, as well as the telomere and silent-mating type locus [114,159]. RNA interference (RNAi) contributes to the assembly of heterochromatin of *S. pombe* [164]. CENP-B homologs are believed to interact with RNAi machinery to facilitate heterochromatin formation at the centromere [165], and aid in the recruitment of Clr4 for H3K9me establishment [152,164]. A disruption of RNAi-directed heterochromatin at the centromeres results in an impairment of CENP-A and kinetochore assembly at the *cnt* [90].

H3K9 methylation by Clr4 can only occur if HDAC Clr6 deacetylates H3K9, and HDAC Clr3 deacetylates H3K14 [159]. Clr6, a homolog of the mammalian HDAC1 and HDAC2 and *Saccharomyces cerevisiae* Rpd3, was initially identified as an essential gene that functions with Clr3 to silence mating-type loci and pericentromeric regions [118]. Research has found that deleting a portion of the repeat heterochromatic regions flanking the *cnt* severely impaired the maintenance of sister chromatid attachment during meiosis I [166]. The removal of any of the RNAi components, particularly *rdp1*, has been found to lead to a decrease in H3K9me2 and Swi6 enrichment at the *dg/dh* repeats. This resulted in a deficiency of both mitotic and meiotic sister chromatid attachment, as well as severe mitotic chromosome segregation defects [198].

Summary of results by chapter

In this thesis, I explore the multifaceted roles of Abp1, a *S. pombe* homolog of human CENP-B. I specifically focus on the functions of Abp1 at the centromeres during the vegetative and meiotic cell cycle, and the impact that a loss of Abp1 has on meiotic progression. Successful meiotic progression is essential for both fertility and reproduction of many organisms, and I hope that the work described in this thesis will reveal further insight into the process of meiosis in both yeast and higher eukaryotes. The experiments performed in this thesis are described in Chapters III-V.

The results of Chapter III reveal the mitotic and meiotic DNA-binding patterns of Abp1, with a focus on the centromeres. Using genome-wide mapping, we have found that Abp1 localizes modestly to the centromeric region, primarily at the pericentromeric *dg/dh* repeats, in asynchronous growing cells [120]. To examine the enrichment of Abp1 at the centromeres during the mitotic cell cycle, I performed ChIP qPCR at multiple time

points during the synchronized mitotic cell cycle. The results of these experiments suggest that Abp1 enrichment remains low throughout the centromeres during the mitotic cell cycle. *abp1* mutants have been reported to exhibit defects in meiosis prompting us to examine the binding patterns of Abp1 during meiosis [125]. The genome-wide binding patterns of Abp1 at 0 and 5 hours post-meiotic induction show a significant increase in Abp1 localization to the *dg/dh* repeats and central core (*cnt*) of each centromere. Abp1 enrichment at non-centromere loci, including *Tf2*s, *LTR*s, and the mating type region, remain relatively unchanged. These data suggest that Abp1 plays a role in centromere function during meiosis, either directly or indirectly through the interaction with other centromere proteins.

In Chapter IV, I examine the impact that Abp1 has on other centromere components, including the essential histone 3 variant Cnp1, which is necessary for centromere identity and function. Genome-wide binding and ChIP qPCR experiments of Cnp1 reveal that vegetative cells lacking *abp1* do not experience a loss of Cnp1 at the *cnt*. However, Cnp1 localization at the *cnt* is impaired in *abp1*Δ cells at both 0 and 5 hours post-meiotic induction. I then investigated if a loss of *abp1* impacts the localization of Scm3, the Cnp1 chaperone of *S. pombe*. ChIP qPCR experiments of Scm3 do not reveal diminished localization in vegetative or meiotic *abp1*Δ cells. This suggests that the reduction of Cnp1 binding at the centromere during meiosis in *abp1*Δ cells is not due to decreased Scm3 localization.

Chapter V evaluates the meiotic progression patterns of wild type and *abp1*Δ cells. Previous studies have shown that mitotically growing *abp1*Δ cells display a slow-growth phenotype, chromosome segregation defects, and other morphological

abnormalities [42,125]. The meiotic progression data show that there is a meiotic delay in *abp1*Δ cells, and that this delay is likely to occur between MI and MII. I hypothesize that the observed meiotic delay is due to chromosome segregation defects in cells lacking *abp1*. I used fluorescence microscopy to monitor the fidelity of the meiotic outcome in wild type and *abp1*Δ cells. These results support my hypothesis that cells lacking *abp1* experience chromosome segregation defects during meiosis.

Finally, in Chapter VI, these results are discussed in the larger context of the importance of faithful chromosome segregation during both mitosis and meiosis. Specifically, I examine and compare the functional relationships among *CENP-B* homologs from *S. pombe* to humans. Additionally, I discuss how work described in this thesis creates new questions concerning the various evolutionary forces that could shape centromere identity and function, chromosome segregation, and successful meiotic outcome.

Figures

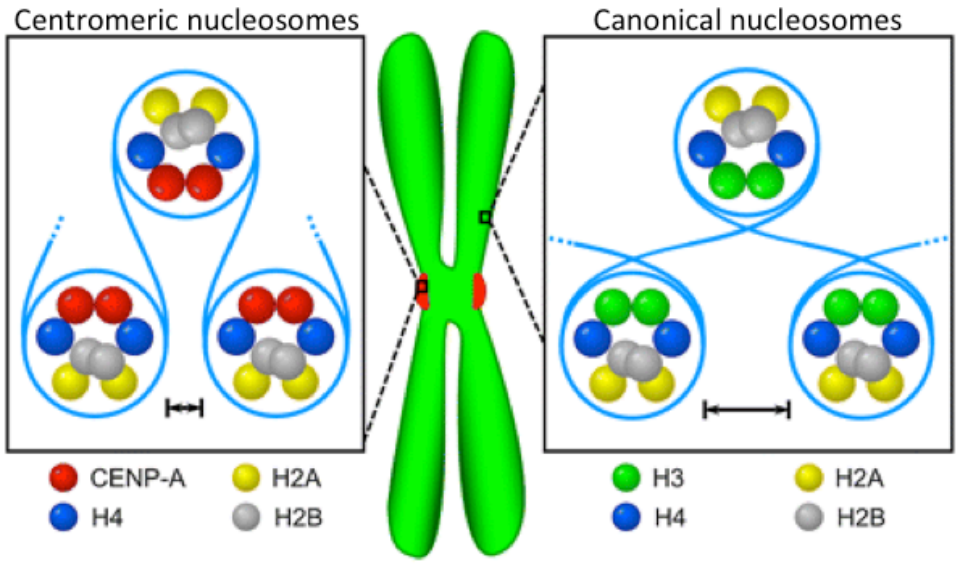

Figure 1. Model of nucleosome positioning on the eukaryotic chromosome. Model shows location of nucleosomes containing the centromere-specific histone 3 variant, CENP-A, at the centromere (left) and the location of nucleosomes containing the canonical histone H3 along the chromosome arms (right). Figure adapted from Panchenko *et al*, PNAS, 2011[174].

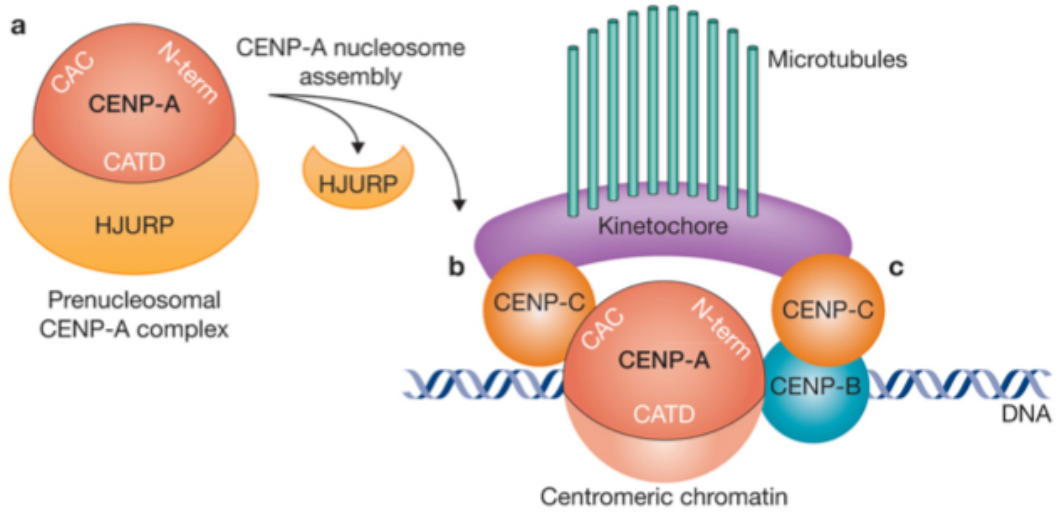

Figure 2. Model of Centromere Protein (CENP) binding at the human centromere. (**a**) The CENP-A targeting domain (CATD) is directly bound by the CENP-A chaperone HJURP, which localizes CENP-A to the centromere. (**b**) Once incorporated into the centromeric DNA chromatin, the CENP-A C-terminus (CAC) directs kinetochore assembly by binding CENP-C, which makes direct contact with the kinetochore complex. (**c**) The CENP-A N-terminus also recruits a low level of CENP-C, possibly through CENP-B, providing an alternative, redundant pathway for kinetochore assembly at the centromere. Figure adapted from French and Straight, Nature Cell Biology, 2013[175].

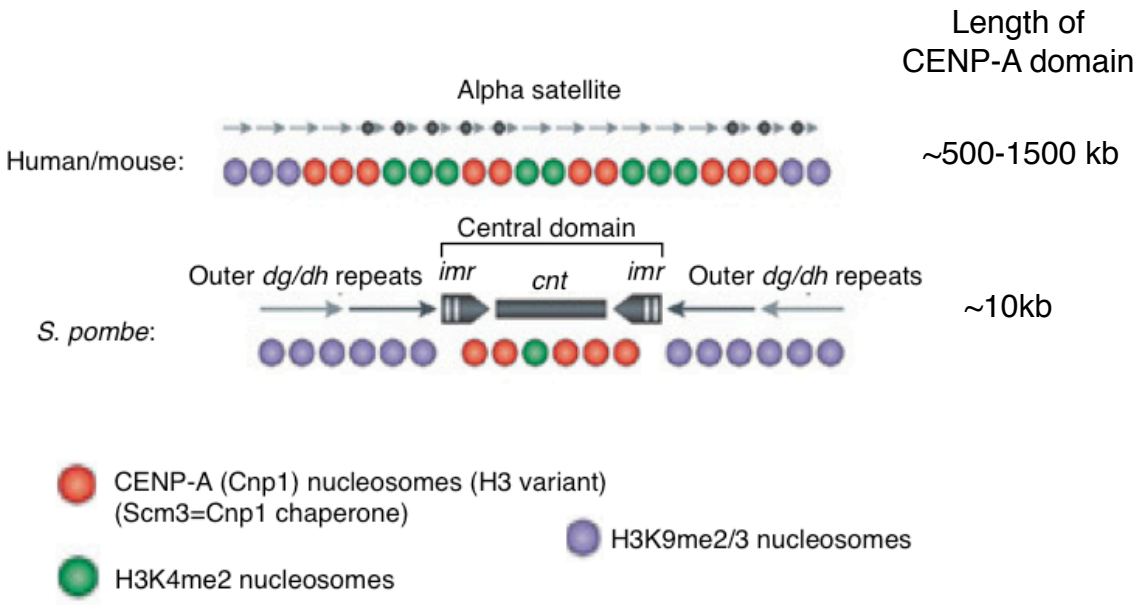

Figure 3. Model of eukaryotic centromeres. Model depicts the structure and epigenetic patterns of the higher eukaryotic human/mouse centromere and the *S. pombe* centromere. Both centromeres contain the centromere-specific histone 3 variant, CENP-A (Cnp1 in *S. pombe*), as well as flanking H3K9me2/3 heterochromatin. Figure modified from Duggan *et al*, Nature, 2010[176].

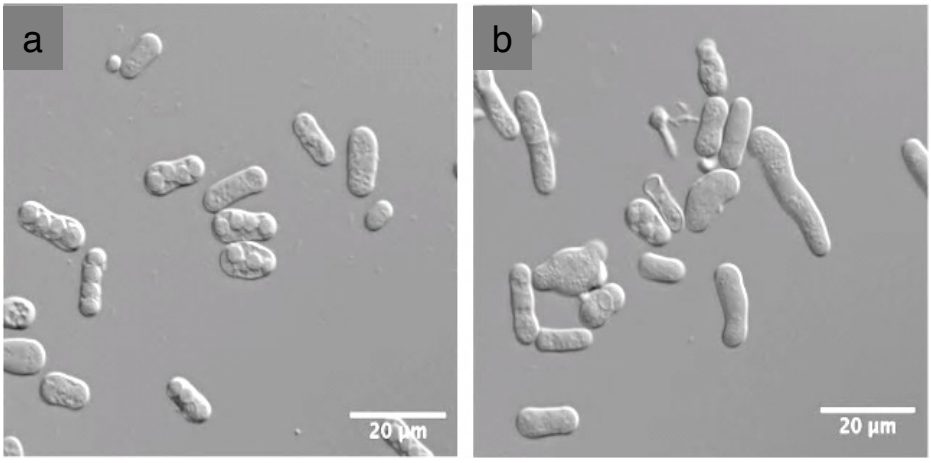

Figure 4. Light microscopy image of diploid *S. pombe* cells after being allowed to sporulate. (a) Wild type *S. pombe* diploid cells and asci and **(b)** *abp1*Δ diploid cells and asci. Cells grown on Edinburgh Minimal Media (EMM) media at 26°C for 2 days to allow sporulation. Image taken on a Zeiss Axioplan 2 microscope.

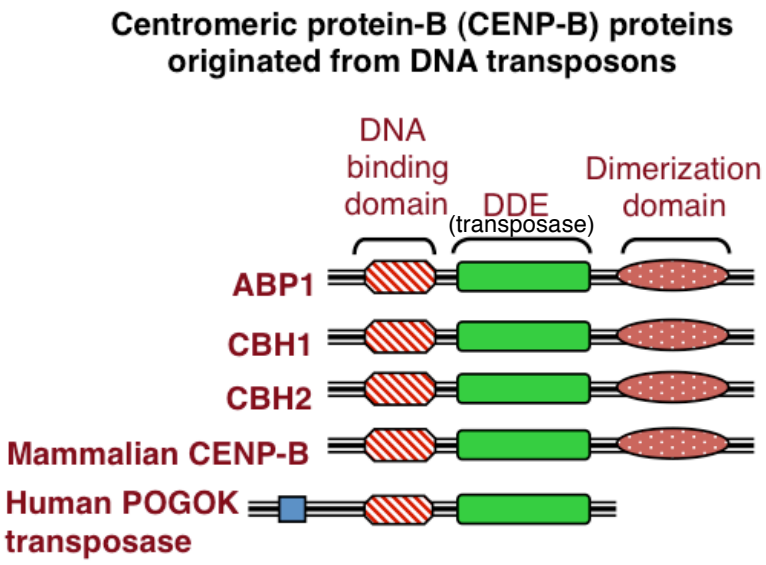

Figure 5. Model comparing mammalian CENP-B with its homologous proteins in *S. pombe*. The CENP-B proteins of *S. pombe*, Abp1, Cbh1, and Cbh2, share similar protein architecture with the mammalian CENP-B and the human *pogo* transposase. Each protein contains a DNA-binding domain at the amino terminus, a large transposase domain with the characteristic DDE motif, and a dimerization domain at the carboxy terminus. Figure modified from Lorenz *et al*, MCB, 2012[177].

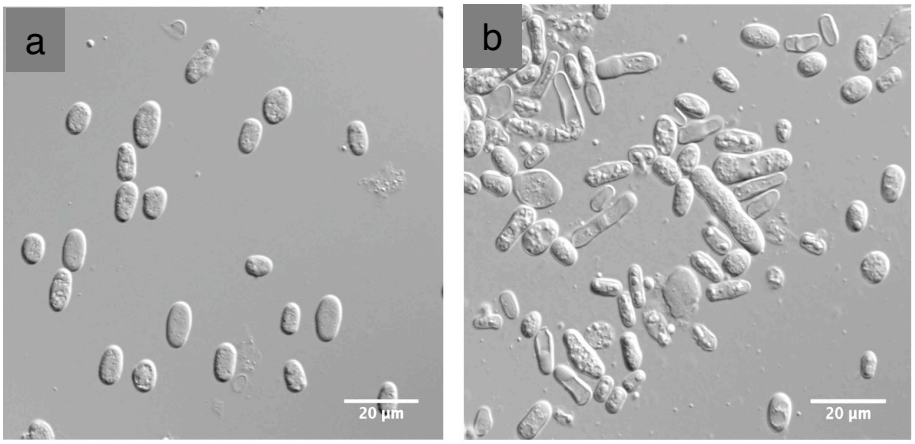

Figure 6. Light microscopy image of haploid *S. pombe* cells. (a) Wild type *S. pombe* haploid cells and **(b)** *abp1*Δ *S. pombe* haploid cells. Cells grown on standard Yeast Extract with Adenine (YEA) media at 30°C until colonies formed, at which time cells were collected for imaging. Image taken on a Zeiss Axioplan 2 microscope.

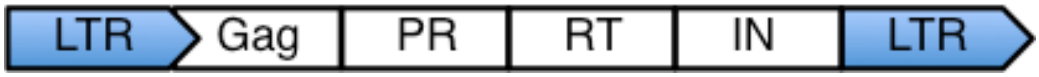

Figure 7. Schematic of the *LTR*-containing *Tf2* retrotransposon of *S. pombe*. Shown is the structure of the *Tf2* retrotransposon, including the protease (PR), reverse transcriptase (RT), and integrase (IN) domains. *LTR* sequences flank the *Tf2* sequence.

Chapter II: Materials and Methods

Strain Construction

Strains were created using standard yeast genetic crosses [178]. *mat2-102* strains were genotyped using colony PCR. *pat1-114* temperature sensitive (*ts)* strains were scored by ectopic haploid meiosis on EMM media at the restrictive temperature of 30°C after 2 days of incubation. *pat1-114* cells were identified by microscopic examinations or staining with iodine vapor for the presence of spores.

Strain growth conditions

All strains were maintained on solid standard rich medium supplemented with 225 mg/liter adenine (YEA) at 30°C or 25°C for *ts* mutants. Haploid *pat1-114* liquid cultures were grown in liquid YEA at the permissive temperature of 25°C. Diploid strains carrying the *ade6-M210/ade6-M216* complementation alleles were grown on media lacking adenine (SC-Ade) to maintain the diploid state.

Meiotic synchronization

The *ts* mutant *pat1-114* was used to synchronize diploid cells in meiosis using nitrogen starvation and G1 arrest. Fresh diploid cells were grown to an OD of 1-2 at the permissive temperature of 25°C in 50ml of SC-Ade media. Cells were then centrifuged and transferred to 100ml EMM2 media containing nitrogen with an initial OD of 0.05-0.1. Strains containing the *abp1*Δ mutation were transferred to EMM2 so that their initial OD was double that of wild type due to their slow-growth phenotype. These cultures were then grown at 25°C for 24 hours to an OD of 0.5-0.6. Cells were then washed three times with sterile water and transferred to 100ml of EMM media containing no nitrogen with an initial OD of 0.4. They were then incubated at 25°C for 15 hours to an OD of 0.8-

1. To initiate meiosis, 1ml of 5% NH4Cl was added to the 100ml EMM-N culture that was then shifted to the restrictive temperature of 34°C [179]. Cells were collected at 0 hours and 5 hours post-meiotic induction. The 0 hour and 5 hour time points refer to the moment before the temperature shift to 34°C and 5 hours after that temperature shift, respectively. For the meiotic delay experiment of WT and *abp1*Δ diploids, cells were collected every 30 minutes and observed under a fluorescence microscope to identify meiotic phases.

Mitotic synchronization

Mitotic synchrony was achieved using strains containing a *ts cdc25-22* allele. Cells were grown in 200mL liquid YEA at the permissive temperature of 26°C overnight and grown to an OD of approximately 0.8. Cells were then diluted to five separate flasks containing 50mL of fresh liquid YEA pre-warmed to 36°C at the initial OD of 0.2. These cultures were incubated at the restrictive temperature of 36°C for four hours to induce G2 arrest. To release from G2 arrest, the cultures were returned to 26°C, and samples were collected to measure the septation index percentage using calcofluor staining. This was done to estimate the mitotic cell cycle stage of each culture [180]. At t=0 minutes, t=40 minutes, t=100 minutes, and t=140 minutes after G2 release at 26°C, 50 mL of culture were collected for ChIP analysis of Abp1 enrichment across the cell cycle. For asynchronous sample, 50mL of culture was collected from cells kept at 26°C for the entirety of their growth.

Calcofluor staining

Calcolfuor staining was used to measure the septation index of mitotically synchronized *cdc25-22* cells [181]. At each time point, 1mL of culture was removed and centrifuged 5,000 rpm for 2 minutes, washed with 1mL ice-cold 1X PBS, and resuspended in 100µl of ice-cold 1X PBS containing calcofluor (1mg/mL). The cells were kept on ice for 10-15 minutes. 3µl of cells were mounted on a slide and examined with the EVOS fluorescence microscope using the DAPI channel.

Chromatin Immunoprecipitation (ChIP)

ChIP assays and ChIP–chip experiments were performed as previously described [114]. For analysis of histones and histone modifications (i.e., Cnp1 and H3K9me2), cells were cross-linked with 3% paraformaldehyde (PFA). For chromatin-associated proteins (i.e., Abp1, HDACs), PFA-cross-linked cells were subjected to second round of cross-linking with dimethyl adipimidate dihydrochloride (DMA). The sonicated, cross-linked chromatin was immunoprecipitated with 2µg of anti-FLAG antibodies (M2, Sigma-Aldrich) coupled either to agarose beads (Abp1-FLAG) or magnetic beads (Cnp1-FLAG and Scm3- FLAG). For ChIP analyses of H3K9me2, 2µg of antibodies against H3K9me2 (ab1220, Abcam) were used in combination with a 20 µL 50% slurry of magnetic protein G beads (L00274, Genscript).

ChIP-chip was done as previously described using Agilent tiling microarrays [114]. ChIP-chip analysis was performed using the R/Bioconductor *ringo* package [182]. Preprocessing was performed using loess normalization. ChIP-enriched regions were defined as three or more adjacent microarray probes with fold-enrichment greater than a two-Gaussian null distribution threshold (greater than 2-fold enrichment). The application

of the two-Gaussian null distribution threshold eliminated single probes that displayed a fold-enrichment greater than 20. The Abp1 binding data represents the mean of two biological replicates. The Cnp1 binding data represents a single ChIP-chip experiment.

Quantitative real-time PCR (qPCR)

qPCR was performed using ChIP DNA and a master mix containing Phire Polymerase (F-122L, Thermo Scientific) on the Applied Biosystems 7500 fast real-time PCR system. SYBR green signal was normalized to a passive ROX reference dye. Triplicate reactions were carried out in 10µl volume for each experiment. Enrichment of ChIP versus input DNA was determined using the $2^{-\Delta\Delta CT}$ method in Microsoft Excel. The relative fold enrichment was quantified using actin as a reference.

Fluorescence microscopy analyses of WT, *abp1*Δ, and *rdp1*Δ asci

Diploid WT and *abp1*Δ strains containing histone H3 tagged with GFP (*hht2-GFP::ura4*$^{+}$) were grown and maintained on SC–Ade media using *ade6-M210*/*ade6-M216* complementation. Single colonies of diploids were plated on EMM media to allow sporulation at 26°C for approximately 2 days, or until the majority of cells formed asci. The fluorescent signals of histone H3-GFP in asci-encased spores on an EMM agar pad were analyzed for abnormal nuclei using the EVOS fluorescence microscope. For analyzing the wild type, *abp1*Δ, and RNAi mutant *rdp1*Δ meiotic products, spore nuclei were visualized by DAPI-stained asci. Each microscopy experiment was performed in duplicates.

Western blot analysis of Cnp1

S. pombe cells (OD 1–2) were collected during vegetative growth and at 0 hours and 5 hours post-meiotic induction. Cells were lysed in HCS buffer (150 mM HEPES pH 7.2, 250 mM NaCl, 0.1% NP-40, 1 mM EDTA, 1 mM dithiothreitol, 1 mM PMSF) and protein inhibitor tablet (1836153, Roche) by acid-washed beads in a bead beater (two times for 30 seconds each with a 2 minute interval on ice). 50 µg of protein extracts were run on a ExpressPlus PAGE Gel, 4-20% (M42012, Genscript) in 1 X MOPS buffer and subjected to overnight western blot transfer at 4°C. Cnp1 was detected using anti-FLAG antibody at a concentration of 1:1000 (A00187, Genscript).

Chapter III: Genome-wide analysis of Abp1 localization during the meiotic cell cycle and meiosis

Summary

Unlike the human *CENP-B*, for which the discovery and function have always been linked to centromeres, a centromeric role for *S. pombe* CENP-B homologs at times seems less straightforward. Abp1 (*ARS*-binding protein 1) was first identified in *S. pombe* as a 60-kDa protein that binds to autonomously replicating sequence (*ARS*) elements, specifically *ars3002* [123]. *ARS* elements act as origins of DNA replication and are present in high density at centromeres [123]. However, its potential centromeric function was quickly appreciated due to its high sequence homology to the human *CENP-B*[123,125] and subsequent studies showing a role for Abp1 in proper assembly of pericentromeric heterochromatin[125,152].

More recent discovery of Abp1 as a regulator of retrotransposons shifts attention away from its original role as a centromeric protein [120,121,177]. The experiments described in Chapter III aim to expand on previous DNA-binding experiments of Abp1, specifically during the synchronized mitotic cell cycle and meiosis. These experiments result in the discovery of a potential novel role for Abp1 at the centromeres during meiosis.

Constitutive low enrichment of Abp1 at the pericentromeres across the mitotic cell cycle

While earlier studies have shown localization of Abp1 to the centromere [42,125,152], our previous genome-wide mapping reveals only a slight binding of Abp1 at centromeres, primarily at the pericentromeric repeats in asynchronous growing cells [120]. Because *S. pombe* has an extended G2 phase, previous reports of Abp1-binding in asynchronous cells likely reflect its binding in G2 [120]. I performed chromatin immunoprecipitation

(ChIP) followed by quantitative PCR (qPCR) to assess the possibility that Abp1 could be preferentially enriched at centromeres during certain phases of the mitotic cell cycle.

Cells were synchronized by the *cdc25-22 ts* mutation, which causes cell cycle arrest in G2 when grown at the restrictive 36°C [180]. Septation index monitoring revealed that ~ 90% of cells synchronously reentered S phase 100 minutes after release from the G2 block **(Figure 8)**. Cells were collected at 0 minutes, 40 minutes, 100 minutes, and 140 minutes after release from G2 arrest for ChIP qPCR analysis of Abp1 binding. These time points correlate with the G2, M/G1, S, and G2 stages of the mitotic cell cycle, respectively, as determined by calcofluor staining **(Figure 8)**. Asynchronous cells were also collected for comparison.

According to the ChIP qPCR data, the levels of Abp1 were not much enriched at the pericentromeric *dg/dh* and *imr* repeats, central core (*cnt*), or the negative control *rpb1* gene in either the asynchronous or synchronized cell populations across the mitotic cell cycle **(Figure 9)**. More specifically, the enrichment values of Abp1 at any given area of the centromere in vegetative cells did not exceed 1.5 fold **(Figure 9)**. In contrast, Abp1 occupancy at the *Tf2-1* element slightly fluctuated during each time point of the mitotic cell cycle, with enrichment values ranging from 1.5-5 fold **(Figure 10)**. Thus, consistent with previous genome-wide bindings [120,121], our analysis of the mitotic cell cycle reveals that Abp1 is barely detectable at the centromeres. As such, it remains unclear whether mitotic chromosome segregation defects observed in *abp1* mutants [125,152] could be explained via its centromeric localization.

Abp1 is dynamically enriched at the centromere central cores upon meiotic entry

Because Abp1 has also been reported to contribute to normal meiosis, I examined genome-wide binding of Abp1 in cells at 0 and 5 hours post-meiotic induction using a ChIP microarray. These time points refer to the moment of meiotic induction at 34°C (0 hr) and 5 hours after this induction (approximately MI). The binding patterns of Abp1 at the chromosomal levels in meiotic cells appeared largely similar to those of vegetative cells **(Figures 11-16)**. More specifically, the binding data revealed that there was little difference in Abp1 occupancy in vegetative cells compared to meiotic cells at *Tf2s* **(Figure 17)**, solo *LTRs* **(Figure 18)**, and the origins of replication (*ars*) **(Figure 19)**, with Abp1 enrichment values ranging from 4-6 fold **(Figures 17-19)**.

Abp1 has also been shown to bind to the mating type locus [120,183] and contribute to the directionality of mating type switching [183]. Therefore, I examined the localization of Abp1 at this region. The enrichment of Abp1 at the mating type locus remained relatively unchanged in vegetative cells compared to meiotic cells, and the prominent binding peaks ranged from 5-7 fold **(Figure 20)**. In addition to binding at retrotransposon sequences and major chromosomal landmarks, Abp1 is known to bind to certain gene promoters [120]. Less than 10 gene promoters were identified that exhibited significant changes (> 2 fold ChIP enrichment) in Abp1 binding. These genes included *glo3* (encodes for a GTPase activating protein), *cam2* (encodes for a myosin I light chain protein), *mod5* (encodes for a cell-end marker protein), *prp11* (encodes for an ATP-dependent RNA helicase), and *tpx1* (encodes for thioredoxin peroxidase) **(Figures 11-16)**. These genes displayed vegetative Abp1 enrichment that was approximately 5-7 fold

greater than meiotic enrichment **(Figure 21)**. However, Gene Ontology (GO) analysis did not reveal any significant GO terms associated with these genes.

Intriguingly, I observed dramatic changes in Abp1 binding at the centromeres as cells entered meiosis. At 0 hours post-meiotic induction, there was a sharp increase of Abp1 enrichment at the pericentromeric *dh* repeats (6 fold enrichment) concomitant with small binding peaks (2 fold enrichment) within the central cores of centromere I **(Figure 22)**, centromere II **(Figure 23)**, and centromere III **(Figure 24)**. In addition, Abp1 displayed a 3 fold enrichment during early meiosis at sites enriched for centromeric tRNAs, which have been shown to act as boundary elements at the centromere **(Figures 23, 24)**. Abp1 in vegetative cells did not exceed 2 fold enrichment at any region of centromeres I-III, with the majority of vegetative enrichment values below 1.5 fold **(Figures 22-24)**.

By 5 hours into meiosis, Abp1 binding at major *dg/dh* repeats was somewhat reduced to 3.5 fold enrichment, but Abp1 binding could still be detected throughout the central cores with 2.5 fold enrichment at centromere I **(Figure 25)**, centromere II **(Figure 26)**, and centromere III **(Figure 27)**. Abp1 localization at the centromeres and *Tf2-1* remained elevated 8 hours post-meiotic induction as shown by ChIP qPCR **(Figure 28)**. At 8 hours-post meiotic induction, Abp1 displayed a 7-10 fold enrichment at central cores I-III, a noticeable increase relative to the pericentromeric *dg* repeat, where Abp1 displayed a 2-3 fold enrichment **(Figure 28)**. One primer pair (*cnt1 and 3*) was used for examining enrichment at both central core I (*cnt1*) and central core III (*cnt3*) because it is complementary to both regions due to the similarity in their DNA sequences. These data suggest that Abp1 occupancy at the central cores of centromeres I-III is maintained, and

possibly increases, as meiosis progresses **(Figures 22-28)**. Thus, these results regarding Abp1 localization suggest a potential specialized role for Abp1 at meiotic centromeres.

Except for the centromeres, these data collectively reveal that Abp1 binding at all *Tf2s*, multiple *LTR*s, origins of replication, and mating type region remains very similar between vegetative and meiotic cells, ranging from 4-6 fold enrichment **(Figures 17-20)**. These data support my hypothesis that Abp1 is exerting a unique role at the centromere during meiosis. The experiments in Chapter IV aim to uncover a relationship between Abp1 and the centromere-specific histone, Cnp1, at the meiotic centromeres.

Figures

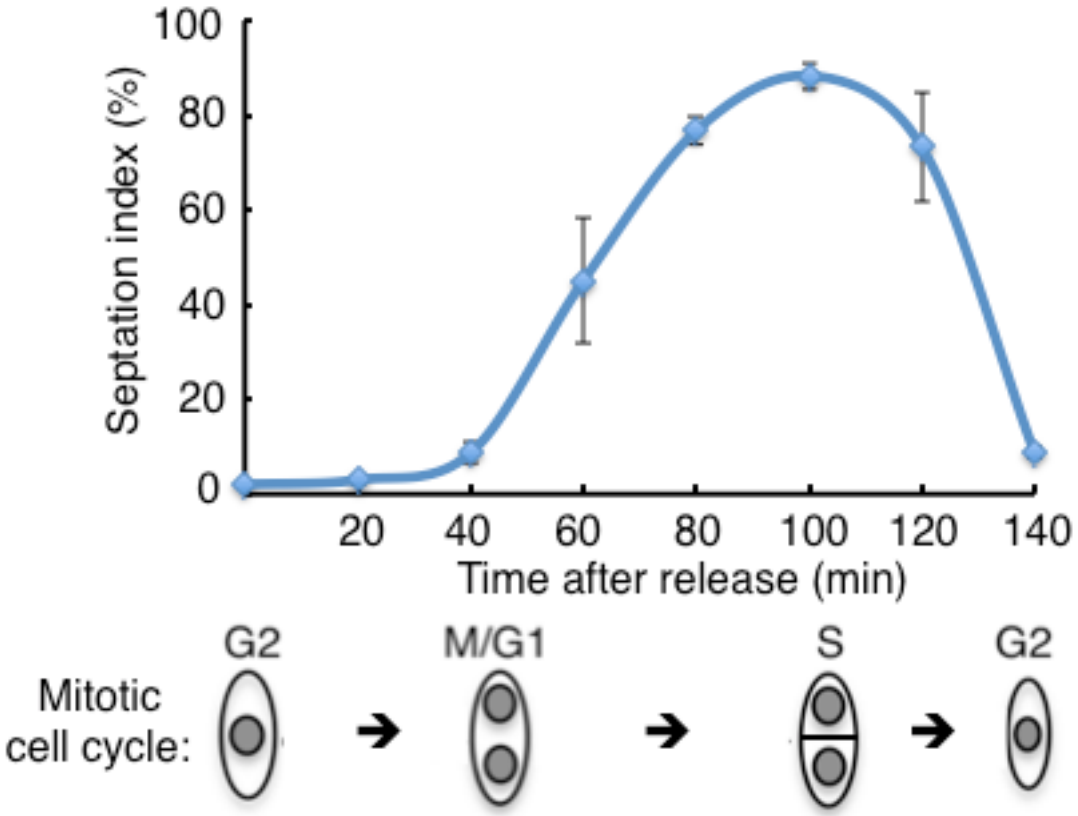

Figure 8. Mitotic synchrony of *S. pombe* using the *cdc25-22* temperature sensitive mutant. The septation index (%) of the synchronized cells represents specific stages of the mitotic cell cycle, as shown in the cell cycle diagram. Error bars represent standard deviation. *n*=3 biological replicates.

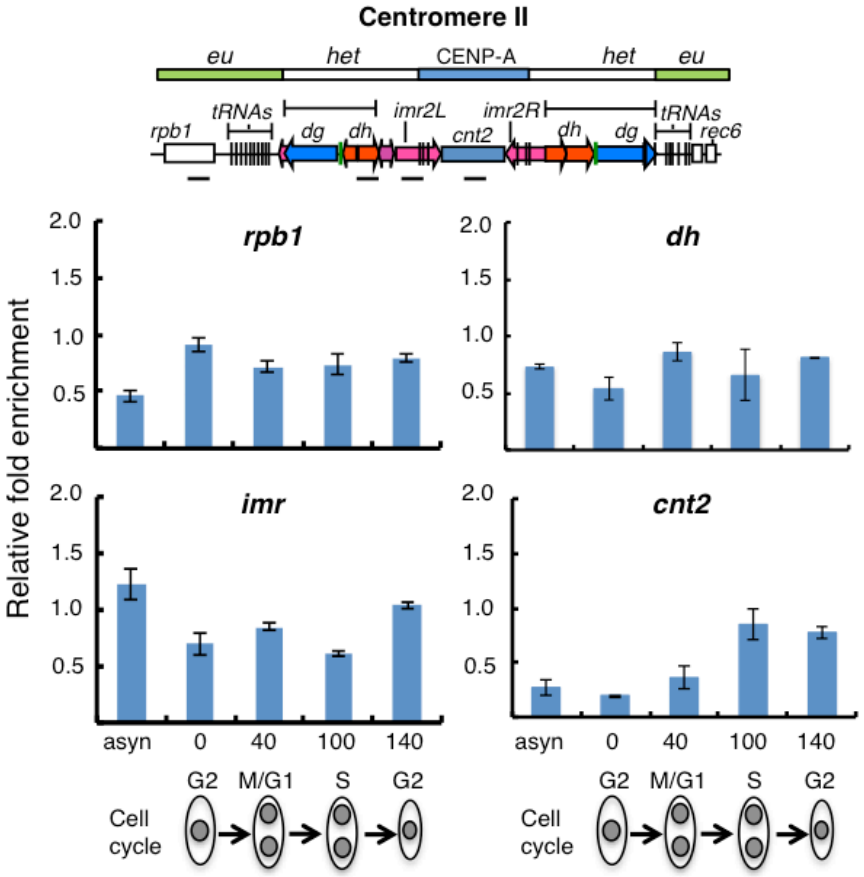

Figure 9. Abp1 displays minimal binding to the centromere during the synchronized mitotic cell cycle. (Upper panel) Schematic of centromere II. The black bars indicate the positions of primers used for qPCR. (Lower panels) Relative fold enrichment of Abp1-FLAG(3X) at t=0 minutes (G2), t=40 minutes (M/G1), t=100 minutes (S), and t=140 minutes (G2) after temperature release. Asynchronous (asyn) cells are also included. Enrichment at the gene *rbp1*, pericentromeric repeat *dh*, inner most region of the centromere (*imr*), and central core of chromosome 2 (*cnt2*) was determined using chromatin immunoprecipitation (ChIP) and qPCR using *act1* gene as a reference. Error bars indicate standard deviation. *n*=3 technical replicates.

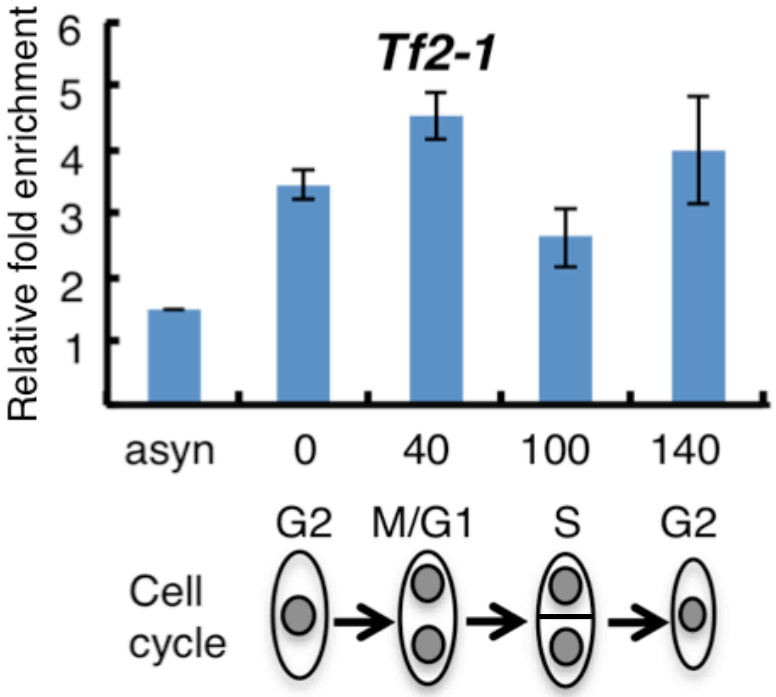

Figure 10. Abp1 remains enriched at *Tf2-1* throughout the mitotic cell cycle. Relative fold enrichment of Abp1-FLAG(3X) at t=0 minutes (G2), t=40 minutes (M/G1), t=100 minutes (S), and t=140 minutes (G2) after temperature release. Asynchronous (asyn) cells are also included. Enrichment at the retrotransposon *Tf2-1* was found using chromatin immunoprecipitation (ChIP) and qPCR using *act1* as a reference. Error bars indicate standard deviation. *n*=3 technical replicates.

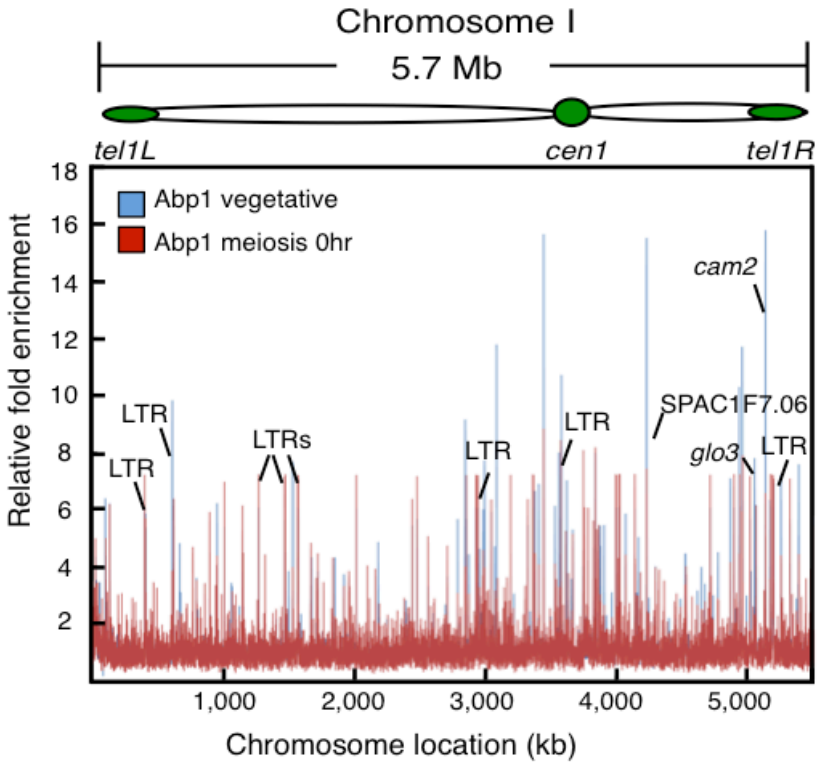

Figure 11. Abp1 displays genome-wide binding on chromosome I in vegetative and meiotic cells using ChIP-chip. (Upper panel) Schematic of chromosome I. (Lower panel) Abp1 binding to chromosome I in vegetative cells (blue) and at t=0 hours meiosis (red). ChIP-chip assays were performed in strains containing Abp1-FLAG(3X). ChIP-chip enrichment of Abp1 relative to whole cell extract (WCE) was plotted against respective chromosomal location. Single probes with fold-enrichment values greater than 20 were removed if the adjacent probes did not show enrichment. Data represent the mean of two biological replicates.

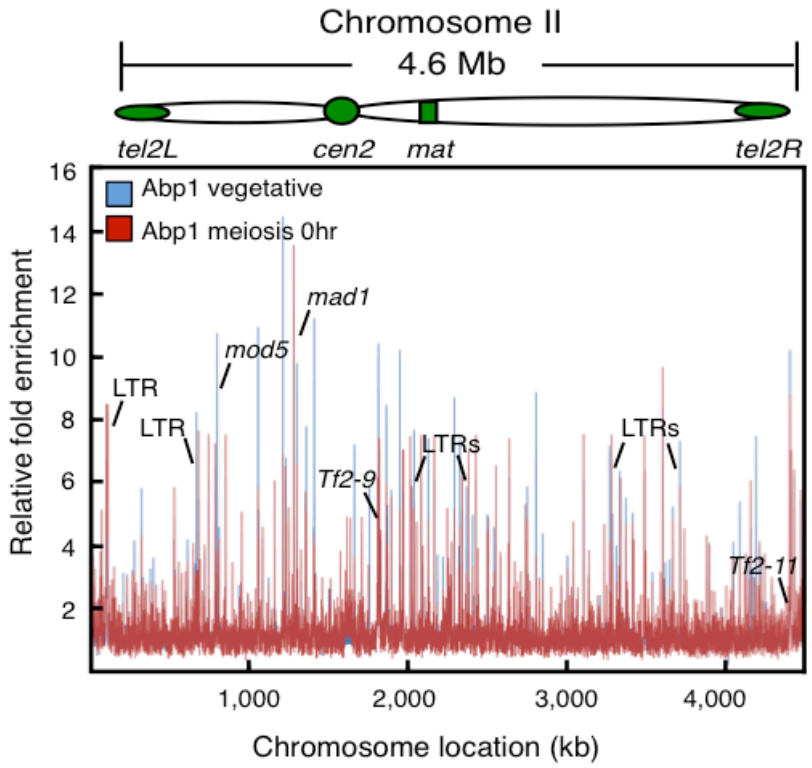

Figure 12. Abp1 displays genome-wide binding on chromosome II in vegetative and meiotic cells using ChIP-chip. (Upper panel) Schematic of chromosome II. (Lower panel) Abp1 binding to chromosome II in vegetative cells (blue) and at t=0 hours meiosis (red). ChIP-chip assays were performed in strains containing Abp1-FLAG(3X). ChIP-chip enrichment of Abp1 relative to WCE was plotted against respective chromosomal location. Single probes with fold-enrichment values greater than 20 were removed if the adjacent probes did not show enrichment. Data represent the mean of two biological replicates.

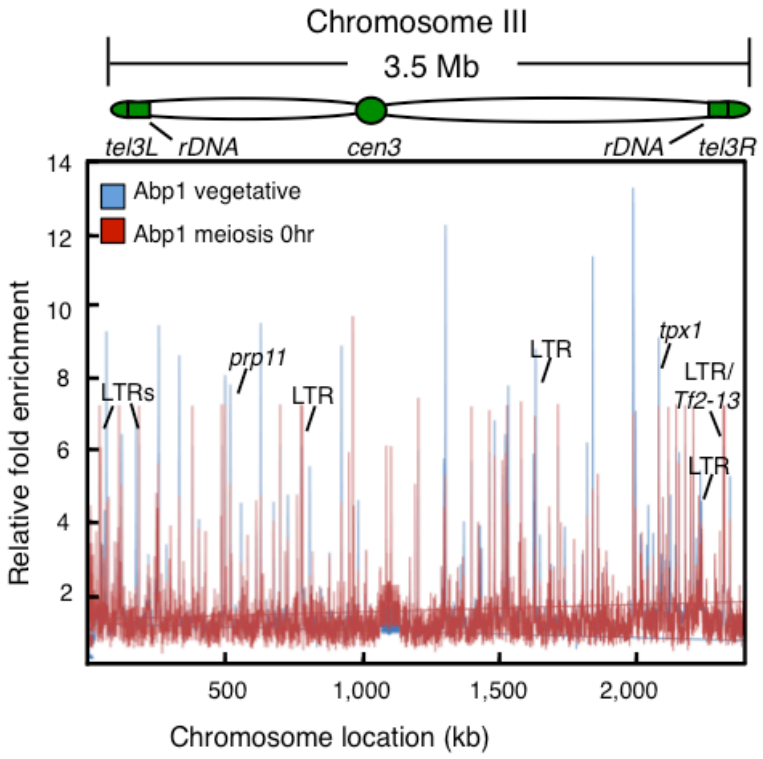

Figure 13. Abp1 displays genome-wide binding on chromosome III in vegetative and meiotic cells using ChIP-chip. (Upper panel) Schematic of chromosome III. (Lower panel) Abp1 binding to chromosome III in vegetative cells (blue) and at t=0 hours meiosis (red). ChIP-chip assays were performed in strains containing Abp1-FLAG(3X). ChIP-chip enrichment of Abp1 relative to WCE was plotted against respective chromosomal location. Single probes with fold-enrichment values greater than 20 were removed if the adjacent probes did not show enrichment. Data represent the mean of two biological replicates.

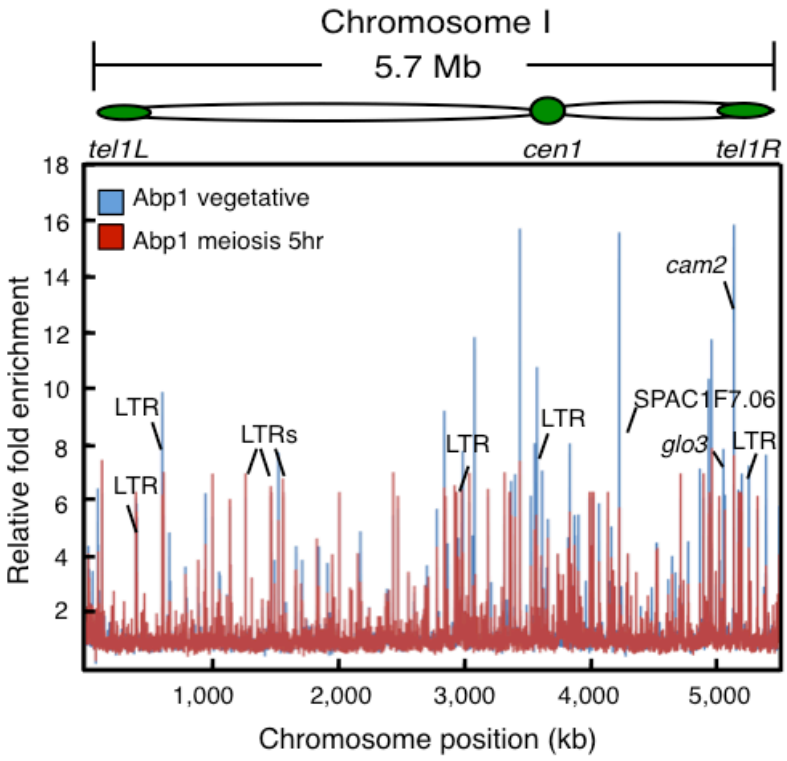

Figure 14. Abp1 displays genome-wide binding on chromosome I in vegetative and meiotic cells using ChIP-chip. (Upper panel) Schematic of chromosome I. (Lower panel) Abp1 binding to chromosome I in vegetative cells (blue) and at t=5 hours meiosis (red). ChIP-chip assays were performed in strains containing Abp1-FLAG(3X). ChIP-chip enrichment of Abp1 relative to WCE was plotted against respective chromosomal location. Single probes with fold-enrichment values greater than 20 were removed if the adjacent probes did not show enrichment. Data represent the mean of two biological replicates.

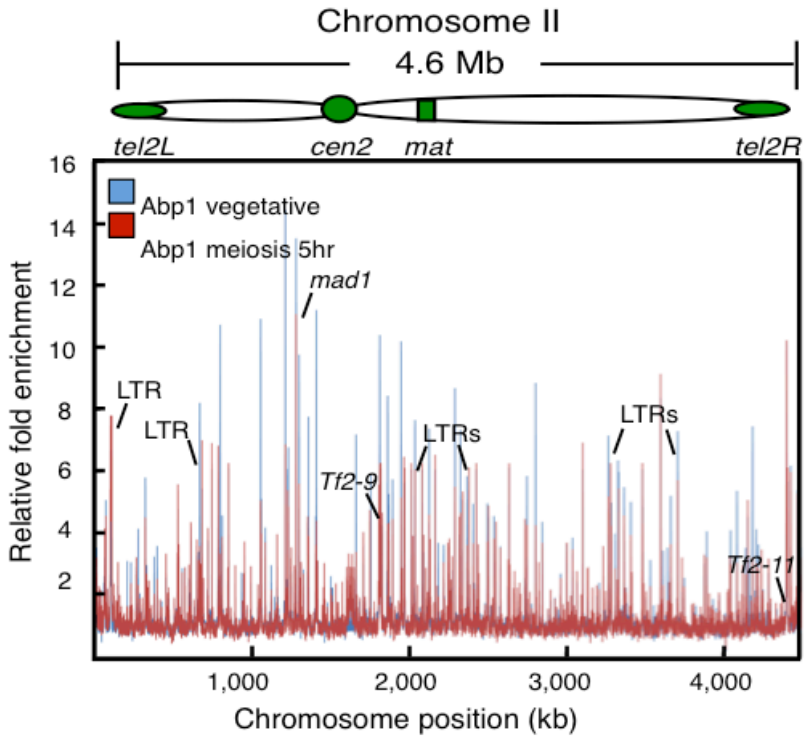

Figure 15. Abp1 displays genome-wide binding on chromosome II in vegetative and meiotic cells using ChIP-chip. (Upper panel) Schematic of chromosome II. (Lower panel) Abp1 binding to chromosome II in vegetative cells (blue) and at t=5 hours meiosis (red). ChIP-chip assays were performed in strains containing Abp1-FLAG(3X). ChIP-chip enrichment of Abp1 relative to WCE was plotted against respective chromosomal location. Single probes with fold-enrichment values greater than 20 were removed if the adjacent probes did not show enrichment. Data represent the mean of two biological replicates.

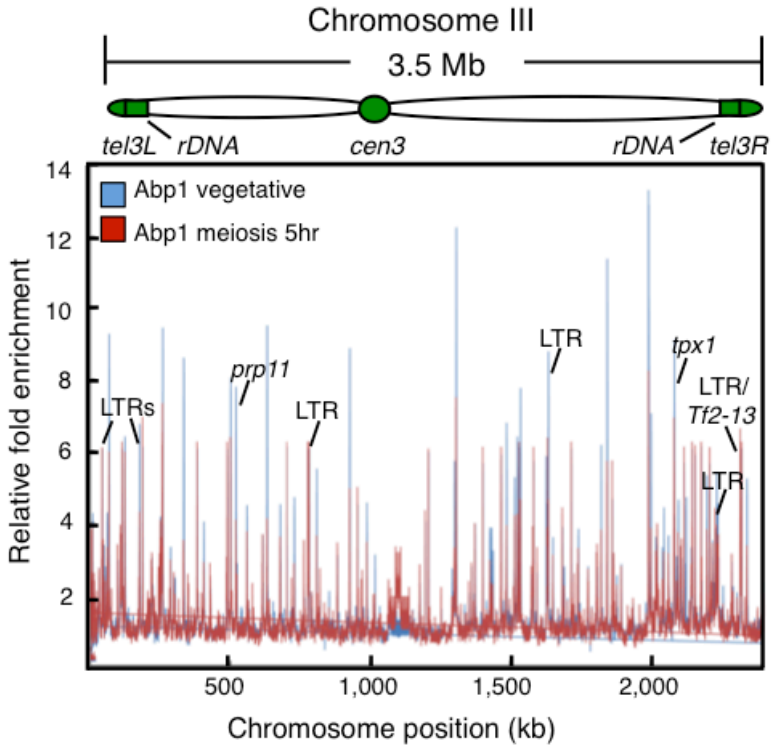

Figure 16. Abp1 displays genome-wide binding on chromosome III in vegetative and meiotic cells using ChIP-chip. (Upper panel) Schematic of chromosome III. (Lower panel) Abp1 binding to chromosome III in vegetative cells (blue) and at t=5 hours meiosis (red). ChIP-chip assays were performed in strains containing Abp1-FLAG(3X). ChIP-chip enrichment of Abp1 relative to WCE was plotted against respective chromosomal location. Single probes with fold-enrichment values greater than 20 were removed if the adjacent probes did not show enrichment. Data represent the mean of two biological replicates.

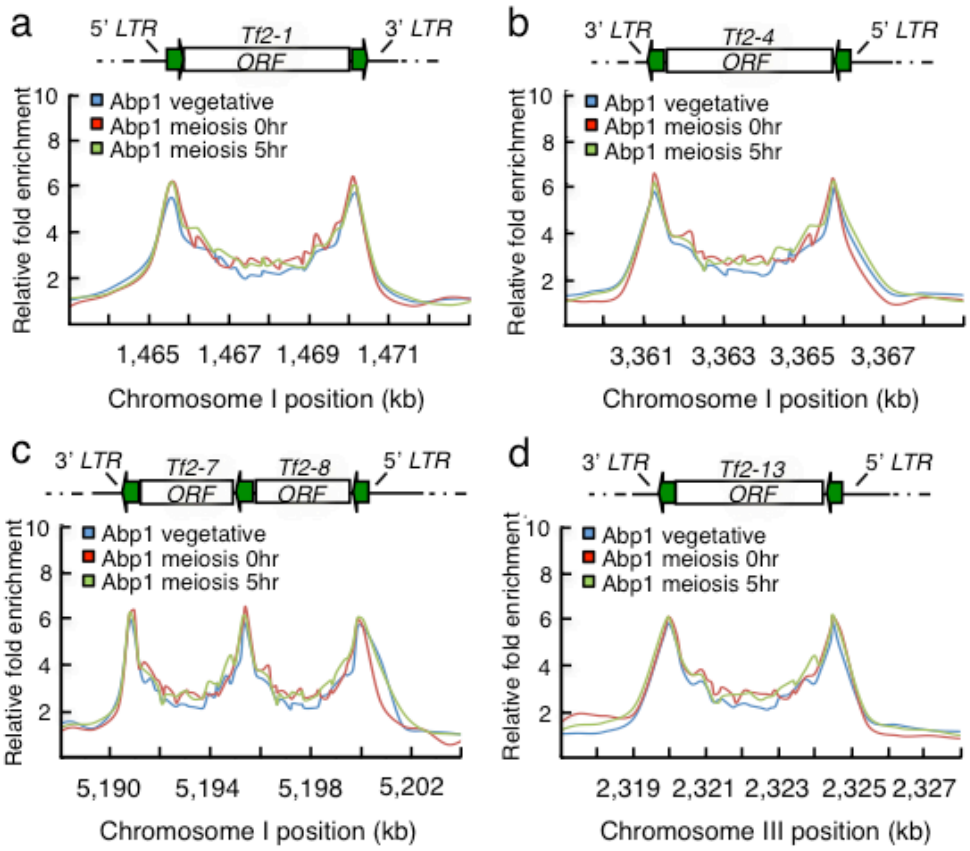

Figure 17. Abp1 enrichment at *Tf2*s is similar between meiotic and vegetative cells. (Upper panel) Schematic of *Tf2* locus. (Lower panel) Abp1-FLAG(3X) enrichment at **(a)** *Tf2-1*, **(b)** *Tf2-4*, **(c)** *Tf2-7/8*, and **(d)** *Tf2-13* in vegetative strains (blue), at t=0 hours meiosis (red) and t=5 hours meiosis (green). ChIP-chip enrichment of Abp1 relative to WCE was plotted against respective chromosomal location. Data represent the mean of two biological replicates.

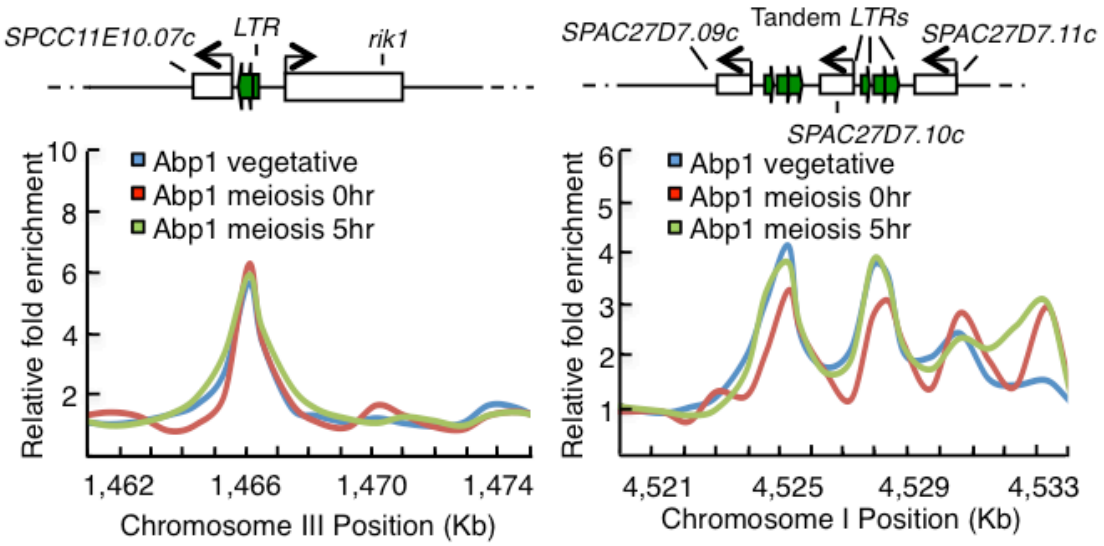

Figure 18. Abp1 enrichment at solo *LTR*s is similar between meiotic and vegetative cells. (Upper panel) Schematic of *LTR* loci. (Lower panel) Abp1-FLAG(3X) enrichment at indicated *LTR* loci in vegetative strains (blue), at t=0 hours meiosis (red) and t=5 hours meiosis (green). ChIP-chip enrichment of Abp1 relative to WCE was plotted against respective chromosomal location. Data represent the mean of two biological replicates.

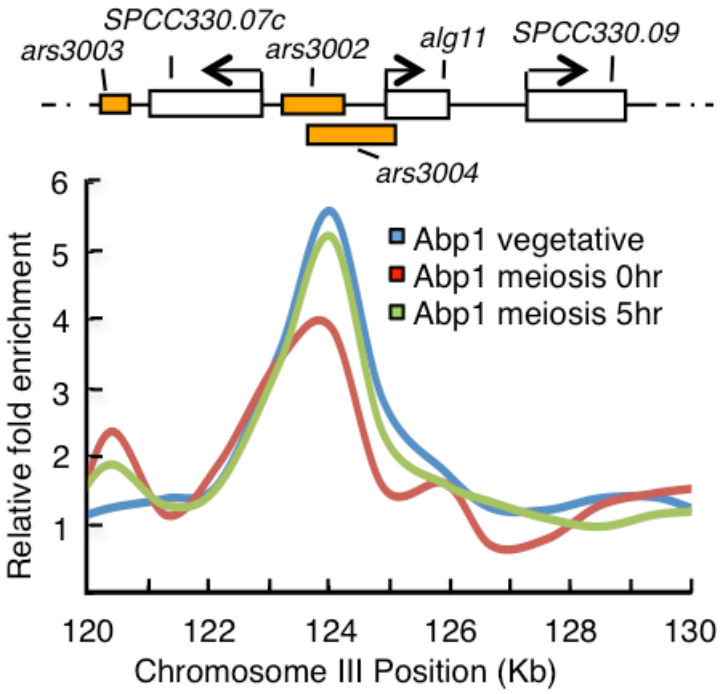

Figure 19. Abp1 enrichment at the autonomously replicating sequence (*ars*) locus is similar between meiotic and vegetative cells. (Upper panel) Schematic of the *ars* (origin of replication). (Lower panel) Abp1-FlAG(3X) enrichment at the origin of replication of chromosome III in vegetative strains (blue), at t=0 hours meiosis (red) and t=5 hours meiosis (green). ChIP-chip enrichment of Abp1 relative to WCE was plotted against respective chromosomal location. Data represent the mean of two biological replicates.

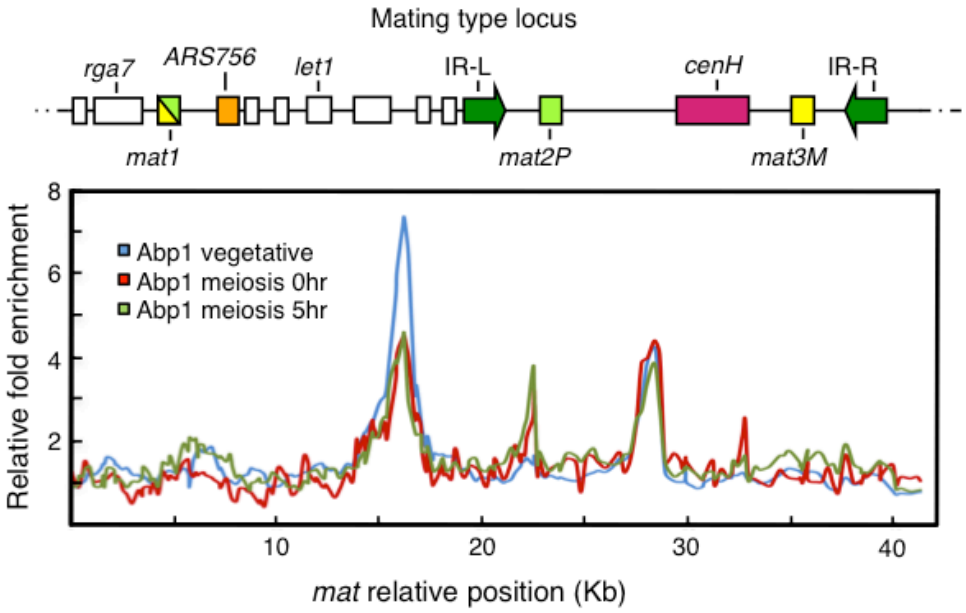

Figure 20. Abp1 enrichment at the mating type locus is similar between meiotic and vegetative cells. (Upper panel) Schematic of mating type locus. (Lower panel) Abp1-FLAG(3X) enrichment at the mating type locus in vegetative strains (blue), at t=0 hours meiosis (red) and t=5 hours meiosis (green). ChIP-chip enrichment of Abp1 relative to WCE was plotted against respective chromosomal location. Data represent the mean of two biological replicates.

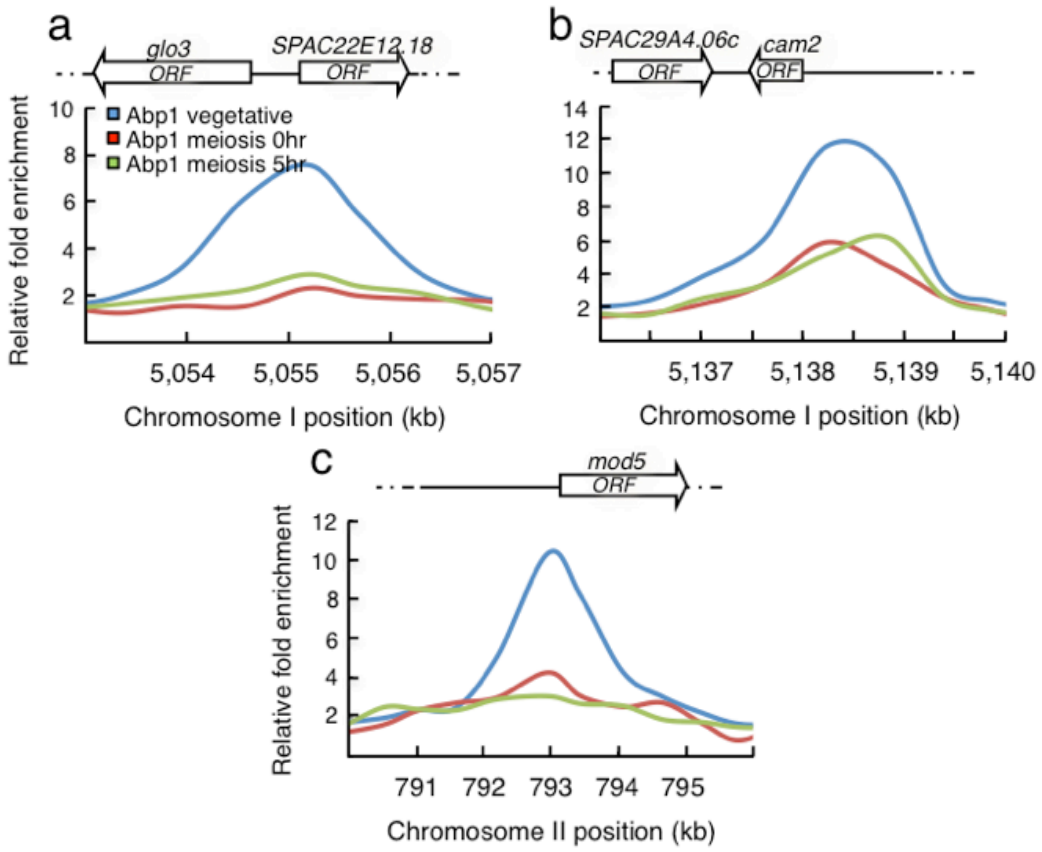

Figure 21. Reduced Abp1 binding at certain gene promoters during meiosis. Abp1 shows increased binding at *glo3* **(a)**, *cam2* **(b)** and *mod5* **(c)** during the vegetative cell cycle (blue) when compared to t=0 hours meiosis (red) and t=5 hours meiosis (green). ChIP-chip enrichment of Abp1 relative to WCE was plotted against respective chromosomal location. Data represent the mean of two biological replicates.

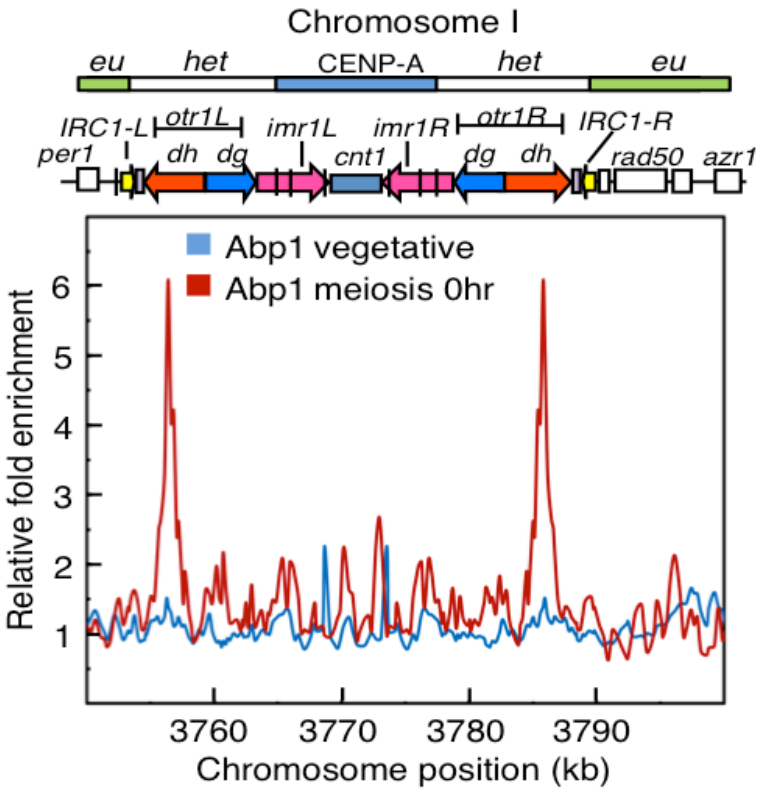

Figure 22. Abp1 displays increased binding at centromere I upon meiotic entry relative to vegetative cells. (Upper panel) Schematic of centromere I. (Lower panel) Abp1 binding to centromere I at t=0 hours meiosis in synchronized *pat1-114* strains (red) and in vegetative strains (blue). ChIP-chip enrichment of Abp1 relative to WCE was plotted against respective chromosomal location. Data represent the mean of two biological replicates.

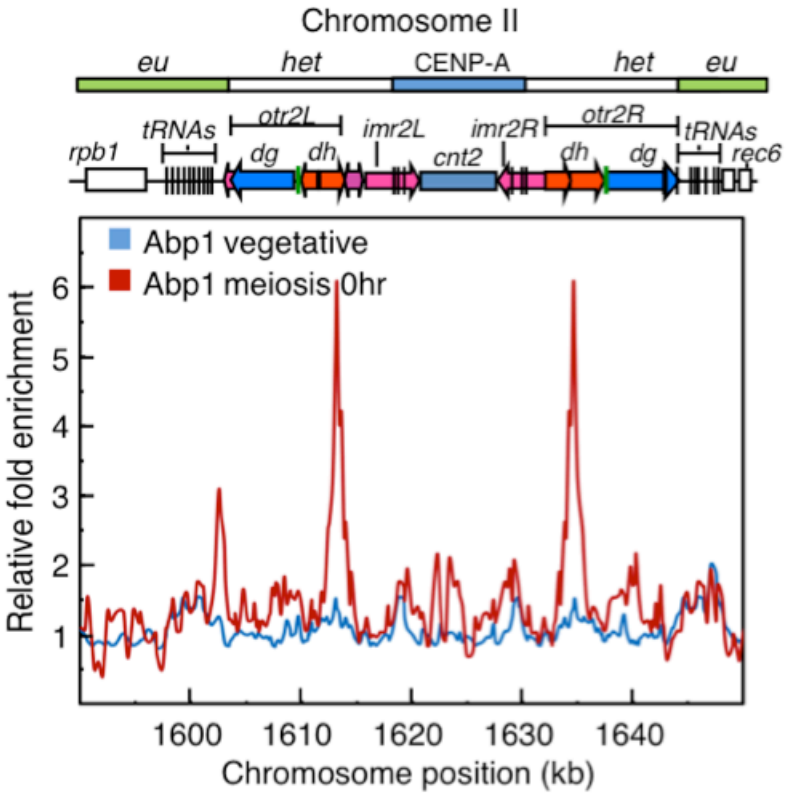

Figure 23. Abp1 displays increased binding at centromere II upon meiotic entry relative to vegetative cells. (Upper panel) Schematic of centromere II. (Lower panel) Abp1 binding to centromere II at t=0 hours meiosis in synchronized *pat1-114* strains (red) and in vegetative strains (blue). ChIP-chip enrichment of Abp1 relative to WCE was plotted against respective chromosomal location. Data represent the mean of two biological replicates.

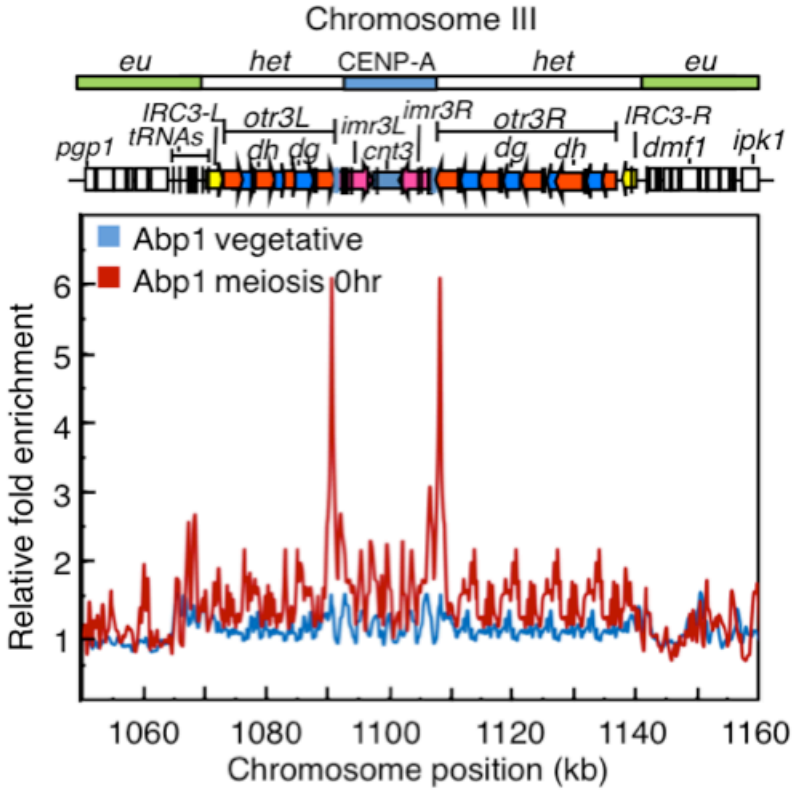

Figure 24. Abp1 displays increased binding at centromere III upon meiotic entry relative to vegetative cells. (Upper panel) Schematic of centromere III (Lower panel) Abp1 binding to centromere III at t=0 hours meiosis in synchronized *pat1-114* strains (red) and in vegetative strains (blue). ChIP-chip enrichment of Abp1 relative to WCE was plotted against respective chromosomal location. Data represent the mean of two biological replicates.

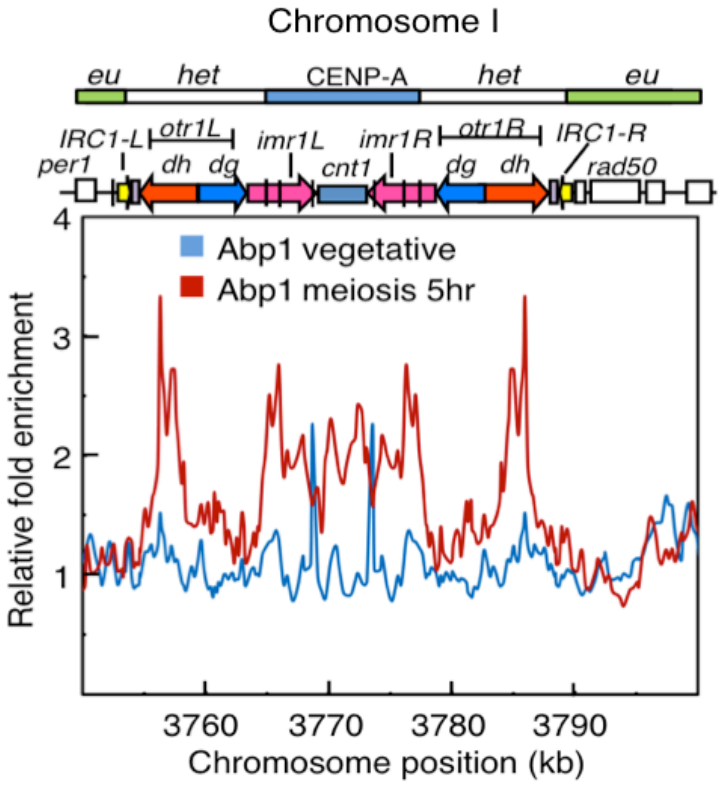

Figure 25. Abp1 displays increased binding at centromere I during meiosis relative to vegetative cells. (Upper panel) Schematic of centromere I. (Lower panel) Abp1 binding to centromere 1 at t=5 hours meiosis in synchronized *pat1-114* strains (red) and in vegetative strains (blue). ChIP-chip enrichment of Abp1 relative to WCE was plotted against respective chromosomal location. Data represent the mean of two biological replicates.

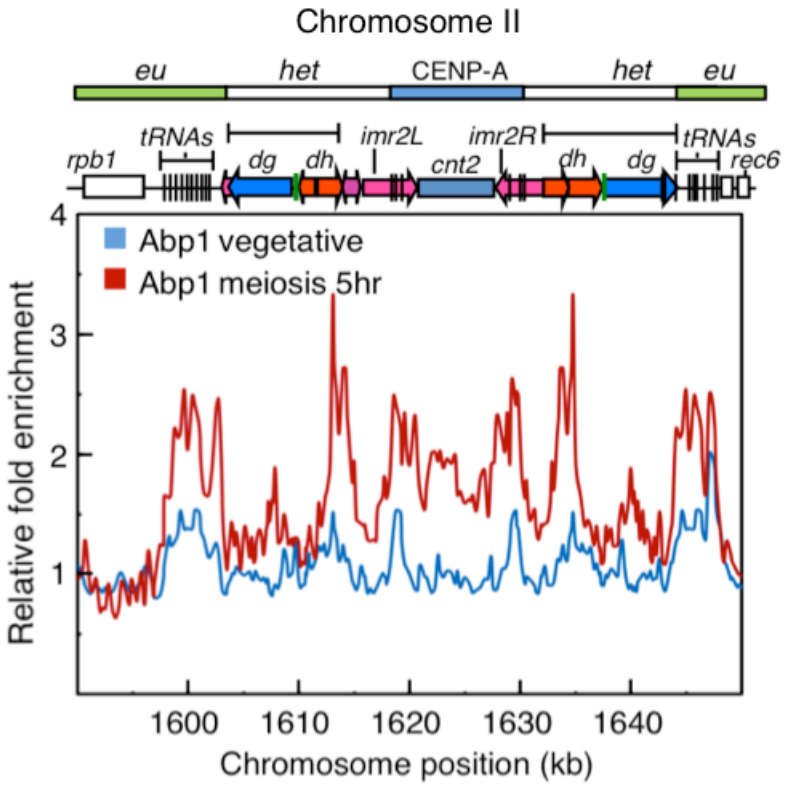

Figure 26. Abp1 displays increased binding at centromere II during meiosis relative to vegetative cells. (Upper panel) Schematic of centromere II. (Lower panel) Abp1 binding to centromere II at t=5 hours meiosis in synchronized *pat1-114* strains (red) and in vegetative strains (blue). ChIP-chip enrichment of Abp1 relative to WCE was plotted against respective chromosomal location. Data represent the mean of two biological replicates.

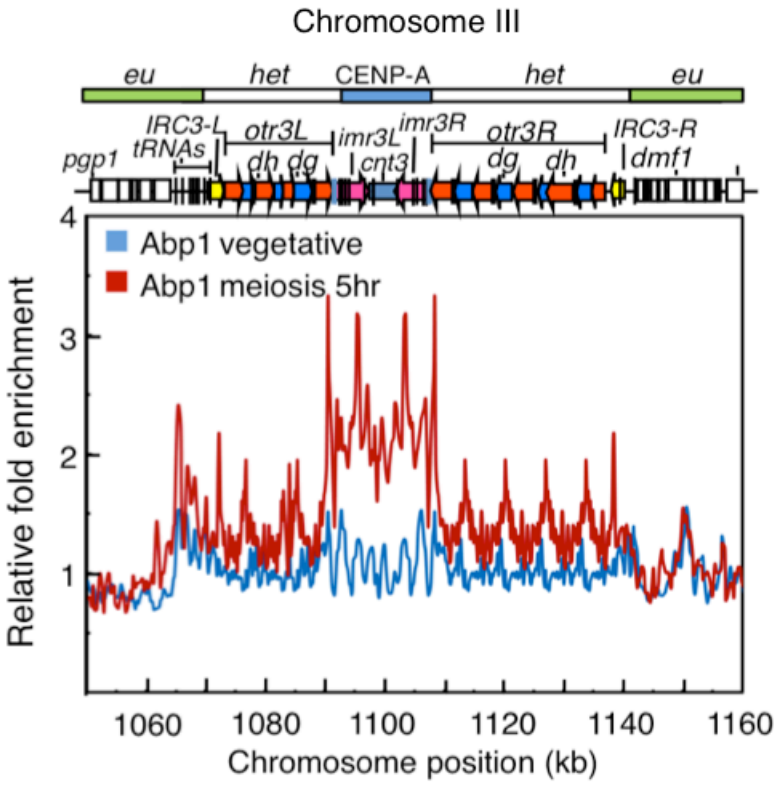

Figure 27. Abp1 displays increased binding at centromere III during meiosis relative to vegetative cells. (Upper panel) Schematic of centromere III. (Lower panel) Abp1 binding to centromere III at t=5 hours meiosis in synchronized *pat1-114* strains (red) and in vegetative strains (blue). ChIP-chip enrichment of Abp1 relative to WCE was plotted against respective chromosomal location. Data represent the mean of two biological replicates.

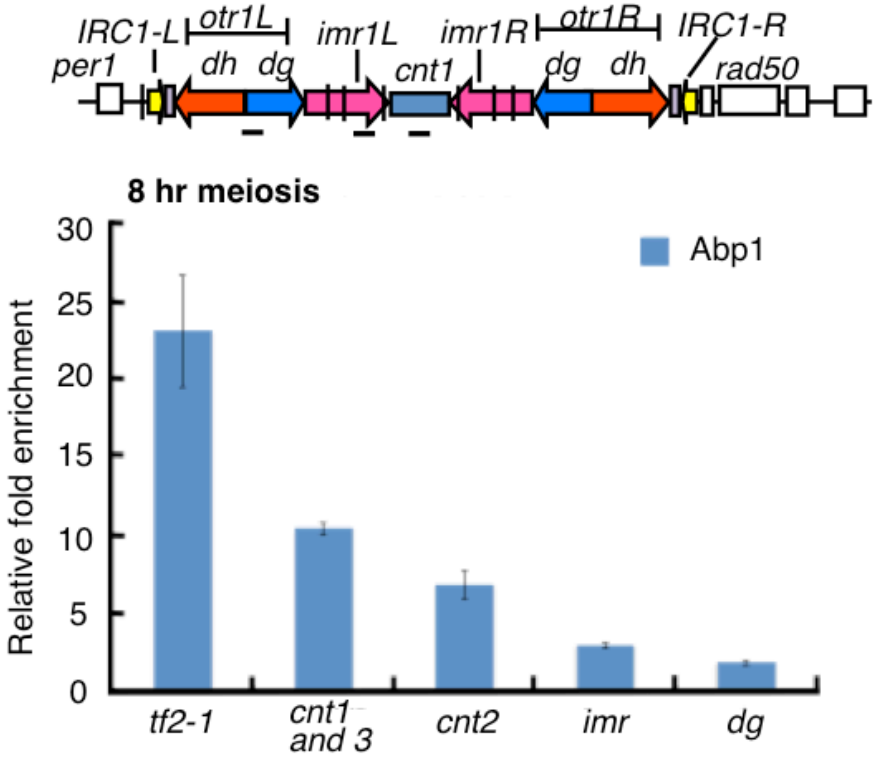

Figure 28. Abp1 remains enriched at the *cnt* region at 8 hours post-meiotic induction. (Upper panel) Schematic of centromere I. The black bars indicate the positions of primers used for qPCR. (Lower panel) Abp1 binding to *Tf2-1* and various regions of the centromere at 8 hours post-meiotic induction in synchronized *pat1-114* strains was assayed by ChIP assay against Abp1-FLAG(3X). Enrichment was determined by qPCR. Error bars indicate standard deviation. *n*=3 technical replicates.

Chapter IV: Investigating the effects of *abp1* loss on the localization of Cnp1, Scm3 and H3K9 methylation at centromeres in mitotic and meiotic cells.

A loss of *abp1* impairs the deposition of Cnp1 at centromeric chromatin in meiosis

Our experiments aim to identify an additional role of Abp1 at the centromeres, specifically during the meiotic cell cycle. We hypothesized that Abp1 may be directly or indirectly interacting with Cnp1, the histone 3 variant found exclusively at the central core of each centromere [21,23]. Cnp1 has been found to be crucial for the epigenetic identification and maintenance of the centromeres [28,55]. Additionally, previous studies have shown that human CENP-B and CENP-A may be physically interacting with each other at the centromeres [34,38,184], and that CENP-B binding near the CENP-A nucleosome stabilizes the CENP-A nucleosome on alphoid DNA in human cells [38]. We believe that a loss of *abp1* may negatively affect the localization and maintenance of Cnp1 at the central core during meiosis, as well as meiotic progression and chromosome segregation.

To investigate whether Abp1 binding at the central cores affects the assembly of Cnp1 chromatin, I performed ChIP qPCR to assess the occupancy of Cnp1 in wild type and *abp1*Δ vegetative and meiotic cells. Robust Cnp1 enrichment (70-80 fold) at the central cores of each of the three centromeres could be detected in vegetative wild type and *abp1*Δ cells **(Figure 29)**. However, compared to wild type, there was a dramatic reduction of Cnp1 enrichment at the centromeres in *abp1*Δ cells under meiotic conditions **(Figures 30 and 31)**.

At 0 hours post-meiotic induction, wild type cells displayed a 350-450 fold enrichment of Cnp1 at central cores I-III, while *abp1*Δ cells displayed ~275 fold enrichment of Cnp1 **(Figure 30)**. More specifically, at *cnt1* and *3*, wild type cells displayed ~450 fold enrichment, while *abp1*Δ cells displayed ~275 fold enrichment (**Figure 30**). However, this reduction of Cnp1 enrichment in *abp1*Δ cells was not found

to be significant (p=0.14, t-test), likely due to the outlier present in the qPCR data **(Table 2)**. At *cnt2*, wild type cells displayed ~325 fold enrichment, while *abp1*Δ cells displayed ~275 fold enrichment **(Figure 30)**. This reduction in Cnp1 enrichment in *abp1*Δ cells was found to be significant (p=0.022, t-test) **(Table 2)**.

At 5 hours post-meiotic induction, wild type cells displayed a 90-130 fold enrichment of Cnp1 at central cores I-III, while *abp1*Δ cells displayed ~70 fold enrichment of Cnp1 **(Figure 31)**. More specifically, at *cnt1* and *3*, wild type cells displayed ~90 fold enrichment, while *abp1*Δ cells displayed ~65 fold enrichment (**Figure 31**). This reduction in Cnp1 enrichment in *abp1*Δ cells was found to be significant (p=0.006, t-test) **(Table 2)**. At *cnt2*, wild type cells displayed ~130 fold enrichment, while *abp1*Δ cells displayed ~90 fold enrichment (**Figure 31**). Again, this reduction in Cnp1 enrichment in *abp1*Δ cells was found to be significant (p=0.0097, t-test) **(Table 2)**.

These results, which are representative of multiple ChIP qPCR experiments, suggest that meiosis-specific enrichment of Abp1 affects Cnp1 localization at the central cores exclusively during meiosis in *S. pombe.* This is shown by the overall decrease of Cnp1 enrichment in meiotic, but not vegetative, cells lacking *abp1,* though not all of the data points showing a decrease in Cnp1 enrichment are statistically significant **(Figures 29-31)**. However, the mechanism causing the decrease of Cnp1 localization at the *cnt* is yet to be determined.

A loss of *abp1* does not impact Scm3 localization to the centromere

In *S. pombe*, deposition of Cnp1 at centromeres is known to be mediated by the histone chaperone Scm3 [22,61]. However, Scm3 can localize at centromeric chromatin independent of Cnp1, but not vice versa [22,61]. ChIP qPCR was used to investigate whether reduced levels of Cnp1 in meiotic *abp1*Δ cells could be due to impaired recruitment of Scm3 to the centromere. Loss of *abp1* did not impair the levels of Scm3 at the central cores in vegetative cells **(Figure 32)** or in meiotic cells **(Figures 33-34)**. Interestingly, at 5 hours post-meiotic induction, Scm3 localization to *cnt1* and *cnt3* was found to be significantly more in *abp1*Δ cells relative to wild type cells (p=0.013, t-test) **(Table 3)**, though the enrichment values for both wild type and *abp1*Δ cells were between 3.5-4 fold **(Figure 34)**. Because Scm3 localization at the centromeres appeared similar between wild type and *abp1*Δ cells, impaired Cnp1 localization in *abp1*Δ cells likely occurs after Cnp1 has been deposited by Scm3. An alternative explanation is that the loss of *abp1* somehow renders Scm3 less effective at depositing Cnp1 to the central cores.

Cnp1 localizes to novel sites in meiotic cells deficient in *abp1*

Reduced binding of Cnp1 at the central cores in meiotic *abp1*Δ cells could be explained by a decrease in the total protein levels of Cnp1. Therefore, I investigated the relative Cnp1 protein levels in vegetative and meiotic wild type and *abp1*Δ cells. The immunoblotting assay revealed no noticeable change in Cnp1 protein levels in vegetative or meiotic *abp1*Δ cells compared to wild type **(Figure 35)**.

Alternatively, low levels of Cnp1 enrichment at the central cores could be a result of mis-deposition of Cnp1 at non-centromeric sites [149]. This possibility was examined by mapping Cnp1 genome-wide at 0 hours post-meiotic induction using a ChIP microarray. I found that meiotic *abp1*Δ cells exhibited reduced levels of Cnp1 enrichment throughout the central cores of chromosomes I-III relative to wild type **(Figures 36-38)**. This reduction in Cnp1 binding to the central cores I-III in *abp1*Δ cells ranged from 5-10 fold **(Figures 36-38)**.

Intriguingly, Cnp1 was detected at non-centromeric sites in meiotic *abp1*Δ cells including the mating-type (*mat*) locus, where Abp1 is normally found **(Figure 39)**. According to the genome-wide binding assay, Cnp1 enrichment at the *mat* locus reached nearly 8 fold in meiotic *abp1*Δ cells compared to the 4 fold enrichment displayed by Cnp1 in wild type cells **(Figure 39)**. This Cnp1 localization in meiotic *abp1*Δ cells corresponded to a prominent peak of Abp1 binding **(Figure 39)**.

ChIP qPCR confirmed that Cnp1 enrichment is significantly increased at the *mat* locus in meiotic *abp1*Δ cells relative to wild type **(Figures 40-41)**. The fold-enrichment of vegetative Cnp1 was found to be less than 2.5 fold for both wild type and *abp1*Δ cells **(Figures 40 and 41; Tables 4 and 5)**. Based on the ChIP qPCR data, Cnp1 displayed a significant increase of enrichment during meiosis in *abp1*Δ cells, reaching ~4 fold at the *mat* locus, compared to just a ~2 fold enrichment in meiotic wild type cells (0 hr: p=0.0001, t-test; 5 hr: p=0.0002, t-test) **(Figures 40-41; Table 4)**. It is possible that a role of Abp1 is to prevent aberrant localization of Cnp1 at the mating type region. These

results suggest an active role for Abp1 in ensuring that Cnp1 is exclusively deposited at the central cores during meiosis.

H3K9me2 levels at the *dg/dh* repeats are decreased in meiotic *abp1*Δ cells

Heterochromatic *dg/dh* repeats are found flanking each centromere of *S. pombe*, and these repeats are enriched in the epigenetic marker for heterochromatin, H3K9 methylation [114,159]. CENP-B homologs are believed to and aid in the recruitment of Clr4 for H3K9me establishment [152,164]. Research has found that the *dg/dh* repeat heterochromatic regions flanking the central core of the centromere are necessary for centromere function, as well as maintenance of sister chromatid attachment during mitosis and meiosis I [166,198]. Removal of all or part of the *dg/dh* sequences results in aberrant sister chromatid separation during mitosis and meiosis I [166,198].

Increased binding of Abp1 at pericentromeric *dg/dh* repeats upon meiotic entry **(Figures 22-27)** suggests a more prominent role of Abp1 in heterochromatin assembly at the centromere during meiosis. Therefore, I was interested in examining if a loss of *abp1* could affect H3K9me enrichment at pericentromeric repeats. The levels of H3K9me2 were assessed at the *dg/dh* repeats in vegetative and meiotic wild type and *abp1*Δ cells. H3K9me2 levels at various centromeric regions were similar in vegetative wild type and *abp1*Δ cells. At the *dg/dh* pericentromeric repeats, H3K9me2 displayed a 4-7 fold enrichment in both vegetative wild type and *abp1*Δ cells **(Figure 42)**. These results are consistent with our findings of minimal Abp1 binding at centromeres during the vegetative cell cycle **(Figures 21-26)**.

However, during meiosis, there was a substantial reduction of H3K9me2 at the *dg/dh* repeats in *abp1*Δ cells relative to wild type **(Figures 43-44)**. More specifically, enrichment of H3K9me2 at both the *dg* and *dh* repeats was significantly decreased by approximately 10 fold in *abp1*Δ cells at 0 hours post-meiotic induction (*dg*: p=0.0002, *t*-test; *dh*: p=0.0001, *t*-test) **(Figure 43; Table 6)**. At 5 hours post-meiotic induction, H3K9me2 enrichment values at both the *dg* and *dh* repeats decreased significantly by approximately 20 fold in *abp1*Δ cells (*dg*: p=0.0001, *t*-test; *dh*: p=0.0001, *t*-test) **(Figure 44; Table 6)**. In addition, the levels of H3K9me2 enrichment at the *mat* locus remained similar among wild type and *abp1*Δ cells during the vegetative cell cycle (15-20 fold enrichment) and at 5 hours post-meiotic induction (50-60 fold enrichment) **(Figure 45; Table 7**), suggesting that heterochromatin defects in meiotic *abp1*Δ cells appear to be restricted to the pericentromeric regions.

Interestingly, enrichment of H3K9me2 remained low (1-2 fold) at *cnt1*, *cnt2*, and *cnt3* in wild type cells during meiosis, but H3K9me2 enrichment in *abp1*Δ cells slightly increased relative to wild type to ~2.5 fold at *cnt1* and *cnt3* 0 hours post-meiotic induction (p=0.036, *t*-test) **(Figure 43; Table 6)**. At 5 hours post-meiotic induction, H3K9me2 enrichment at *cnt2* in *abp1*Δ cells increased relative to wild type to ~8 fold, which was found to be significant (p=0.0002, *t*-test) **(Figure 44; Table 6)**. It is possible that the encroachment of H3K9me2 into the *cnt* regions in cells lacking *abp1* could interfere with the structure and function of the *cnt*, leading to defects in kinetochore assembly and chromosome segregation.

Figures

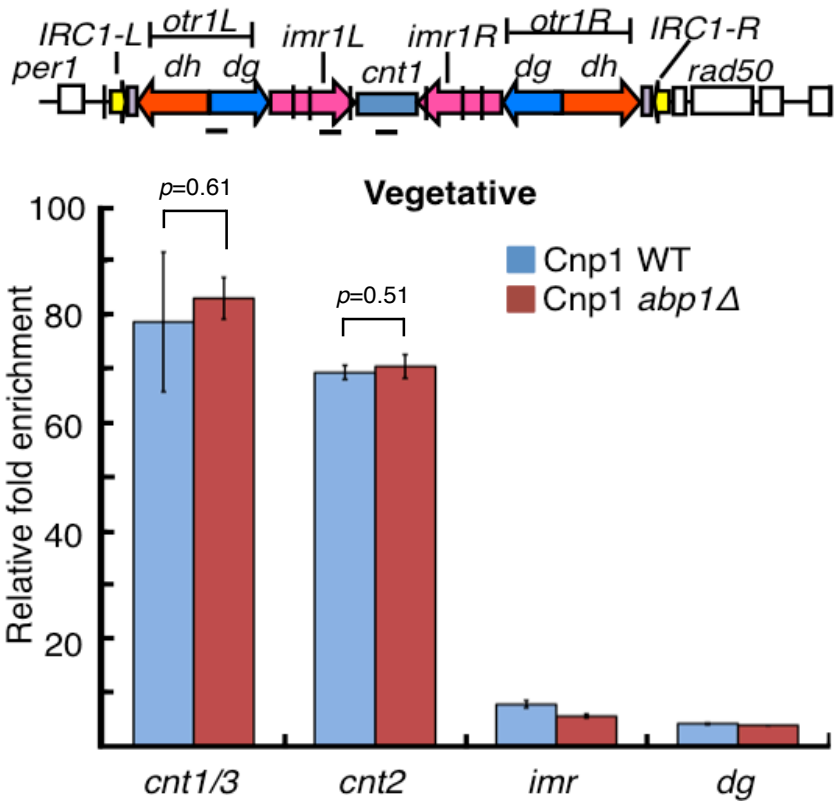

Figure 29. Cnp1 localization to the centromere during the vegetative cell cycle is similar between wild type and *abp1*Δ cells. (Upper panel) Schematic of centromere I. The black bars indicate the positions of primers used for qPCR. (Lower panel) Cnp1-FLAG enrichment at centromere central cores I and III (*cnt1*/*3*), II (*cnt2*), innermost repeat (*imr*), and pericentromeric repeat *dg* in vegetative WT strains (blue) and *abp1*Δ strains (red). Enrichment was determined by ChIP qPCR. Error bars indicate standard deviation. *n*=3 technical triplicates.

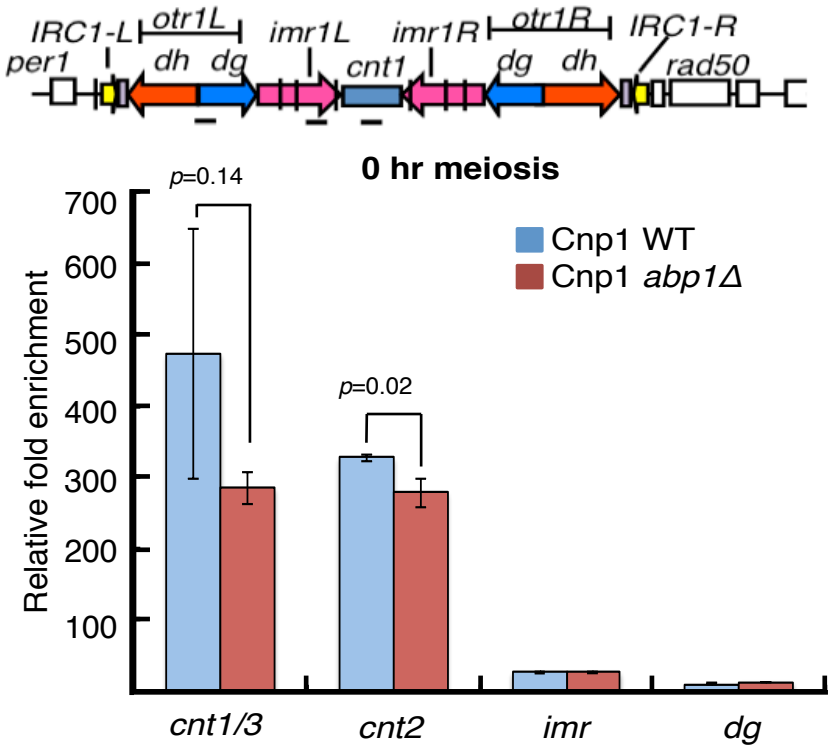

Figure 30. Cnp1 localization to the centromere upon meiotic entry is decreased in *abp1*Δ cells. (Upper panel) Schematic of centromere I. The black bars indicate the positions of primers used for qPCR. (Lower panel) Cnp1-FLAG enrichment at centromere central cores I and III (*cnt1/3*), II (*cnt2*), innermost repeat (*imr*), and pericentromeric repeat *dg* at t=0 hours meiosis of WT strains (blue) and *abp1*Δ strains (red). Enrichment was determined by ChIP qPCR. Error bars indicate standard deviation. *n*=3 technical triplicates.

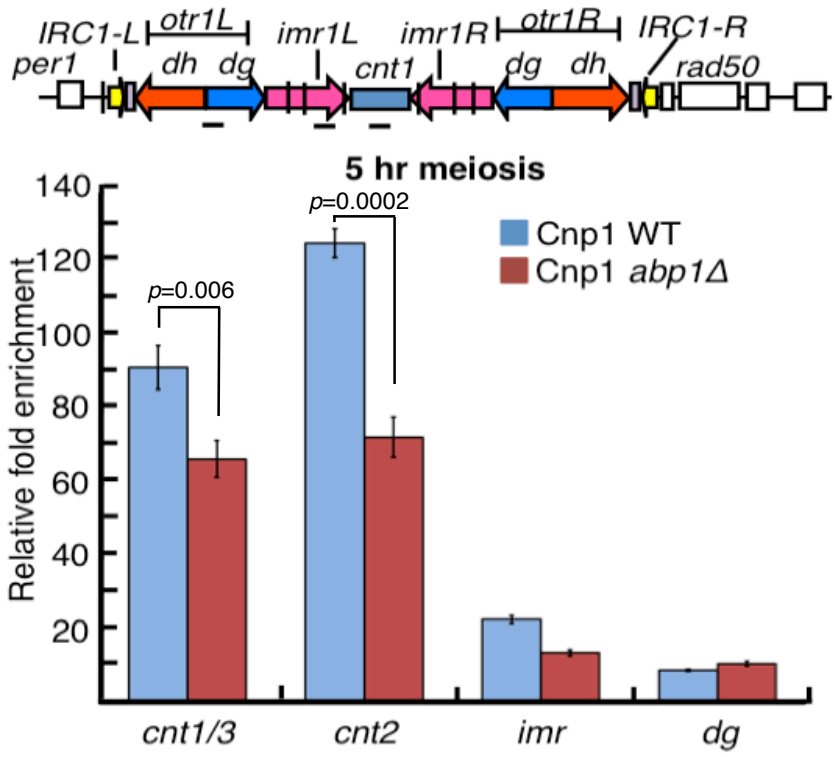

Figure 31. Cnp1 localization to the centromere during early meiosis is decreased in *abp1*Δ. (Upper panel) Schematic of centromere I. The black bars indicate the positions of primers used for qPCR. (Lower panel) Cnp1-FLAG enrichment at centromere central cores I and III (*cnt1*/*3*), II (*cnt2*), innermost repeat (*imr*), and pericentromeric repeat *dg* at t=0 hours meiosis of WT strains (blue) and *abp1*Δ strains (red). Enrichment was determined by ChIP qPCR. Error bars indicate standard deviation. *n*=3 technical triplicates.

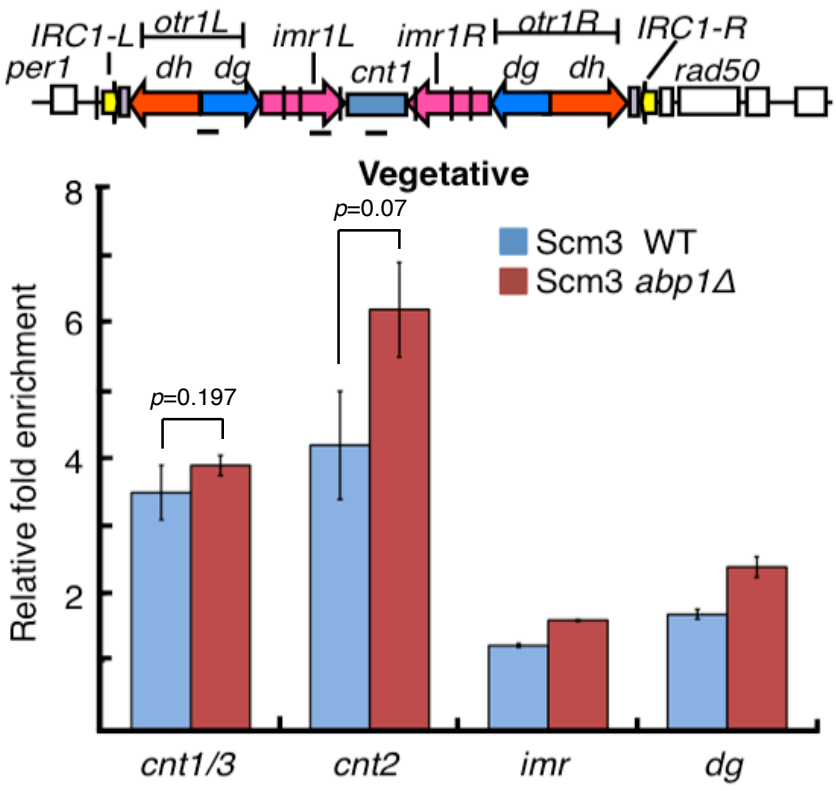

Figure 32. Scm3 localization remains similar between WT and *abp1*Δ cells during the vegetative cell cycle. (Upper panel) Schematic of centromere I. The black bars indicate the positions of primers used for qPCR. (Lower panel) Scm3-FLAG enrichment at centromere central cores I and III (*cnt1*/*3*), II (*cnt2*), innermost repeat (*imr*), and pericentromeric repeat *dg* at t=0 hours meiosis of WT strains (blue) and *abp1*Δ strains (red). Enrichment was determined by ChIP qPCR. Error bars indicate standard deviation. *n*=3 technical triplicates.

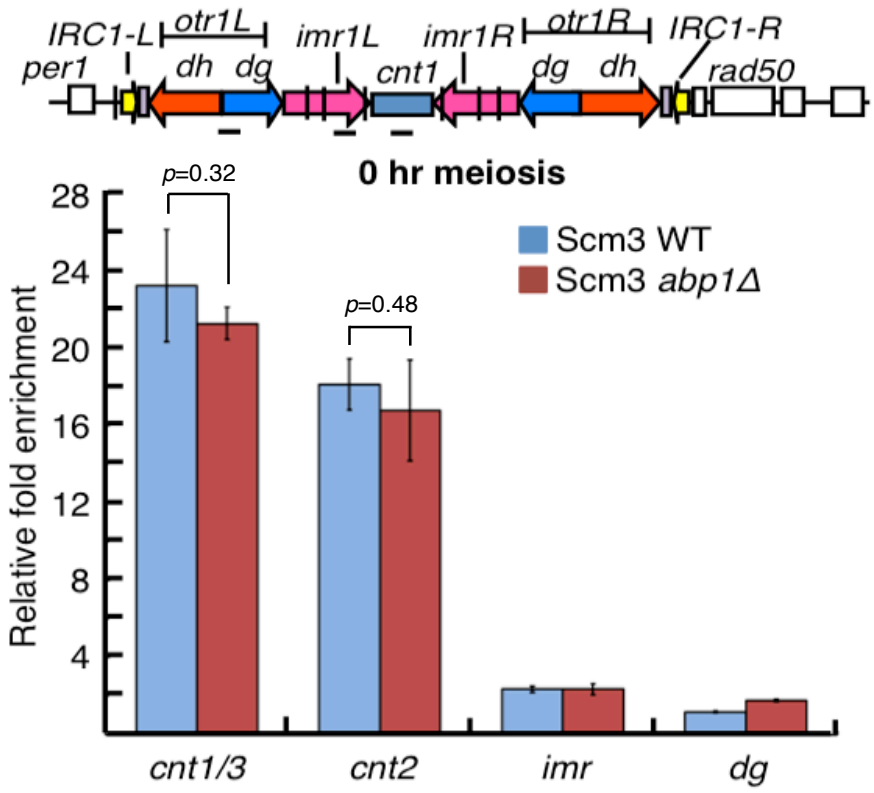

Figure 33. Scm3 localization remains similar between WT and *abp1*Δ cells upon meiotic entry. (Upper panel) Schematic of centromere I. The black bars indicate the positions of primers used for qPCR. (Lower panel) Scm3-FLAG enrichment at centromere central cores I and III (*cnt1/3*), II (*cnt2*), innermost repeat (*imr*), and pericentromeric repeat *dg* at t=0 hours meiosis of WT strains (blue) and *abp1*Δ strains (red). Enrichment was determined by ChIP qPCR. Error bars indicate standard deviation. *n*=3 technical triplicates.

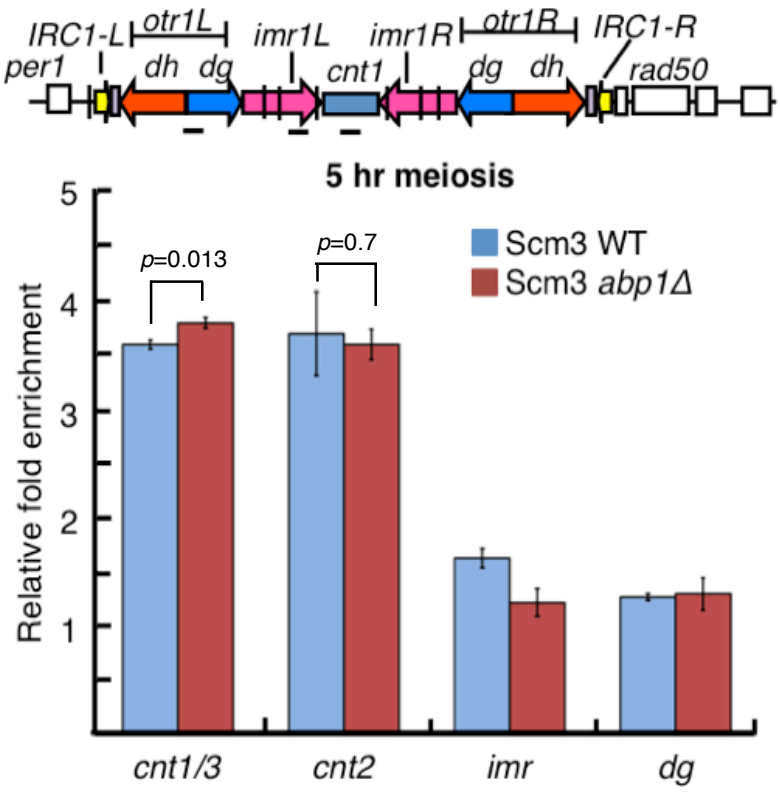

Figure 34. Scm3 localization remains similar during meiosis between WT and *abp1*Δ cells. (Upper panel) Schematic of centromere I. The black bars indicate the positions of primers used for qPCR. (Lower panel) Scm3-FLAG enrichment at centromere central cores I and III (*cnt1*/*3*), II (*cnt2*), innermost repeat (*imr*), and pericentromeric repeat *dg* at t=0 hours meiosis of WT strains (blue) and *abp1*Δ strains (red). Enrichment was determined by ChIP qPCR. Error bars indicate standard deviation. *n*=3 technical triplicates.

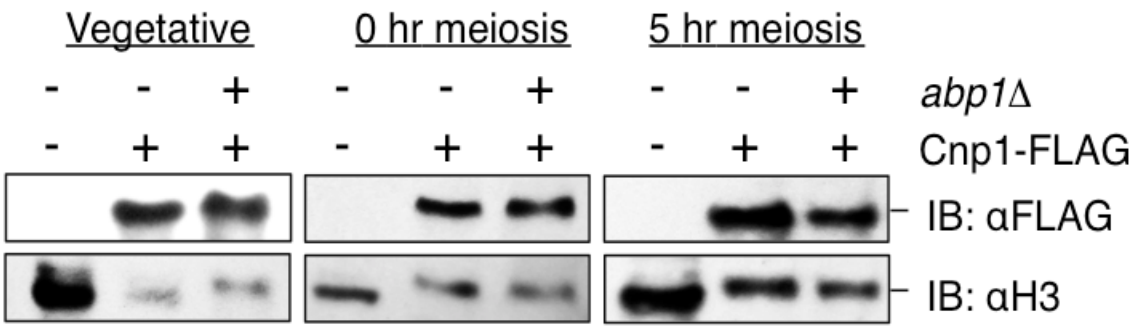

Figure 35. Cnp1 protein levels remain similar in vegetative and meiotic WT and *abp1*Δ cells. Cnp1-FLAG was examined by Western blot with anti-FLAG antibody (M2, Sigma) in WT and *abp1*Δ cells. Cells were collected from vegetative cultures and cultures synchronized at t=0 hours and t=5 hours meiosis. H3 (ab1791, Abcam) was used as a loading control. Data represent a single western blot experiment.

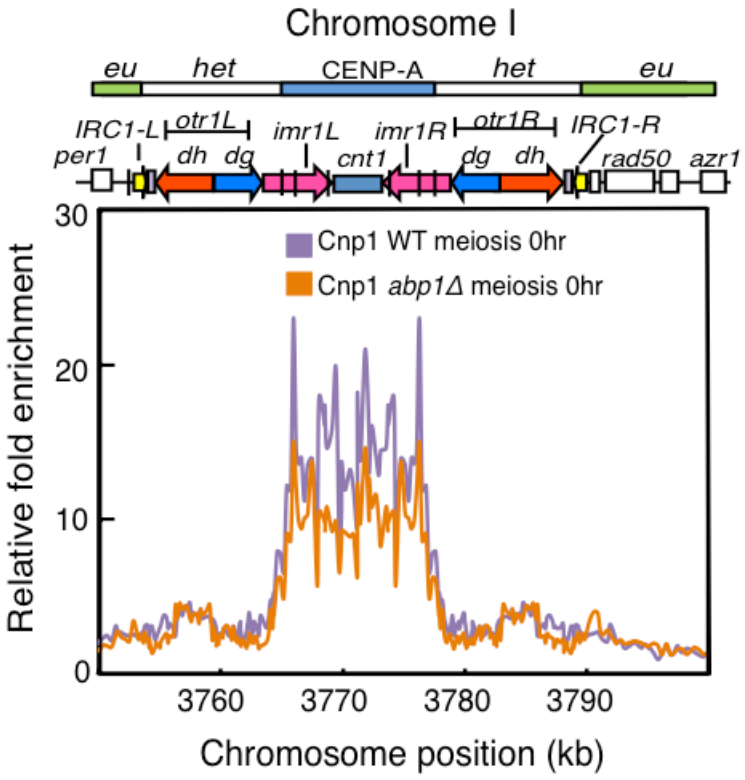

Figure 36. The loss of *abp1* leads to decreased localization of Cnp1 to centromere I upon meiotic entry. (Upper panel) Schematic of centromere I. (Lower panel) Cnp1-FLAG binding to centromere I at t=0 hours of meiosis in WT (blue) and *abp1*Δ (red). ChIP-chip enrichment of Cnp1 relative to WCE was plotted against respective chromosomal location. Data represent a single microarray experiment.

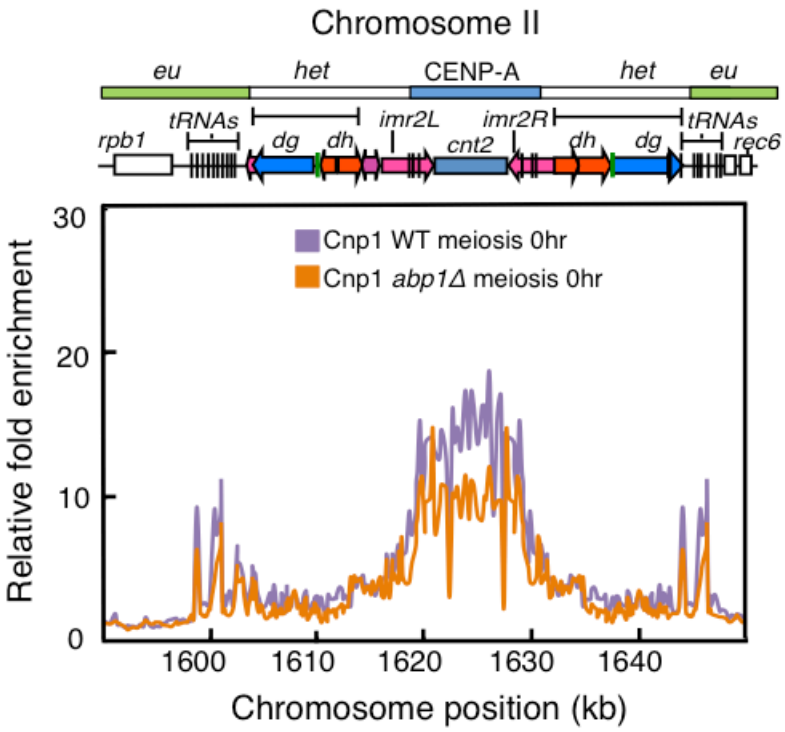

Figure 37. The loss of *abp1* leads to decreased localization of Cnp1 to centromere II upon meiotic entry. (Upper panel) Schematic of centromere II. (Lower panel) Cnp1-FLAG binding to centromere II at t=0 hours of meiosis in WT (blue) and *abp1*Δ (red). ChIP-chip enrichment of Cnp1 relative to WCE was plotted against respective chromosomal location. Data represent a single microarray experiment.

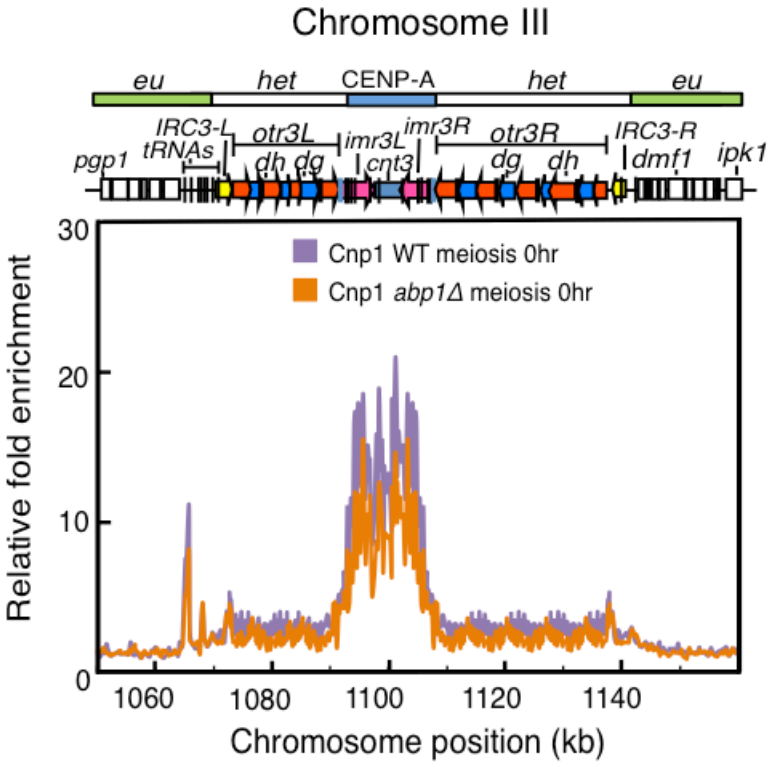

Figure 38. The loss of *abp1* leads to decreased localization of Cnp1 to centromere III upon meiotic entry. (Upper panel) Schematic of centromere III. (Lower panels) Cnp1-FLAG binding to centromere III at t=0 hours of meiosis in WT (blue) and *abp1*Δ (red). ChIP-chip enrichment of Cnp1 relative to WCE was plotted against respective chromosomal location. Data represent a single microarray experiment.

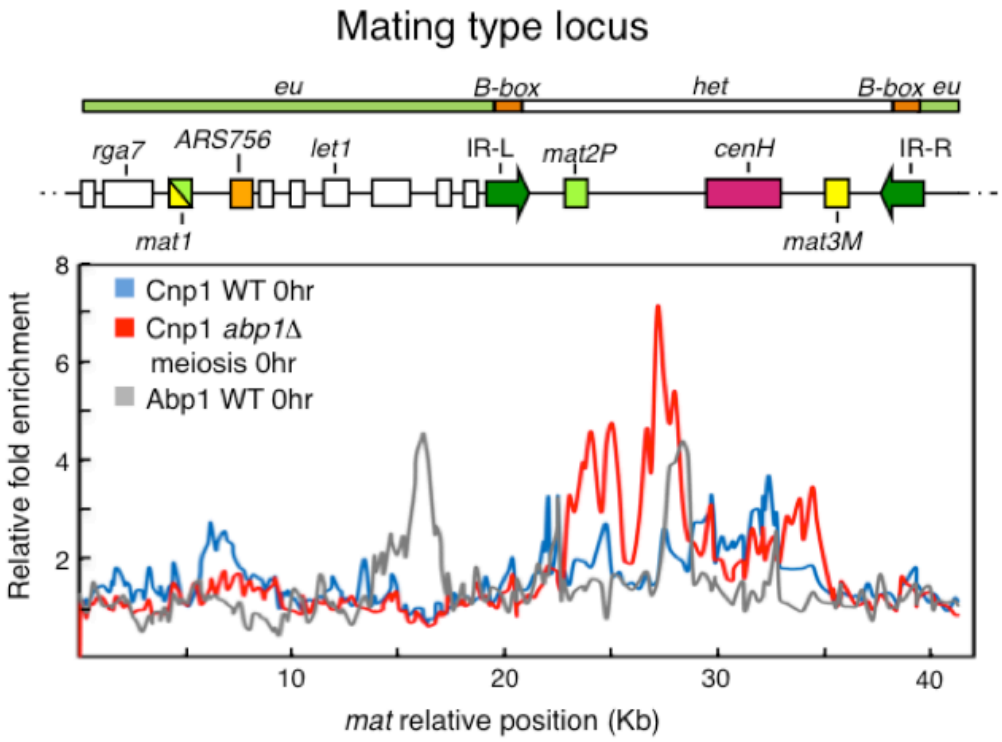

Figure 39. Cnp1 localizes to the silent *mat* locus in *abp1*Δ cells during meiosis.
(Upper panel) Schematic of the mating type locus on chromosome II.
(Lower panel) Localization of Cnp1 in WT (blue), Cnp1 in *abp1*Δ (red) and Abp1 (grey) at the mating type locus at t=0 hours meiosis. Meiotic cells were synchronized using *pat1-114*. ChIP assays were performed in strains containing Cnp1-FLAG and Abp1-FLAG(3X). ChIP-chip enrichments of Cnp1 and Abp1 relative to WCE were plotted against respective chromosomal location. Cnp1 data represent a single microarray experiment. Abp1 data represent the mean of two biological replicates.

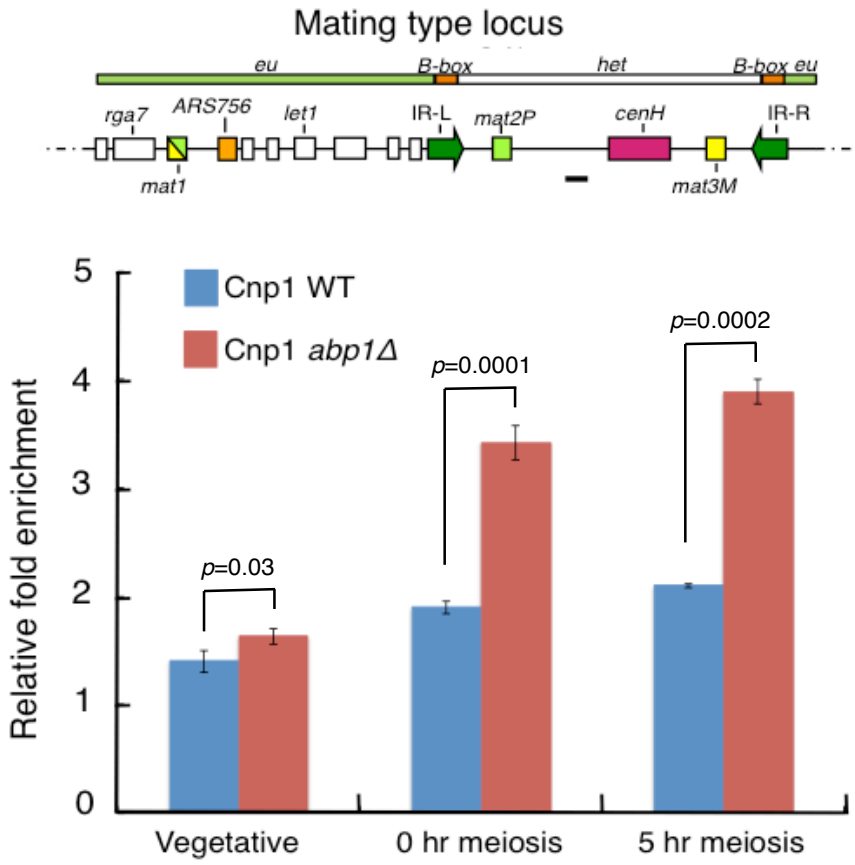

Figure 40. Cnp1 enrichment at the silent *mat* locus is significantly increased in *abp1*Δ meiotic cells. (Upper panel) Schematic of the *mat* locus. The black bar indicates the position of primers used for qPCR. (Lower panel) Cnp1-FLAG enrichment at the *mat* region in WT (blue) and *abp1*Δ (red). Enrichment was determined by ChIP qPCR. Error bars indicate standard deviation. *n*=3 technical triplicates.

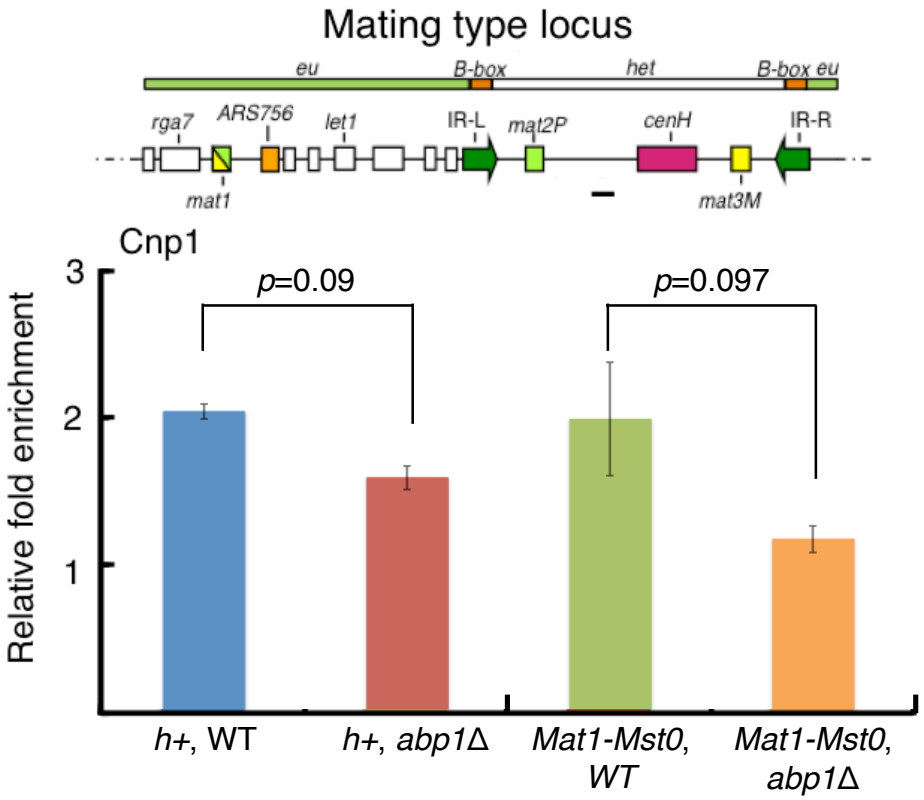

Figure 41. Cnp1 enrichment at the silent *mat* locus is similar between WT and *abp1*Δ vegetative cells. (Upper panel) Schematic of the *mat* locus. The black bar indicates the position of primers used for qPCR. (Lower panel) Cnp1-FLAG enrichment at the silent *mat* region in WT *h+* (blue); WT *Mat1-Mst0* (green); *abp1*Δ *h+* (red); *abp1*Δ *Mat1-Mst0* (orange) vegetative strains. Enrichment was determined by ChIP qPCR. Error bars indicate standard deviation. *n*=3 technical replicates.

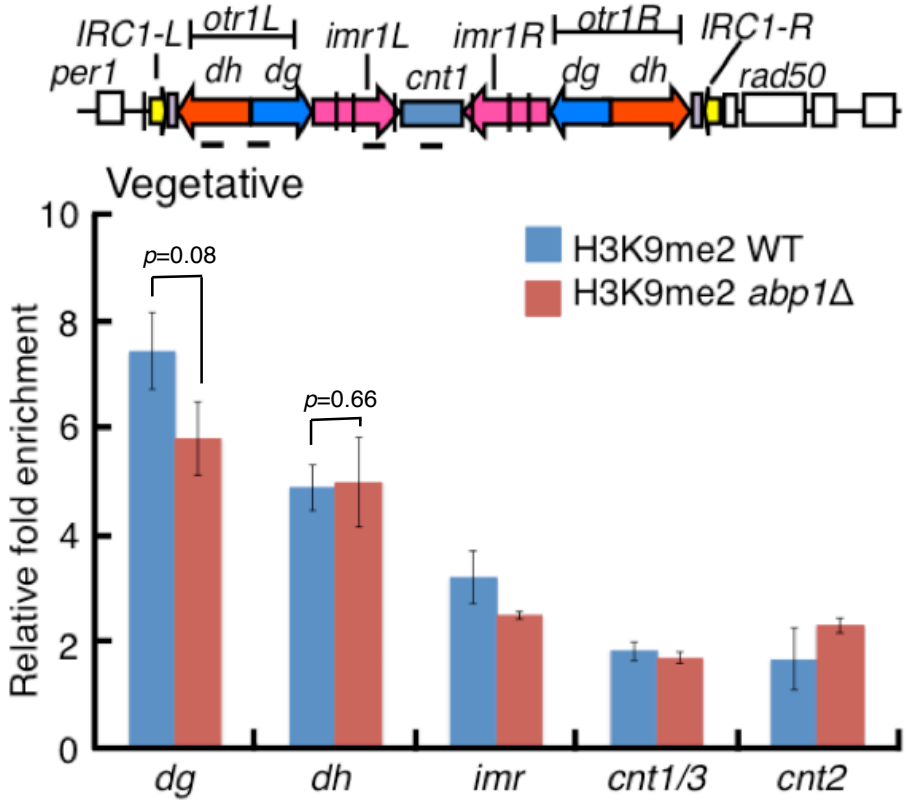

Figure 42. H3K9me2 enrichment is similar between vegetative WT and *abp1*Δ cells at the centromere. (Upper panel) Schematic of centromere I. The black bars indicate the positions of primers used for qPCR. (Lower panel) H3K9me2 enrichment at multiple centromere loci in vegetative WT (blue) and *abp1*Δ (red) cells. Enrichment was determined by ChIP qPCR. Error bars indicate standard deviation. *n*=3 technical replicates.

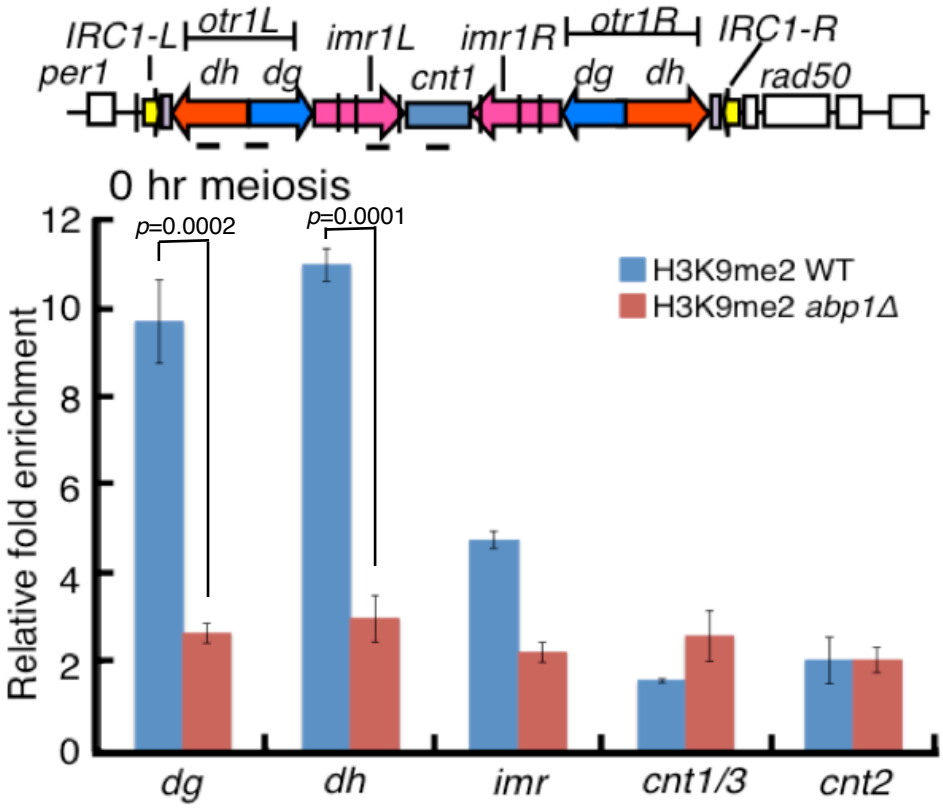

Figure 43. H3K9me2 enrichment is significantly decreased at the *dg/dh* pericentromeric repeats in *abp1*Δ cells upon meiotic entry. (Upper panel) Schematic of centromere I. The black bars indicate the positions of primers used for qPCR. (Lower panel) H3K9me2 enrichment at multiple centromere loci in WT (blue) and *abp1Δ* (red) cells at t=0 hours meiosis. Enrichment was determined by ChIP qPCR. Error bars indicate standard deviation. *n*=3 technical triplicates.

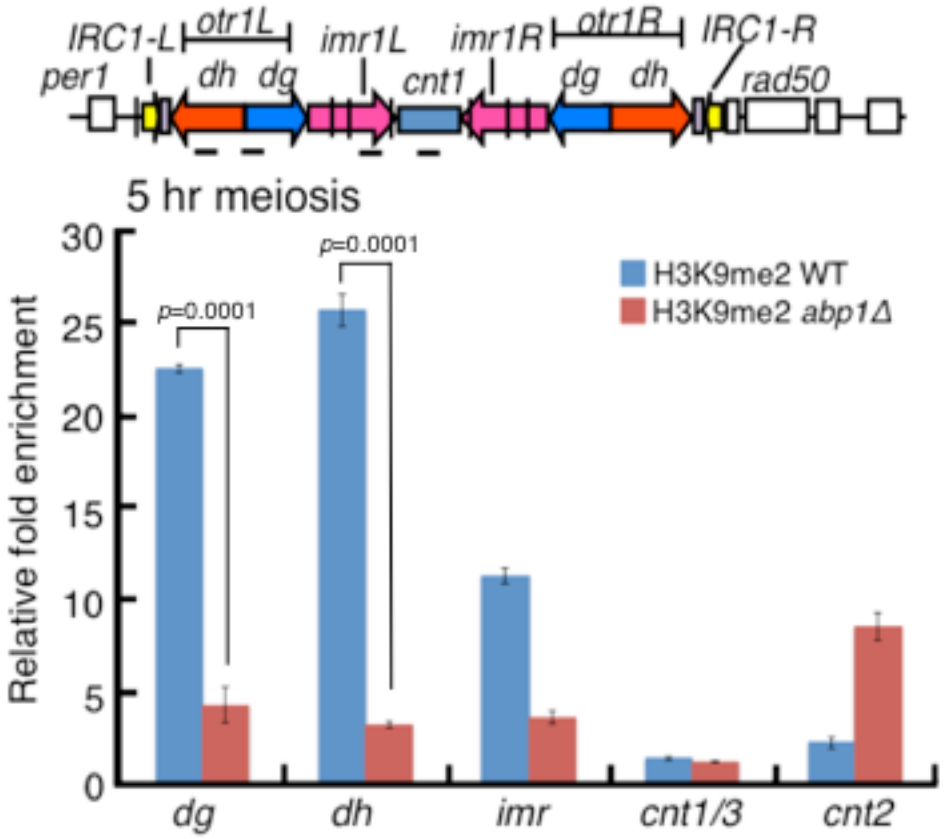

Figure 44. H3K9me2 enrichment is significantly decreased at the *dg/dh* pericentromeric repeats in *abp1*Δ cells during meiosis. (Upper panel) Schematic of centromere I. The black bars indicate the positions of primers used for qPCR. (Lower panel) H3K9me2 enrichment at multiple centromere loci in WT (blue) and *abp1*Δ (red) cells at t=5 hours meiosis. Enrichment was determined by ChIP qPCR. Error bars indicate standard deviation. *n*=3 technical triplicates.

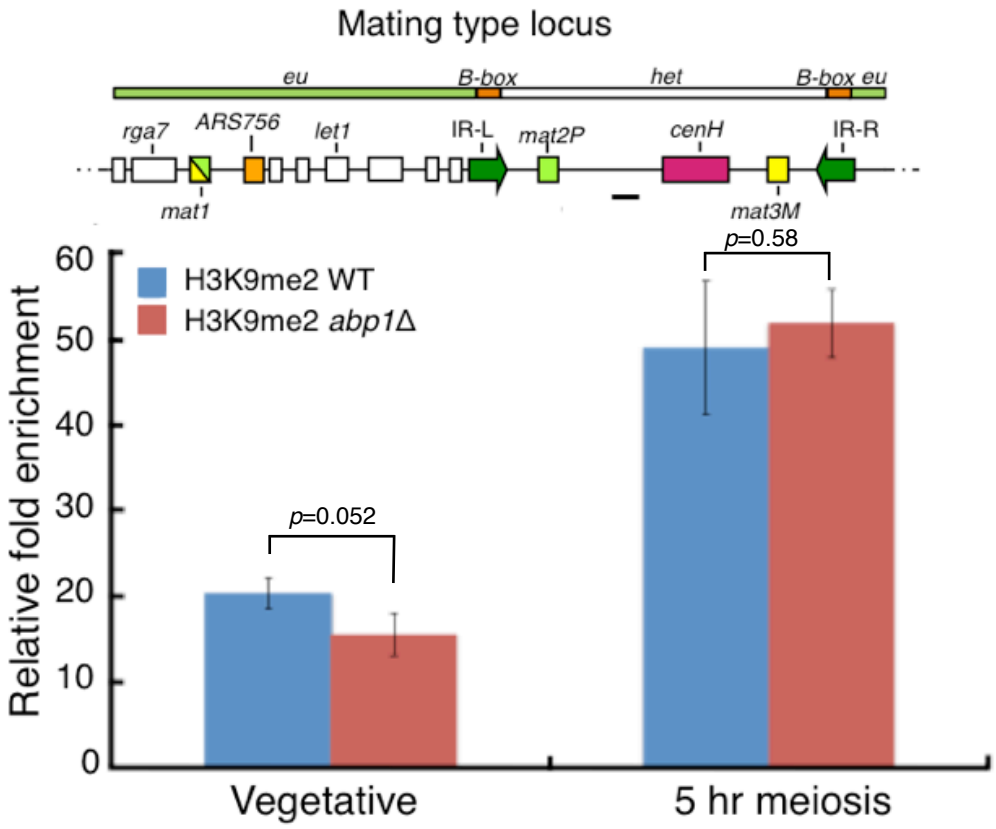

Figure 45. H3K9me2 enrichment at the mating type region is similar between vegetative and meiotic WT and *abp1*Δ cells. (Upper panel) Schematic of the mating type locus. The black bar indicates the position of primers used for qPCR. (Lower panel) H3K9me2 enrichment at the mating type locus in vegetative and meiotic WT (blue) and *abp1*Δ (red) cells. Enrichment was determined by ChIP qPCR. Error bars indicate standard deviation. *n*=3 technical triplicates.

Chapter V: Meiotic progression and fidelity of chromosome segregation in the presence and absence of Abp1

Abp1 and RNAi are important for proper meiotic progression and chromosome segregation

Previous studies have shown that a loss of *abp1* results in meiotic defects, such as decreased asci formation, abnormal asci shape, and decreased spore viability [42,125]. I wanted to further explore the possible causes of meiotic defects in *abp1* mutants. In particular, results from chapters III-IV showing Abp1-dependent localization of Cnp1 point us to the possibility that Abp1 could directly affect the process of meiotic progression such as chromosome segregation.

To investigate this idea, I analyzed the meiotic cell cycle in wild type and *abp1*Δ cells. The results of this experiment reveal that *abp1*Δ diploid cells exhibited a delay in completing meiosis **(Figure 46).** Approximately 90% of wild type cells completed meiosis within 11 hours, while only 70% of *abp1*Δ cells completed meiosis within 11 hours. The meiotic delay of *abp1*Δ cells appeared to be most pronounced at the transitional period between MI and MII, as highlighted by the yellow vertical bar **(Figure 46)**. Additionally, *abp1*Δ cells displayed a loss of meiotic synchrony, as detected by light and fluorescence microscopy of sample cells taken at 30-minute intervals during the entirety of meiosis **(Figure 46)**.

To examine the meiotic products of live cells, I monitored the spore nuclei in wild type and *abp1*Δ cells expressing a histone H3 that is tagged with a green fluorescent protein (H3-GFP). A noticeable fraction of *abp1*Δ cells displayed meiotic chromosome segregation defects, shown by the increased frequency of aberrant asci **(Figure 47)**. *abp1*Δ asci experienced a slightly higher rate (17%) of unequal distribution of H3-GFP among spores compared to wild type (10.8%). The proportion of micronuclei formed in

*abp1*Δ asci (4.7%) was also found to be slightly higher when compared to wild type (3.3%) **(Figure 47)**. Further analysis of the histone H3-GFP data revealed that *abp1*Δ asci displayed a greater incidence (50%) than wild type (33%) of having two adjacent spores with a stronger GFP signal than the remaining two, an indication of MI chromosome segregation defects **(Figure 48).**

To further investigate the impact that a loss of *abp1* has on meiotic progression, fluorescence microscopy was used to visualize nuclei in asci stained with the DNA dye 4',6-diamidino-2-phenylindole (DAPI). This DNA staining technique allowed visualization of the entire DNA content of each nucleus, rather than just histone H3 that was used in the previous GFP experiment. Whereas ~ 98% wild type asci displayed equal DAPI-staining of DNA in each spore, only 85% *abp1*Δ asci appeared normal **(Figure 49)**. Notably, 14.5% of the observed *abp1*Δ asci contained micronuclei compared to just ~2% of wild type (p=0.009; t-test) **(Table 8)**.

Collectively, our data suggest a positive role for Abp1 in the deposition and/or maintenance of Cnp1 at meiotic centromere central cores, as well as H3K9me2 enrichment at the *dg/dh* pericentromeric repeats, both of which are critical for maintaining the fidelity of chromosome segregation and cell cycle progression [28,55,90,165,166]. The mislocalization of Cnp1 to areas of the genome outside of the *cnt* in meiotic *abp1*Δ cells, including the mating type locus **(Figure 39),** may also be contributing to the observed chromosome segregation defects **(Figures 47-49)**.

Because *abp1*Δ cells displayed reduced levels of H3K9me2 at meiotic pericentromeric heterochromatin, I asked whether the RNAi mutant, *rdp1*Δ, would also exhibit defective meiotic asci since it has been shown to display reduced H3K9me at the

pericentromeric *dg/dh* repeats [164]. The purpose of this experiment was to identify a possible correlation between the decrease of H3K9me2 at the *dg/dh* repeats and observed increase of micronuclei in the *abp1*Δ strains.

This experiment revealed that *rdp1*Δ asci had an increased rate of micronuclei formation during meiosis. More specifically, 36% of *rdp1*Δ asci contained micronuclei compared to just ~2% of the wild type asci, which was found to be significant (p=0.0062, *t*-test) **(Figure 50; Table 9)**. Impaired H3K9me at pericentromeric repeats, either by a loss of *abp1* or a loss of *rdp1*, likely contributed to increased micronuclei formation during meiosis **(Figure 50)**. I hypothesize that the increased micronuclei formation in *abp1*Δ and *rdp1*Δ cells may be the result of meiosis I chromosome segregation defects caused by the insufficient cohesion of sister chromatid centromeres due to decreased pericentromeric H3K9me2 enrichment. This phenomenon has been reported in meiotic *S. pombe* cells [166].

LTR insertion into centromere central core negatively affects meiotic chromosome segregation in _abp1_Δ strains.

Abp1 primarily binds to solo *LTR*s and *LTR*s associated with full-length *Tf* retrotransposons [120,121,140,141,142], and a loss of Abp1 results in significant increased *Tf2* expression, which is increased further by an additional loss of Cbh1 or Cbh2 [120]. Centromeres of *S. pombe* do not normally contain an *LTR* sequence, and it is possible that the cell uses surveillance mechanisms involving Abp1 to prevent an *LTR*, or full-length *Tf2* transposable elements, from entering the centromere [120]. I hypothesized that the disruption of the centromeres by an *LTR* or *Tf2* retrotransposon would negatively impact

its role in chromosome segregation in both mitosis and meiosis, particularly in *abp1*Δ cells.

DAPI-stained asci were assessed from either wild type or ***abp1*Δ** diploids in which one parent contained a *ura4*$^{+}$inserted into the central core of centromere I (*cnt1:: ura4*$^{+}$) while the other parent contained an *LTR* inserted into the coding sequence of *cnt1:: ura4*$^{+}$ (*cnt1:: ura4-LTR*) rendering *ura4* nonfunctional. These strains were compared to those in which one parent contained a *ura4*$^{+}$inserted into the central core of centromere I (*cnt1:: ura4*$^{+}$) while the other parent contained the nonfunctional minigene *ura4 DS/E* inserted at *cnt* (*cnt1:: ura4-DS/E*), which contains a 268-bp deletion within the coding sequence of *ura4*, as a negative control against *cnt1:: ura4-LTR*.

Interestingly, for wild type cells containing the alleles *cnt1::ura4-LTR* and *cnt1::ura4*$^{+}$*,* 5% asci exhibited micronuclei, while only ~2% of wild type asci containing both *cnt1:: ura4-DS/E* and *cnt1:: ura4*$^{+}$ exhibited micronuclei (p=0.08, t-test) **(Figure 49; Table 8)**. However, for *abp1*Δ, this difference was found to be significant (p=0.018; t-test): asci in *abp1*Δ carrying *cnt1::ura4-LTR* and *cnt1::ura4*$^{+}$ exhibited ~20% micronuclei compared to 16% micronuclei in *abp1*Δ asci containing both *cnt1:: ura4-DS/E* and *cnt1:: ura4*$^{+}$ **(Figure 49; Table 8).**

Overall, these results suggest that the loss of *abp1* leads to meiotic defects, including a delay in meiotic progression **(Figure 46)** and abnormal chromosome segregation **(Figures 49 and 50)**. These defects may be due to the decrease of H3K9me2 enrichment at the pericentromeric *dg/dh* repeats observed in *abp1*Δ meiotic cells **(Figures 33 and 34)**, which could negatively affect sister chromatid cohesion during meiosis I [166]. The decrease in meiotic Cnp1 enrichment to the central cores of

centromeres in *abp1*Δ cells **(Figures 30, 31, 36-38)**, as well as the associated aberrant increase of Cnp1 enrichment to the mating type locus **(Figures 39 and 40)**, are also factors likely contributing to the observed meiotic chromosome segregation defects **(Figures 47-50)**, as Cnp1 has been shown to be important for centromere function and maintenance [28,55]. The meiotic chromosome segregation defects in both wild type and *abp1*Δ cells are exacerbated slightly by the presence of ectopic *LTR* sequences in the *cnt* relative to cells with either no marker in *cnt1* or *cnt1::ura4-DS/E* **(Figure 49; Table 8)**. Future experiments are still needed to assess whether Abp1 can mitigate the detrimental effects of the presence of retrotransposons in the *cnt* by localizing to and preventing these retroelements from interfering with proper chromatin assembly of the centromere central cores.

Figures

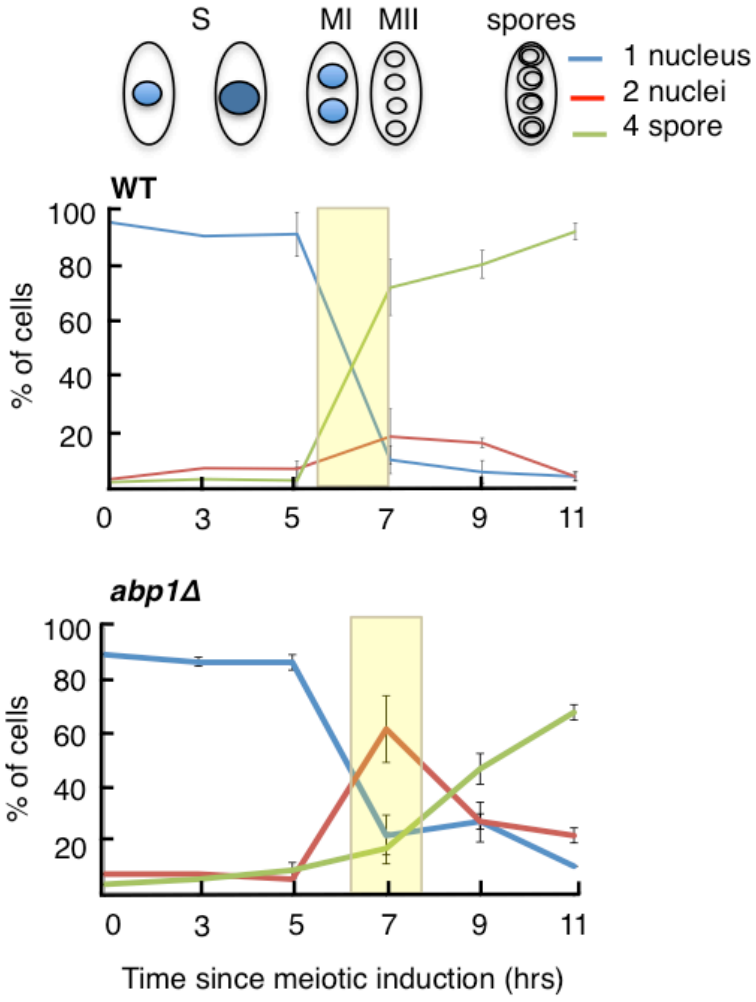

Figure 46. *abp1*Δ cells display a delay and loss of synchrony during meiosis. (Upper panel) Schematic of *S. pombe* meiotic cell cycle. (Lower panel) Results of meiotic synchrony experiment in WT (top) and *abp1*Δ (bottom) cells. The percentage of cells with 1 nucleus (blue), 2 nuclei (red), and 4 spores (green) are depicted on the graphs. The yellow bar highlights the time period during which the meiotic progression is especially different between *abp1*Δ and WT. Error bars were created using the standard deviation from two biological replicates.

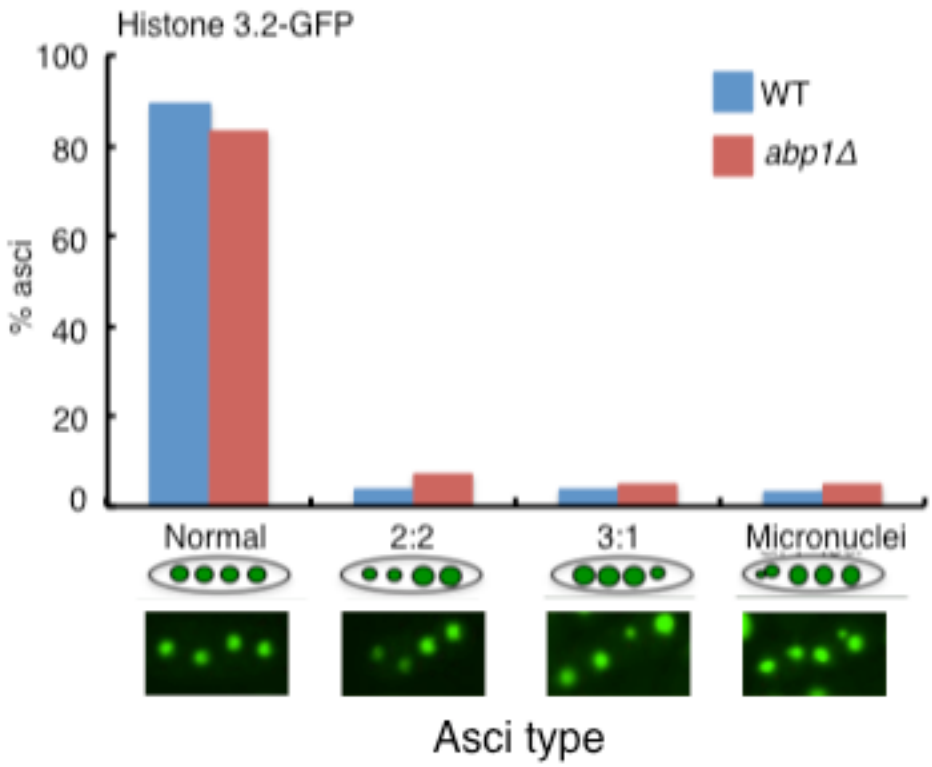

Figure 47. *abp1*Δ cells display an increased incidence of abnormal meiotic chromosome segregation. The percentage of WT (blue) and *abp1*Δ (red) asci that appear to have normal chromosome segregation versus abnormal chromosome segregation based on a histone H3.2-GFP tag (*hht2-GFP::ura4*$^{+}$) analysis using an EVOS fluorescence microscope. (WT *n*=1021, *abp1*Δ *n*=951).

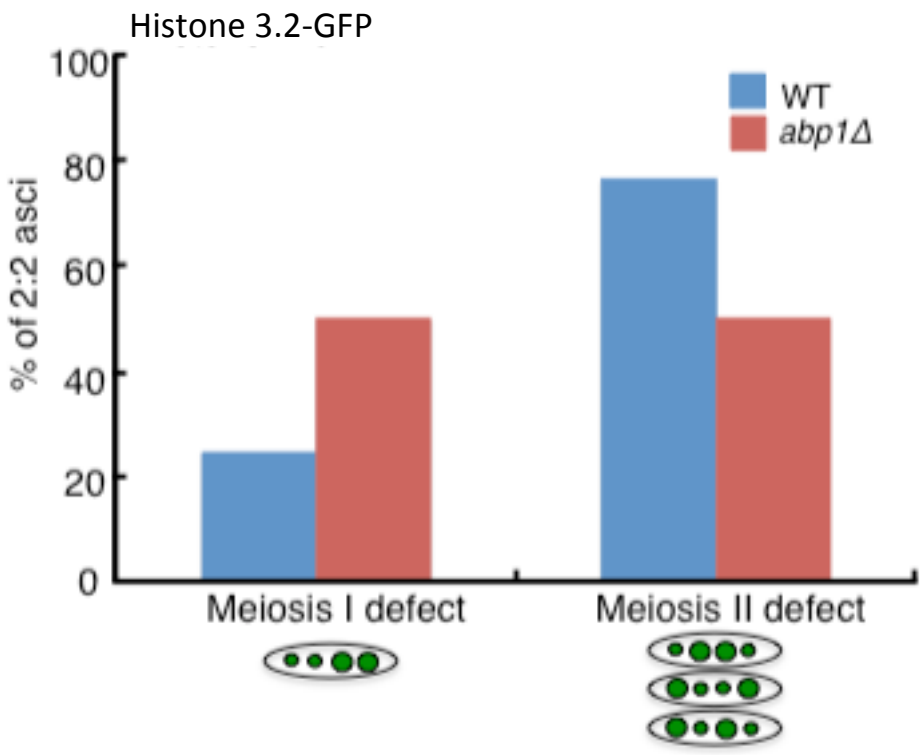

Figure 48. *abp1*Δ cells display increased defects in Meiosis I chromosome segregation. The percentage of WT (blue) and *abp1*Δ (red) asci that appear to have normal chromosome segregation versus abnormal chromosome segregation based on a histone H3.2-GFP tag (*hht2-GFP::ura4*$^{+}$) analysis using an EVOS fluorescence microscope (WT *n*=41, *abp1*Δ *n*=66).

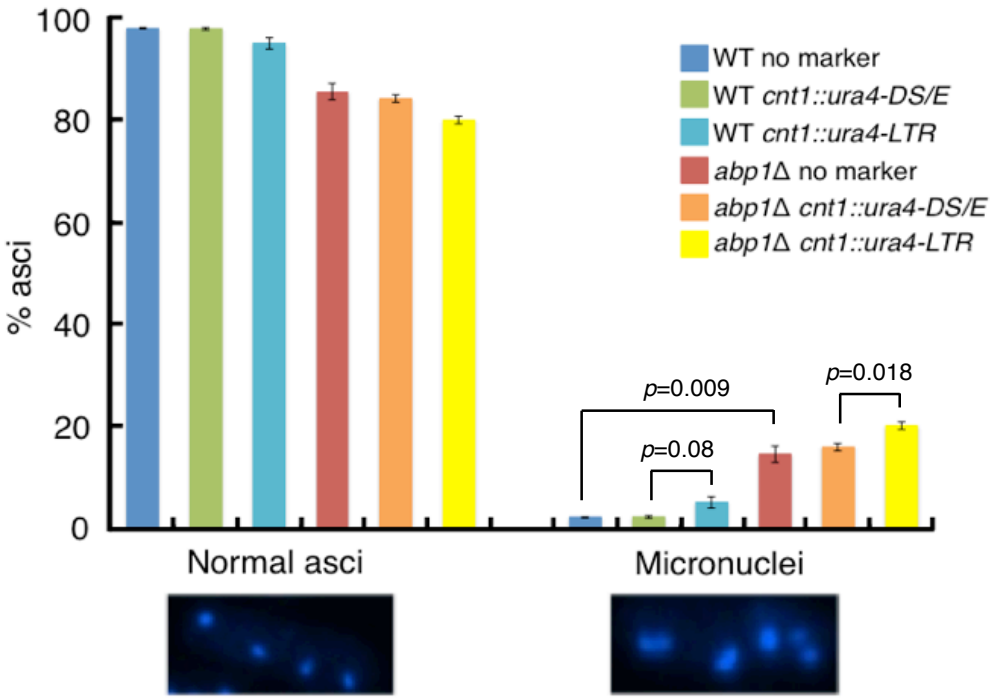

Figure 49. Chromosome segregation defects in meiotic *abp1*Δ cells. The percentage normal asci (left) and asci containing micronuclei (right) from WT strains with no *cnt1* marker (blue), *cnt1::ura4-DS/E* (green), and *cnt1::ura4-LTR* (teal) versus *abp1*Δ strains with no *cnt1* marker (red), *cnt1::ura4-DS/E* (orange), and *cnt1::ura4-LTR* (yellow). Results based on DAPI analysis using an EVOS fluorescence microscope (no *cnt1* marker: WT *n*=594, *abp1*Δ *n*=652; *cnt1::ura4-DS/E*: WT *n*=634, *abp1*Δ *n*=615; *cnt1::ura4-LTR*: WT *n*=427, *abp1*Δ *n*=264). Error bars indicate standard deviation. *n*=2 biological replicates.

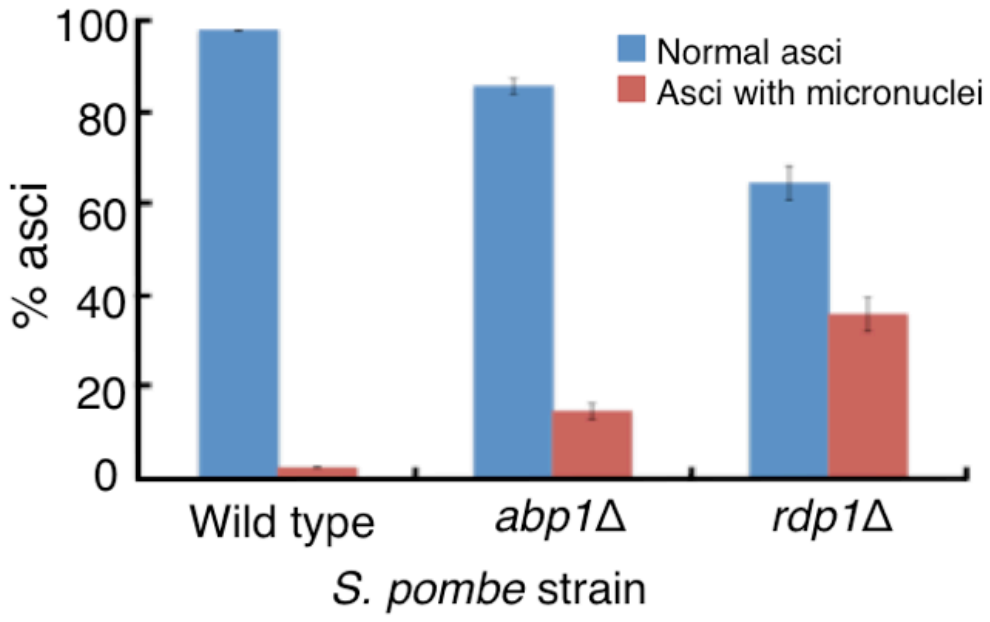

Figure 50. *abp1*Δ and *rdp1*Δ cells display an increased incidence of abnormal meiotic chromosome segregation. The percentage of normal asci (blue) and asci with micronuclei (red) in WT, *abp1*Δ, and *rbp1*Δ cells based on DAPI analysis using an EVOS fluorescence microscope (WT *n*=594, *abp1*Δ *n*=652, *rdp1*Δ *n*=392). Error bars indicate standard deviation. *n*=2 biological replicates.

Chapter VI: Discussion

A novel role for a *S. pombe* CENP-B homolog in meiosis

Earlier works identify a centromeric role for the *S. pombe* CENP-B homologs in the formation of pericentromeric heterochromatin [43,152]. More recent findings reveal a genome-wide function for *S. pombe* CENP-Bs in the suppression and genome organization of *Tf2* retrotransposons [120,121,177]. In this dissertation, I have described a novel meiosis-specific role for Abp1, the most prominent *S. pombe* CENP-B member, in ensuring proper localization of Cnp1 at centromeres critical for maintaining accurate chromosome segregation. In the following sections, I will address these findings within the larger context of the known biology of CENP-Bs that include the mammalian CENP-B, the likely mechanisms of Abp1-mediated localization of Cnp1 and its contribution to meiotic chromosome segregation, and potential insights stemming from our work regarding the evolutionary forces driving the domestication of CENP-Bs from DNA transposases within the fission yeast lineage.

The paradox of CENP-B functions: from *S. pombe* to mice, monkeys, and humans

The eukaryotic centromere is a highly specialized region of the chromosome that is the site of kinetochore assembly and microtubule attachment during cell division, ensuring accurate segregation of chromosomes to daughter cells during cell division [5-7]. Both sequence-specific and nonspecific DNA-binding proteins including epigenetic factors contribute to the assembly of a functional centromere [8-10, 15,186]. The repetitive nature of regional centromeres has long posed a significant challenge to its study. The identification of centromere proteins CENP-A-C in humans provided the key initial

discovery for elucidating the molecular pathway controlling the assembly of centromeric chromatin [29,187].

The human CENP-B has been shown to have dual centromeric functions, facilitating de novo assembly of functional centromeres and suppression of new centromeres by promoting heterochromatin at sites containing its alpha-satellite DNA binding sequences [188]. In addition, CENP-B binding is thought to increase centromere strength and the frequency of faithful chromosome segregation, at least partially through the stabilization of the CENP-A-H4 nucleosome [34]. CENP-B may exert these roles through stabilization of binding of other centromere and/or kinetochore proteins, such as CENP-C [41].

Most initial studies of *S. pombe* CENP-Bs focused on their roles at centromeres [42,43,152]. In particular, it was proposed that the three *S. pombe* CENP-Bs contribute to the assembly of heterochromatin by acting in a redundant fashion in recruiting the HP1 protein Swi6 to pericentromeres [152]. Thus, there was already parallel evidence for both human and fission yeast CENP-B proteins having roles in heterochromatin formation at centromeres. However, whereas the evidence linking human CENP-B to the centromeric function of CENP-A has been well-documented [34,188], a direct role for *S. pombe* CENP-Bs in mediating Cnp1 function has not been established. Our current work provides the first evidence for a fission yeast CENP-B member as an important factor in ensuring the localization and likely proper functions of Cnp1 at centromeres during meiosis. These findings thus further strengthen the functional commonality between human CENP-B and *S. pombe* CENP-Bs. Nevertheless, despite human CENP-B being a constitutive and highly expressed human centromeric protein [189], a major source of autoantigens in certain

autoimmune diseases [190], and having very high conservation across mammals (96% nucleotide identity between humans and mouse) [187], its cellular and physiological functions remain puzzling. First, CENP-B is not found on all mammalian centromeres such as those on the Y chromosome of humans and mice [41]. However, research has suggested that the centromere of the human Y chromosome, relative to the centromere of other chromosomes, contains approximately 80% and 60% of CENP-A and CENP-C enrichment, respectively [41]. Additionally, the human and mouse Y chromosomes have both been found to display increased mitotic chromosome segregation defects [41]. Second, African green monkey chromosomes whose centromeres consist largely of alpha-satellite DNA [191], and human marker chromosomes with neocentromeres that do not contain alphoid-DNA (analphoid), appear to lack CENP-B binding, though their centromeres are functional and contain adequate levels of CENP-C [192,193,194]. Third, *CENP-B* null mice, while having lower body and testis weights and uterine dysfunctions [40,195], have normal development and are fertile [39,40,195,196]. These findings collectively suggest that while our results might reveal a remarkable convergence of functions in some respect between human CENP-B and those of fission yeast, they likely have divergent modes of functions due to their independent origin of domestication [122] and evolution to recognize different DNA-binding motifs in different lineage (*CENP-B* box in mammals [197] and AT-rich sequences in *S. pombe* [177]). As such, cautions are warranted for any conclusion pertaining to their "conserved" functions.

Abp1-mediated localization of Cnp1 at meiotic centromeres

Our ChIP analysis revealed that except for the centromeres, Abp1 binding across the genome remains similar as cells transit from the mitotic cycle to meiosis. These data support our hypothesis that Abp1 is exerting a unique role at the centromere during meiosis. The dynamic binding of Abp1 displaying multiple peaks at pericentromeric *dg/dh* repeats, boundary elements such as tRNA clusters, and the central core *cnt* regions suggests that Abp1 contribution to centromere function is likely to be multifaceted. Indeed, pericentromeric heterochromatin and Cnp1 localization at the *cnt* are impaired in meiotic cells deficient in *abp1*.

It has been found that the Clr4 H3K9 methyltransferase and intact pericentromeric heterochromatin are both necessary to establish Cnp1 chromatin at the *cnt* on a minichromosome [160]. Even though the *cnt* is not enriched for heterochromatin factors such as H3K9me, Swi6, and RNAi machinery [114], incorporation of the *cnt* sequence on a minichromome in cells deficient in any of the above heterochromatin factors fails to localize Cnp1 and establish a functional centromere [160,161]. However, heterochromatin and RNAi become dispensable for Cnp1 localization once a functional centromere has been established [90]. Thus, it is unlikely that impaired Cnp1 localization in meiotic *abp1*Δ cells is due to reduced H3K9me levels at pericentromeric repeats. However, RNAi–mediated heterochromatin is required for proper chromosome segregation during mitosis and meiosis through Swi6-mediated recruitment of cohesin proteins at pericentromeres critical for the cohesion of sister chromatids [198]. Consistent with these findings, meiotic cells lacking the RNAi component Rdp1 appears to exhibit a higher incidence of chromosome missegregation than that seen in *abp1*Δ cells **(Figure 50)**. I hypothesize that

the meiotic delay observed at the transition point from MI to MII of *abp1*Δ cells **(Figure 46)** is likely due to insufficient cohesion of sister chromatid centromeres because of decreased H3K9me2 enrichment at the *dg/dh* pericentromeric repeats **(Figure 50)**.

While a decrease in H3K9me at the *dg/dh* repeats is unlikely to affect Cnp1 function at the *cnt* [90], it has been suggested that an increase in H3K9me at the *cnt* is detrimental for centromere formation and activation [199]. In this situation, intact centromeric chromatin is epigenetically silenced and is unable to be recognized for kinetochore assembly [199]. Therefore, loss of *abp1* could compromise the tRNA boundary partitioning heterochromatin from the central cores, and thereby allowing heterochromatin to spread into the *cnt* region and hinder Cnp1 localization. Consistent with this idea, H3K9me2 enrichment was detected, though modest, at the *cnt* regions of all three centromeres in meiotic *abp1*Δ cells.

The presence of Abp1 throughout the *cnt* suggests that Abp1 could contribute to Cnp1 localization by directly interacting with Cnp1 protein. This possibility is reminiscent of that of human CENP-B promoting CENP-A binding at human centromere via physical interaction with CENP-A and other centromeric proteins [34,188]. However, support for this scenario is somewhat tempered by our inability thus far to detect physical interaction between Abp1 and Cnp1 (Panariello and Meyer, data not shown).

While Cnp1 chromatin lacks the typical heterochromatin marker such as H3K9me and Swi6, its transcriptional silencing requires the HDAC activities of Clr3 and Clr6 [118]. These HDACs have been shown to be recruited by Abp1 to silence *Tf2* retrotransposons [120]. Therefore, I hypothesize that Abp1 could contribute to Cnp1 localization by recruiting these HDACs to the *cnt* regions to promote the assembly of Cnp1 chromatin.

Supporting this hypothesis is that Clr2, a component of the SHREC complex that contains Clr3 strongly localizes to the central core in vegetative cells, which suggests a central core-specific function of at least Clr2 of the SHREC complex [142]. In addition, Clr6 has been shown to be required for preventing inappropriate deposition of ectopic Cnp1 to noncentromeric sites [149]. In support of this scenario, preliminary ChIP analysis reveals that Cnp1 localization is impaired in meiotic cells deficient for either *clr2* or *clr3* (Meyer, data not shown), and that meiotic cells lacking *clr6* display chromosome segregation defects, possibly through a decrease in sister chromatid cohesion at the centromere (Stahl, data not shown).

The role of Abp1 in the suppression of meiotic neocentromeres

Heterochromatin is known to play a positive and negative role in the formation of centromeres. Loss of native centromeres results in neocentromere formation at regions adjacent to heterochromatin such as subtelomere [200]. On the other hand, while heterochromatin itself is not needed for centromere inactivation, it can prevent the reactivation of inactive centromeres by rendering the centromere as unrecognizable so that it is unable to direct kinetochore assembly [199]. Interestingly, Cre-lox mediated excision of centromere II, which contains the relatively nearby heterochromatic *mat* locus, did not result in neocentromere formation at the *mat* locus [201]. This finding suggests that not all heterochromatin domains are suitable for the formation of CENP-A chromatin. In other words, certain heterochromatin domains might contain factors that antagonize the deposition of CENP-A. In this regard, Cnp1 was found to localize at the silent *mat* locus in meiotic cells lacking Abp1, which is normally enriched at this region

in both vegetative and meiotic cells **(Figures 39 and 40)**. It is possible that akin to human CENP-B, Abp1 possesses dual roles: facilitating Cnp1 localization at native centromeres while suppressing neocentromere formation by preventing aberrant localization of Cnp1 at certain genomic sites such as the silent *mat* locus. These dual roles likely reinforce each other to ensure that each chromosome has only one functional centromere, critical for maintaining not only the integrity of the chromosome but also the fidelity of the chromosome segregation process.

The nature of meiotic chromosome segregation defects in *abp1Δ* cells

Wild type cells completed meiosis I and II within 11 hours and in a highly synchronized manner, similarly to published data [202]. However, *abp1*Δ cells displayed a delay of meiotic completion. This delay appeared most pronounced between MI and MII, as shown by the accumulation of cells with two nuclei, suggesting a stalling between MI and MII **(Figure 46)**. This stalling in *abp1*Δ cells could be due to various factors, such as chromosome segregation defects, inadequate cohesion between sister chromatids, or defects in the kinetochore-centromere interaction. *S. pombe* undergoes an ordered meiosis in which the two adjacent spores on one side of the tetrad are products of MII. This arrangement allows us to determine whether chromosome missegregation happened in MI or MII. Our results indicate that *abp1*Δ asci may contain a greater incidence of Meiosis I (MI) chromosome segregation defects compared to wild type. This is due to a greater percentage of *abp1*Δ asci with two spores adjacent to each other on one side of the ascus containing a higher content of histone H3 compared to the other two spores on the other side having lower content of histone H3 **(Figure 48)**.

This experiment was expanded upon by observing chromosome segregation in wild type and *abp*1Δ asci using DAPI staining. This allows visualization of the entire DNA content of each ascus. As expected, these results supported the results obtained from the histone H3-GFP experiments, as 97.8% of wild type asci and 85.5% of *abp1*Δ asci displayed normal chromosome segregation, while the remaining asci contained micronuclei **(Figure 49)**. I believe that the greater percentage of micronuclei observed in *abp1*Δ asci when using DAPI staining may be due to the robust staining properties of DAPI. In the histone H3-GFP experiments, the formation of micronuclei may have not been observed at as high of a rate because the lagging chromosome may have contained too little of the GFP signal to be detectable.

Potential forces driving the domestication of CENP-Bs within the *Schizosaccharomyces* lineage

While the mammalian genome has only one *CENP-B* gene copy [122], *CENP-B*-like genes are prevalent within the *Schizosaccharomyces* lineage. While *S. pombe* has 3 CENP-B-like genes (*abp1*, *cbh1*, *cbh2*), the closely related *S. octosporus* and *S. cryophilus* have 5 and 6 copies, respectively. Surprisingly, the more distantly related *S. japonicus* has no CENP-B-like genes [203]. Whereas, the centromeres of *S. pombe, S. octosporus, and S. cryophilus* lack transposons, *S. japonicus* centromeres still retain many retrotransposon sequences [203], with some that are still active [204]. Furthermore, *S. octosporus* and *S. cryophilus* have appeared to successfully eradicate all retrotransposons from their genomes [203]. Our current work could help shed light on the potential origin and biological forces driving the domestication of CENP-B-like genes within the *Schizosaccharomyces*

lineage. Considering that the still active *Tf2* retrotransposons are under the regulatory controls of Abp1 in *S. pombe* [120,121], it is likely that the ancestral centromeres of the *S. pombe* lineage were replete with retrotransposons similar to those of *S. japonicus*. Thus, perhaps one potential driving force behind the domestication of Abp1 and its kindreds is to control the detrimental effects of retrotransposon activities at centromeres, particularly at the centromere central cores. Consistent with this hypothesis, the mere insertion of an *LTR* sequence within the *cnt* region results in the further elevated incidence of chromosome missegregation in meiotic cells deficient in *abp1* **(Figure 49)**.

It is possible that insertion of multiple *LTRs* or full-length retrotransposons might cause a more drastic disruption to centromere function. Furthermore, this hypothesis would lead to the prediction that the proliferation and retention of *CENP-B*-like genes in *S. octosporus, and S. cryophilus* that no longer contain any active retrotransposon is likely due to their evolved specialized function at centromeres. Our works pave the way for these exciting future experiments that could elucidate the mechanisms by which CENP-B-like genes could mold the evolutionary architecture of centromeres not only within the *Schizosaccharomyces* lineage but other lineages including that of mammals. Collectively, these future studies could yield important conceptual understandings of the various forces shaping the evolution of eukaryotic genomes.

Appendix:

Table 1: Strains used in this study

Strain:	Genotype:
LM28	*mat1Msmt0, ade6-M216, abp1-FLAG::KanMX, pat1-114*
LM29	*mat2-102, ade6-M210, abp1-FLAG::KanMX, ura4-DS/E, pat1-114*
LM41	*mat1Msmt0, ade6-M216, abp1Δ::KanMX, pat1-114*
LM47	*mat2-102, ade6-M210, abp1Δ::KanMX, pat1-114*
LM140	*mat1Msmt0, ade6-M210, abp1-FLAG::KanMX, cdc25-22*
LM169	*h-, ade6-M210, scm3-FLAG(hph), pat1-114*
LM171	*h+,ade6-M216,abp1Δ::KanMX,scm3-FLAG (hph),cnp1+::GFP[lys1+], pat1-114*
LM173	*h+, ade6-M216, scm3-flag(hph), cnp1+::GFP[lys1+], pat1-114*
LM175	*h-,ade6-M210,abp1Δ::KanMX,scm3-FLAG (hph),cnp1+::GFP[lys1+],pat1-114*
LM189	*h+, ade6-M210, Scm3-pk(hph), cnp1-FLAG::KanMX, Abp1-myc::KanMX, pat1-114*
LM190	*h-, ade6-M216, cnp1-FLAG::KanMX, abp1-myc::KanMX, leu1 WT, ura4 WT, pat1-114*
LM191	*h+, ade6-M216, scm3-pk(hph), cnp1-FLAG::KanMX, abp1-myc::KanMX, pat1-114*
LM194	*h+, ade6-M216, hh+2-GFP::ura4+, mcherry-atb2-hph, abp1Δ::KanMX*
LM195	*h-, ade6-M216, hh+2-GFP::ura4+, mcherry-atb2-hph, leu1-32*
LM197	*h+, ade6-M210, hh+2-GFP::ura4+, mcherry-atb2-hph, leu1-32*
LM223	*h+, ade6-M216, abp1Δ::KanMX, cnp1-FLAG::KanMX, pat1-114*
LM226	*h-, ade6-M210, abp1Δ::KanMX, cnp1-FLAG::KanMX, pat1-114*
LM234	*mat1Mst0, ade6-M216, cnp1-FLAG::KanMX, leu1-32, pat1-114*
LM235	*mat1Mst0, ade6-M216, cnp1-FLAG::KanMX,abp1Δ::KanMX, leu1-32, pat1-114*
LM282	*h-, ade6-M210, hh+2-GFP::ura4+, mcherry-atb2-hph, abp1Δ::KanMX, leu1-32*
LM293	*h+, ade6-M210, abp1Δ::KanMX, Cnp1-FLAG:;KanMX, pat1-114*
HC200	*mat1Msmt0, ade6-M216, ura4-DS/E, OtrR1::ura4+, his2, leu1-32*
HC476	*mat1Msmt0, ade6-M210, ura4-D18, his2, leu1-32, abp1Δ::KanMX*
HC2505	*mat1Msmt0, ade6-M210, his2, ura4-D18, cnt1::ura4, leu1-32*
HC2540	*h+, ade6-M216, ura4-D18, cnt1::ura4-LTR, leu1-32*
HC2565	*h+, ade6-M216, ura4-D18, cnt1::ura4, leu1-32, abp1Δ::KanMX*
HC2566	*mat1Msmt0, ade6-M210, his,2 ura4-D18, cnt1::ura4-LTR, leu1-32, abp1Δ::KanMX*
HC2620	*mat1Msmt0, ade6-M216, his2, ura4-D18, cnt1::ura4-DS/E, leu1-32*
HC2533	*h+, ade6-M210, ura4-D18, cnt1::ura4+, leu1-32*
HC2627	*mat1Msmt0, ade6-M210, his2, ura4-D18, cnt1::ura4-LTR, a1Da2D, abp1Δ::KanMX*
HC2625	*mat1-Msmt-0, ade6-M210, his2, ura4-D18, cnt1::ura4-LTR, a1Da2D*
HC2497	*h+, ade6-M216, ura4-D18, cnt1::ura4+, leu1-32*
HC2621	*mat1Msmt0, ade6-M210, his2, ura4-D18, cnt1::ura4-DS/E, leu1-32,*
HC1807	*mat1-Msmt-0, ade6-M210, his2, OtrR1::ura4, leu1-32, rdp1Δ::KanMX*
HC1809	*h+, ade6-M216, OtrR1::ura4, leu1-32, rdp1Δ::KanMX*

Table 2. *t*-test analysis of Cnp1-FLAG ChIP qPCR at the centromere. *t*- and *p*-values were calculated using an unpaired *t*-test of the wild type and *abp1*Δ ChIP qPCR values. Technical triplicates (values indicated below) were used. Significant *p*-values are in bold font ($p<0.05$). **(Figures 29-31)**.

qPCR locus	WT qPCR values	*abp1*Δ qPCR values	Statistic	Veg	0 hr meiosis	5 hr meiosis
cnt1/3	**Veg: 71.6, 70.8, 94**	**Veg: 87.4, 82.5, 79.6**	***t*-value**	0.55	1.85	5.25
	0hr: 331, 416, 671	**0hr: 298.3, 293.3, 259**	***p*-value**	0.61	0.14	**0.006**
	5hr: 97.1, 84.9, 93.4	**5hr: 70.6, 69.3, 60.6**				
cnt2	**Veg: 69.6, 68, 70.6**	**Veg: 72.9, 69.9, 68.6**	***t*-value**	0.72	4.36	12
	0hr: 330, 321, 331	**0hr: 292, 263.4**	***p*-value**	0.51	**0.022**	**0.0002**
	5hr: 131, 123.3, 123	**5hr: 78, 74, 67**				
imr	**Veg: 7.3, 8.4, 7.2**	**Veg: 5, 5.5, 5.8**	***t*-value**	4.83	0.3	11.66
	0hr: 26.4, 28, 25	**0hr: 27.7, 25, 27.4**	***p*-value**	**0.008**	0.78	**0.0003**
	5hr: 22, 23.2, 24.2	**5hr: 15, 14, 13.2**				
dg	**Veg: 4.2, 4.2, 3.8**	**Veg: 5.8, 3.7, 3.6**	***t*-value**	2.14	4.56	4.64
	0hr: 9.8, 10, 11.5	**0hr: 12.8, 12.9, 13.2**	***p*-value**	0.12	**0.01**	**0.0097**
	5hr: 9.4, 9.4, 8.9	**5hr: 11.9, 11.4, 10.5**				

Table 3. *t*-test analysis of Scm3-FLAG ChIP qPCR at the centromere. *t*- and *p*-values were calculated using an unpaired *t*-test of the wild type and *abp1*Δ ChIP qPCR values. Technical triplicates (values indicated below) were used. Significant *p*-values are in bold font ($p<0.05$). **(Figures 32-34)**.

qPCR locus	WT qPCR values	*abp1*Δ qPCR values	Statistic	Veg	0 hr meiosis	5 hr meiosis
cnt1/3	**Veg: 3.3, 3.2, 3.9**	**Veg: 3.7, 4, 3.9**	***t*-value**	1.54	1.12	5.21
	0hr: 26.6, 21.7, 21.4	**0hr: 21.3, 22.1, 20.4**	***p*-value**	0.197	0.32	**0.013**
	5hr: 1.3, 1.3, 1.2	**5hr: 3.9, 3.8**				
cnt2	**Veg: 4.3, 5, 3.3**	**Veg: 6.7, 5.7**	***t*-value**	2.76	0.77	0.413
	0hr: 19.5, 16.9, 17.8	**0hr: 19, 17.4, 13.9**	***p*-value**	0.07	0.48	0.7
	5hr: 3.9, 4, 3.2	**5hr: 3.5, 3.7, 3.6**				
imr	**Veg: 1.23, 1.21, 1.3**	**Veg: 1.6, 1.62, 1.61**	***t*-value**	18.76	0.018	4.52
	0hr: 2.5, 2.5, 2.3	**0hr: 2.7, 2.2, 2.2**	***p*-value**	**0.0001**	0.99	**0.011**
	5hr: 1.7, 1.5, 1.7	**5hr: 1.2, 1.4, 1.1**				
dg	**Veg: 1.8, 1.7, 1.6**	**Veg: 2.6, 2.4, 2.6**	***t*-value**	7.85	12.56	0.221
	0hr: 1.2, 1.2, 1.1	**0hr: 1.8, 1.8, 1.7**	***p*-value**	**0.0014**	**0.0002**	0.835
	5hr: 1.3, 1.3, 1.2	**5hr: 1.5, 1.2, 1.2**				

Table 4. *t*-test analysis of Cnp1-FLAG ChIP qPCR at the mating type region. *t*- and *p*- values were calculated using an unpaired *t*-test of the wild type and *abp1*Δ ChIP qPCR values. Technical triplicates (values indicated below) were used. Significant *p*-values are in bold font ($p<0.05$). **(Figure 40)**.

qPCR locus	WT qPCR values	*abp1*Δ qPCR values	Statistic	Veg	0 hr meiosis	5 hr meiosis
Mating type region	**Veg: 1.3, 1.4, 1.5**	**Veg: 1.7, 1.6, 1.6**	***t*-value**	3.37	33.1	13.5
	0hr: 1.9, 2, 1.8	**0hr: 3.3, 3.4, 3.35**	***p*-value**	**0.03**	**0.0001**	**0.0002**
	5hr: 2, 2.3, 2	**5hr: 3.8, 4, 2.9**				

Table 5. *t*-test analysis of vegetative Cnp1-FLAG ChIP qPCR at the mating type region. *t*- and *p*- values were calculated using an unpaired *t*-test of the wild type and *abp1*Δ ChIP qPCR values. Technical triplicates (values indicated below) were used. No significant *p*-values were found ($p<0.05$). **(Figure 41)**.

qPCR locus	WT qPCR values	*abp1*Δ qPCR values	Statistic	*h+*, veg	*mat1*, veg
Mating type region	*h+:* 2.5, 2.3, 2.5	*h+:* 2, 2.4, 2.9	*t*-value	2.19	2.16
	Mat1: 1.7, 2.1, 2.1	*Mat1:* 1.6, 1.7, 1.5	*p*-value	0.09	0.097

Table 6. *t*-test analysis of H3K9me2 ChIP qPCR at the centromere. *t*- and *p*- values were calculated using an unpaired *t*-test of the wild type and *abp1*Δ ChIP qPCR values. Technical triplicates (values indicated below) were used. Significant *p*-values are in bold font ($p<0.05$). **(Figures 42-44)**.

qPCR locus	WT qPCR values	*abp1*Δ qPCR values	Statistic	Veg	0 hr meiosis	5 hr meiosis
cnt1/3	**Veg: 1.9, 1.7**	**Veg: 1.8, 1.6, 1.6**	***t*-value**	1.08	3.09	2.48
	0hr: 1.6, 1.6, 1.5	**0hr: 3.2, 2.5, 2.1**	***p*-value**	0.36	**0.036**	0.089
	5hr: 1.3, 1.3, 1.2	**5hr: 3.9, 3.8**				
cnt2	**Veg: 42.1, 2.6, 3.7**	**Veg: 7.5, 10.5, 8.5**	***t*-value**	5.99	0.029	13.37
	0hr: 1.8, 2.6, 1.7	**0hr: 2.4, 1.8, 2**	***p*-value**	**0.004**	0.978	**0.0002**
	5hr: 3.9, 4, 3.2	**5hr: 3.5, 3.7, 3.6**				
imr	**Veg: 3.5, 3.5, 2.6**	**Veg: 2.4, 2.6, 2.5**	***t*-value**	2.43	14.83	21.54
	0hr: 4.6, 4.7, 5	**0hr: 2.2, 2.5, 2**	***p*-value**	0.07	**0.0001**	**0.0002**
	5hr: 1.7, 1.5, 1.7	**5hr: 1.2, 1.4, 1.1**				
dg	**Veg: 6.9, 8**	**Veg: 5.9, 5, 6.4**	***t*-value**	1.67	12.48	34.4
	0hr: 9.3, 10.8, 9	**0hr: 29, 2.6, 2.5**	***p*-value**	0.08	**0.0002**	**0.0001**
	5hr: 1.3, 1.3, 1.2	**5hr: 1.5, 1.2, 1.2**				
dh	**Veg: 5.2, 4.6**	**Veg: 4.6, 5.8, 4.9**	***t*-value**	0.48	21.38	22.52
	0hr: 10.5, 11.3, 11.1	**0hr: 3.6, 2.6, 2.7**	***p*-value**	0.66	**0.0001**	**0.0001**
	5hr: 1.3, 1.3, 1.2	**5hr: 1.5, 1.2, 1.2**				

Table 7. *t*-test analysis of H3K9me2 ChIP qPCR at the mating type region. *t*- and *p*-values were calculated using an unpaired *t*-test of the wild type and *abp1*Δ ChIP qPCR values. Technical triplicates (values indicated below) were used. No significant *p*-values were found ($p<0.05$). **(Figure 45)**.

qPCR locus	WT qPCR values	*abp1*Δ qPCR values	Statistic	Veg	5 hr meiosis
Mating type region	**Veg: 18.3, 21.7, 21.1**	**Veg: 12.7, 17.2, 16.6**	***t*-value**	2.74	0.61
	5 hr: 43.2, 54.4	**5 hr: 48.3, 56.3, 51.2**	***p*-value**	0.052	0.58

Table 8. *t*-test analysis of DAPI-stained asci assay. *t*- and *p*- values were calculated using an unpaired *t*-test of the percentage of cells containing micronuclei in wild type and *abp1*Δ cells. Biological replicates (values indicated below) were used (n=2). Significant *p*-values are in bold font (p<0.05). **(Figure 49)**.

Strain comparison	**% micronuclei**	**% micronuclei**	***t*-value**	***p*-value**
	1st strain values (%)	**2nd strain values (%)**		
1. WT vs *abp1*Δ (both no *cnt1* marker)	**97.9, 97.7**	**84.3, 86.7**	10.23	**0.009**
2. WT vs *abp1*Δ (both *cnt1::ura4-DS/E)*	**97.6, 98**	**83.9, 84.3**	46.56	**0.0005**
3. WT vs *abp1*Δ (both *cnt1::ura4-LTR)*	**95.8, 94.1**	**79.4, 80.4**	15.29	**0.0042**
4. WT no *cnt1* marker vs WT *cnt1::ura4-DS/E*	**97.9, 97.7**	**97.6, 98**	0.153	0.89
5. WT no *cnt1* marker vs WT *cnt1::ura4-LTR*	**97.9, 97.7**	**95.8, 94.1**	3.45	0.074
6. WT *cnt1::ura4-DS/E* vs WT *cnt1::ura4-LTR*	**97.6, 98**	**95.8, 94.1**	3.32	0.08
7. *abp1*Δ no *cnt1* marker vs *abp1*Δ *cnt1::ura4-DSE*	**84.3, 86.7**	**83.9, 84.3**	1.13	0.37
8. *abp1*Δ no *cnt1* marker vs *abp1*Δ *cnt1::ura4-LTR*	**84.3, 86.7**	**79.4, 80.4**	4.25	0.051
9. *abp1*Δ *cnt1::ura4-DS/E* vs *abp1*Δ *cnt1::ura4-LTR*	**83.9, 84.3**	**79.4, 80.4**	7.31	**0.018**

Table 9. *t*-test analysis of DAPI-stained asci assay. *t*- and *p*- values were calculated using an unpaired *t*-test of the percentage of cells containing micronuclei in wild type, *abp1*Δ, and *rdp1*Δ cells. Biological replicates (n=2; values below) were used. Significant *p*-values are in bold font (p<0.05). **(Figure 50)**.

Strain comparison	% micronuclei	% micronuclei	*t*-value	*p*-value
	1st strain values (%)	2nd strain values (%)		
1. WT vs *abp1*Δ	**97.9, 97.7**	**84.3, 86.7**	10.2312	**0.0094**
2. WT vs *rdp1*Δ	**97.9, 97.7**	**67, 61.7**	12.6137	**0.0062**

Bibliography

1. Riley, R., Flavell, R. B. & Jones, K. A First View of the Meiotic Process [and Discussion]. *... of the Royal ...* (1977).
2. Griffiths, A., Miller, J. H., Suzuki, D. T. & Lewontin, R. C. Historical development of the chromosome theory. (2000).
3. Barr, M. L. The sex chromosomes in evolution and in medicine. *Canadian Medical Association Journal* (1966).
4. Murray, A. W. & Szostak, J. W. Chromosome segregation in mitosis and meiosis. *Annual review of cell biology* (1985).
5. Polizzi, C. & Clarke, L. The chromatin structure of centromeres from fission yeast: differentiation of the central core that correlates with function. *J. Cell Biol.* **112,** 191–201 (1991).
6. Schulman, I. G. & Bloom, K. Genetic dissection of centromere function. *Mol. Cell. Biol.* (1993).
7. Henikoff, S. & Furuyama, T. Epigenetic Inheritance of Centromeres. *Cold Spring Harbor Symposia on Quantitative Biology* **75,** 51–60 (2011).
8. Brinkley, B. R., Tousson, A. & Valdivia, M. M. The kinetochore of mammalian chromosomes: structure and function in normal mitosis and aneuploidy. *Basic Life Sci.* **36,** 243–267 (1985).
9. Mitchison, T. J. Microtubule dynamics and kinetochore function in mitosis. *Annual review of cell biology* (1988).
10. Haaf, T., Warburton, P. E. & Willard, H. F. Integration of human alpha-satellite DNA into simian chromosomes: centromere protein binding and disruption of normal chromosome segregation. *Cell* **70,** 681–696 (1992).
11. Saunders, W. S. *et al.* Chromosomal instability and cytoskeletal defects in oral cancer cells. *Proc. Natl. Acad. Sci. U.S.A.* **97,** 303–308 (2000).
12. Fukasawa, K. Centrosome amplification, chromosome instability and cancer development. *Cancer Lett.* **230,** 6–19 (2005).
13. Pacchierotti, F., Adler, I.-D., Eichenlaub-Ritter, U. & Mailhes, J. B. Gender effects on the incidence of aneuploidy in mammalian germ cells. *Environ. Res.* **104,** 46–69 (2007).
14. Hassold, T. & Hunt, P. To err (meiotically) is human: the genesis of human aneuploidy. *Nat. Rev. Genet.* **2,** 280–291 (2001).
15. Cleveland, D. W., Mao, Y. & Sullivan, K. F. Centromeres and kinetochores: from epigenetics to mitotic checkpoint signaling. *Cell* **112,** 407–421 (2003).
16. MacLennan, M., Crichton, J. H. & Playfoot, C. J. Oocyte development, meiosis and aneuploidy. *Seminars in cell & ...* (2015).
17. Nagaoka, S. I., Hassold, T. J. & Hunt, P. A. Human aneuploidy: mechanisms and new insights into an age-old problem. *Nat. Rev. Genet.* **13,** 493–504 (2012).
18. Knouse, K. A., Wu, J., Whittaker, C. A. & Amon, A. Single cell sequencing reveals low levels of aneuploidy across mammalian tissues. *Proc. Natl. Acad. Sci. U.S.A.* **111,** 13409–13414 (2014).
19. Templado, C., Vidal, F. & Estop, A. Aneuploidy in human spermatozoa.

Cytogenetic and genome research (2011).
20. Danylevska, A., Kovacovicova, K., Awadova, T. & Anger, M. The frequency of precocious segregation of sister chromatids in mouse female meiosis I is affected by genetic background. *Chromosome Res.* **22,** 365–373 (2014).
21. Palmer, D. K., O'Day, K., Wener, M. H., Andrews, B. S. & Margolis, R. L. A 17-kD centromere protein (CENP-A) copurifies with nucleosome core particles and with histones. *J. Cell Biol.* **104,** 805–815 (1987).
22. Williams, J. S., Hayashi, T., Yanagida, M. & Russell, P. Fission yeast Scm3 mediates stable assembly of Cnp1/CENP-A into centromeric chromatin. *Mol. Cell* (2009).
23. Palmer, D. K., O'Day, K., Trong, H. L., Charbonneau, H. & Margolis, R. L. Purification of the centromere-specific protein CENP-A and demonstration that it is a distinctive histone. *Proc. Natl. Acad. Sci. U.S.A.* **88,** 3734–3738 (1991).
24. De Rop, V., Padeganeh, A. & Maddox, P. S. CENP-A: the key player behind centromere identity, propagation, and kinetochore assembly. *Chromosoma* **121,** 527–538 (2012).
25. Earnshaw, W. C. *et al.* Esperanto for histones: CENP-A, not CenH3, is the centromeric histone H3 variant. *Chromosome Res.* **21,** 101–106 (2013).
26. Skene, P. J. & Henikoff, S. Histone variants in pluripotency and disease. *Development* **140,** 2513–2524 (2013).
27. Bloom, K. S. Centromeric heterochromatin: the primordial segregation machine. *Annual review of genetics* (2013).
28. Sullivan, K. F., Hechenberger, M. & Masri, K. Human CENP-A contains a histone H3 related histone fold domain that is required for targeting to the centromere. *J. Cell Biol.* **127,** 581–592 (1994).
29. Earnshaw, W. C. & Migeon, B. R. Three related centromere proteins are absent from the inactive centromere of a stable isodicentric chromosome. *Chromosoma* **92,** 290–296 (1985).
30. Van Hooser, A. A. *et al.* Specification of kinetochore-forming chromatin by the histone H3 variant CENP-A. *J. Cell. Sci.* **114,** 3529–3542 (2001).
31. Castillo, A. G. *et al.* Plasticity of fission yeast CENP-A chromatin driven by relative levels of histone H3 and H4. *PLoS Genet.* **3,** e121 (2007).
32. Okamoto, Y., Nakano, M., Ohzeki, J.-I., Larionov, V. & Masumoto, H. A minimal CENP-A core is required for nucleation and maintenance of a functional human centromere. *EMBO J.* **26,** 1279–1291 (2007).
33. Sullivan, B. A. & Karpen, G. H. Centromeric chromatin exhibits a histone modification pattern that is distinct from both euchromatin and heterochromatin. *Nat. Struct. Mol. Biol.* **11,** 1076–1083 (2004).
34. Fachinetti, D. *et al.* A two-step mechanism for epigenetic specification of centromere identity and function. *Nat Cell Biol* **15,** 1056–1066 (2013).
35. Masumoto, H., Masukata, H., Muro, Y., Nozaki, N. & Okazaki, T. A human centromere antigen (CENP-B) interacts with a short specific sequence in alphoid DNA, a human centromeric satellite. *J. Cell Biol.* **109,** 1963–1973 (1989).
36. Muro, Y. *et al.* Centromere protein B assembles human centromeric alpha-satellite DNA at the 17-bp sequence, CENP-B box. *J. Cell Biol.* **116,** 585–596

(1992).
37. Tanaka, Y., Nureki, O., Kurumizaka, H. & Fukai, S. Crystal structure of the CENP-B protein–DNA complex: the DNA-binding domains of CENP-B induce kinks in the CENP-B box DNA. *The EMBO …* (2001).
38. Fujita, R. *et al.* Stable complex formation of CENP-B with the CENP-A nucleosome. *Nucleic Acids Res.* **43,** 4909–4922 (2015).
39. Perez-Castro, A. V. *et al.* Centromeric protein B null mice are viable with no apparent abnormalities. *Dev Biol* **201,** 135–143 (1998).
40. Hudson, D. F. *et al.* Centromere protein B null mice are mitotically and meiotically normal but have lower body and testis weights. *J. Cell Biol.* **141,** 309–319 (1998).
41. Fachinetti, D. *et al.* DNA Sequence-Specific Binding of CENP-B Enhances the Fidelity of Human Centromere Function. *Dev. Cell* **33,** 314–327 (2015).
42. Baum, M. & Clarke, L. Fission yeast homologs of human CENP-B have redundant functions affecting cell growth and chromosome segregation. *Mol. Cell. Biol.* **20,** 2852–2864 (2000).
43. Irelan, J. T., Gutkin, G. I. & Clarke, L. Functional redundancies, distinct localizations and interactions among three fission yeast homologs of centromere protein-B. *Genetics* **157,** 1191–1203 (2001).
44. Saitoh, H. *et al.* CENP-C, an autoantigen in scleroderma, is a component of the human inner kinetochore plate. *Cell* **70,** 115–125 (1992).
45. Tomkiel, J., Cooke, C. A., Saitoh, H., Bernat, R. L. & Earnshaw, W. C. CENP-C is required for maintaining proper kinetochore size and for a timely transition to anaphase. *J. Cell Biol.* **125,** 531–545 (1994).
46. Falk, S. J. *et al.* Chromosomes. CENP-C reshapes and stabilizes CENP-A nucleosomes at the centromere. *Science* **348,** 699–703 (2015).
47. Klare, K. *et al.* CENP-C is a blueprint for constitutive centromere-associated network assembly within human kinetochores. *J. Cell Biol.* **210,** 11–22 (2015).
48. Nicklas, R. B. How cells get the right chromosomes. *Science* (1997).
49. Gorbsky, G. J. Cell cycle checkpoints: arresting progress in mitosis. *Bioessays* **19,** 193–197 (1997).
50. Gorbsky, G. J. The spindle checkpoint and chromosome segregation in meiosis. *FEBS J.* **282,** 2471–2487 (2015).
51. Bernat, R. L., Delannoy, M. R., Rothfield, N. F. & Earnshaw, W. C. Disruption of centromere assembly during interphase inhibits kinetochore morphogenesis and function in mitosis. *Cell* **66,** 1229–1238 (1991).
52. Rago, F. & Cheeseman, I. M. The functions and consequences of force at kinetochores. *J. Cell Biol.* (2013).
53. Henikoff, S., Ahmad, K. & Malik, H. S. The centromere paradox: stable inheritance with rapidly evolving DNA. *Science* **293,** 1098–1102 (2001).
54. Melters, D. P. *et al.* Comparative analysis of tandem repeats from hundreds of species reveals unique insights into centromere evolution. *Genome Biol.* **14,** R10 (2013).
55. Black, B. E., Brock, M. A., Bédard, S., Woods, V. L. & Cleveland, D. W. An epigenetic mark generated by the incorporation of CENP-A into centromeric

nucleosomes. *Proc. Natl. Acad. Sci. U.S.A.* **104,** 5008–5013 (2007).
56. Warburton, P. E. *et al.* Immunolocalization of CENP-A suggests a distinct nucleosome structure at the inner kinetochore plate of active centromeres. *Curr. Biol.* **7,** 901–904 (1997).
57. Shelby, R. D., Vafa, O. & Sullivan, K. F. Assembly of CENP-A into centromeric chromatin requires a cooperative array of nucleosomal DNA contact sites. *J. Cell Biol.* **136,** 501–513 (1997).
58. Nechemia-Arbely, Y., Fachinetti, D. & Cleveland, D. W. Replicating centromeric chromatin: spatial and temporal control of CENP-A assembly. *Exp. Cell Res.* **318,** 1353–1360 (2012).
59. Stoler, S. *et al.* Scm3, an essential Saccharomyces cerevisiae centromere protein required for G2/M progression and Cse4 localization. *Proc. Natl. Acad. Sci. U.S.A.* **104,** 10571–10576 (2007).
60. Shivaraju, M., Camahort, R., Mattingly, M. & Gerton, J. L. Scm3 is a centromeric nucleosome assembly factor. *J. Biol. Chem.* **286,** 12016–12023 (2011).
61. Pidoux, A. L. *et al.* Fission Yeast Scm3: A CENP-A Receptor Required for Integrity of Subkinetochore Chromatin. *Mol. Cell* **33,** 299–311 (2009).
62. Sanchez-Pulido, L., Pidoux, A. L., Ponting, C. P. & Allshire, R. C. Common ancestry of the CENP-A chaperones Scm3 and HJURP. *Cell* **137,** 1173–1174 (2009).
63. Foltz, D. R. *et al.* Centromere-specific assembly of CENP-a nucleosomes is mediated by HJURP. *Cell* **137,** 472–484 (2009).
64. Takahashi, K., Takayama, Y., Masuda, F., Kobayashi, Y. & Saitoh, S. Two distinct pathways responsible for the loading of CENP-A to centromeres in the fission yeast cell cycle. *Philos Trans R Soc Lond B Biol Sci* **360,** 595–597 (2005).
65. Takayama, Y. *et al.* Biphasic incorporation of centromeric histone CENP-A in fission yeast. *Mol. Biol. Cell* **19,** 682–690 (2008).
66. Jansen, L. E. T., Black, B. E., Foltz, D. R. & Cleveland, D. W. Propagation of centromeric chromatin requires exit from mitosis. *J. Cell Biol.* **176,** 795–805 (2007).
67. Lermontova, I. *et al.* Loading of Arabidopsis centromeric histone CENH3 occurs mainly during G2 and requires the presence of the histone fold domain. *Plant Cell* **18,** 2443–2451 (2006).
68. Schuh, M., Lehner, C. F. & Heidmann, S. Incorporation of Drosophila CID/CENP-A and CENP-C into centromeres during early embryonic anaphase. *Curr. Biol.* **17,** 237–243 (2007).
69. Black, B. E. *et al.* Structural determinants for generating centromeric chromatin. *Nature* **430,** 578–582 (2004).
70. Vermaak, D., Hayden, H. S. & Henikoff, S. Centromere targeting element within the histone fold domain of Cid. *Mol. Cell. Biol.* **22,** 7553–7561 (2002).
71. Bodor, D. L., Valente, L. P., Mata, J. F., Black, B. E. & Jansen, L. E. T. Assembly in G1 phase and long-term stability are unique intrinsic features of CENP-A nucleosomes. *Mol. Biol. Cell* **24,** 923–932 (2013).

72. Bassett, E. A. *et al.* Epigenetic centromere specification directs aurora B accumulation but is insufficient to efficiently correct mitotic errors. *J. Cell Biol.* **190,** 177–185 (2010).
73. Black, B. E. *et al.* Centromere identity maintained by nucleosomes assembled with histone H3 containing the CENP-A targeting domain. *Mol. Cell* **25,** 309–322 (2007).
74. Fujita, Y. *et al.* Priming of centromere for CENP-A recruitment by human hMis18alpha, hMis18beta, and M18BP1. *Dev. Cell* **12,** 17–30 (2007).
75. Régnier, V. *et al.* CENP-A is required for accurate chromosome segregation and sustained kinetochore association of BubR1. *Mol. Cell. Biol.* **25,** 3967–3981 (2005).
76. Liu, S.-T., Rattner, J. B., Jablonski, S. A. & Yen, T. J. Mapping the assembly pathways that specify formation of the trilaminar kinetochore plates in human cells. *J. Cell Biol.* **175,** 41–53 (2006).
77. Guse, A., Carroll, C. W., Moree, B., Fuller, C. J. & Straight, A. F. In vitro centromere and kinetochore assembly on defined chromatin templates. *Nature* **477,** 354–358 (2011).
78. Barnhart, M. C. *et al.* HJURP is a CENP-A chromatin assembly factor sufficient to form a functional de novo kinetochore. *J. Cell Biol.* **194,** 229–243 (2011).
79. Mendiburo, M. J., Padeken, J., Fülöp, S., Schepers, A. & Heun, P. Drosophila CENH3 is sufficient for centromere formation. *Science* **334,** 686–690 (2011).
80. Gascoigne, K. E. *et al.* Induced ectopic kinetochore assembly bypasses the requirement for CENP-A nucleosomes. *Cell* **145,** 410–422 (2011).
81. Hori, T., Shang, W.-H., Takeuchi, K. & Fukagawa, T. The CCAN recruits CENP-A to the centromere and forms the structural core for kinetochore assembly. *J. Cell Biol.* **200,** 45–60 (2013).
82. Tomonaga, T. *et al.* Overexpression and mistargeting of centromere protein-A in human primary colorectal cancer. *Cancer Res.* **63,** 3511–3516 (2003).
83. Hewawasam, G. *et al.* Psh1 is an E3 ubiquitin ligase that targets the centromeric histone variant Cse4. *Mol. Cell* **40,** 444–454 (2010).
84. Ranjitkar, P. *et al.* An E3 ubiquitin ligase prevents ectopic localization of the centromeric histone H3 variant via the centromere targeting domain. *Mol. Cell* **40,** 455–464 (2010).
85. Moreno-Moreno, O., Medina-Giró, S., Torras-Llort, M. & Azorín, F. The F box protein partner of paired regulates stability of Drosophila centromeric histone H3, CenH3(CID). *Curr. Biol.* **21,** 1488–1493 (2011).
86. Dunleavy, E. M. *et al.* The cell cycle timing of centromeric chromatin assembly in Drosophila meiosis is distinct from mitosis yet requires CAL1 and CENP-C. *PLoS Biol.* **10,** e1001460 (2012).
87. Perpelescu, M., Nozaki, N., Obuse, C., Yang, H. & Yoda, K. Active establishment of centromeric CENP-A chromatin by RSF complex. *J. Cell Biol.* **185,** 397–407 (2009).
88. Lagana, A. *et al.* A small GTPase molecular switch regulates epigenetic centromere maintenance by stabilizing newly incorporated CENP-A. *Nat Cell Biol* **12,** 1186–1193 (2010).

89. Steiner, F. A. & Henikoff, S. Diversity in the organization of centromeric chromatin. *Curr. Opin. Genet. Dev.* **31,** 28–35 (2015).
90. Folco, H. D., Pidoux, A. L., Urano, T. & Allshire, R. C. Heterochromatin and RNAi are required to establish CENP-A chromatin at centromeres. *Science* (2008).
91. Lee, C., Wevrick, R., Fisher, R. B., Ferguson-Smith, M. A. & Lin, C. C. Human centromeric DNAs. *Hum. Genet.* **100,** 291–304 (1997).
92. Donovan, P. J., De Miguel, M. P., Hirano, M. P., Parsons, M. S. & Lincoln, A. J. Germ cell biology--from generation to generation. *Int. J. Dev. Biol.* **45,** 523–531 (2001).
93. Vjestica, A., Merlini, L., Dudin, O., Bendezu, F. O. & Martin, S. G. Microscopy of Fission Yeast Sexual Lifecycle. *J Vis Exp* (2016). doi:10.3791/53801
94. Gilbert, S. F. *Developmental Biology*. (2000).
95. Hunter, N. Meiotic Recombination: The Essence of Heredity. *Cold Spring Harb Perspect Biol* (2015).
96. Sen, A. & Caiazza, F. Oocyte maturation: a story of arrest and release. *Front Biosci (Schol Ed)* **5,** 451–477 (2013).
97. Kuliev, A. & Verlinsky, Y. Meiotic and mitotic nondisjunction: lessons from preimplantation genetic diagnosis. *Hum. Reprod. Update* **10,** 401–407 (2004).
98. Koehler, K. E. & Hassold, T. J. Human aneuploidy: lessons from achiasmate segregation in Drosophila melanogaster. *Ann Hum Genet* **62,** 467–479 (1998).
99. Herbert, M., Kalleas, D., Cooney, D., Lamb, M. & Lister, L. Meiosis and maternal aging: insights from aneuploid oocytes and trisomy births. *Cold Spring Harb Perspect Biol* **7,** a017970–a017970 (2015).
100. Diego-Alvarez, D. *et al.* Application of quantitative fluorescent PCR with short tandem repeat markers to the study of aneuploidies in spontaneous miscarriages. *Hum. Reprod.* **20,** 1235–1243 (2005).
101. Verdaasdonk, J. S. & Bloom, K. Centromeres: unique chromatin structures that drive chromosome segregation. *Nat. Rev. Mol. Cell Biol.* **12,** 320–332 (2011).
102. Hoffman, C. S., Wood, V. & Fantes, P. A. An Ancient Yeast for Young Geneticists: A Primer on the Schizosaccharomyces pombe Model System. *Genetics* **201,** 403–423 (2015).
103. Wixon, J. Featured organism: Schizosaccharomyces pombe, the fission yeast. *Comp Funct Genomics* **3,** 194–204 (2002).
104. Yanagida, M. The model unicellular eukaryote, Schizosaccharomyces pombe. *Genome Biol.* **3,** COMMENT2003–COMMENT2003 (2002).
105. Forsburg, S. L. & Nurse, P. Cell cycle regulation in the yeasts Saccharomyces cerevisiae and Schizosaccharomyces pombe. *Annu Rev Cell Biol* **7,** 227–256 (1991).
106. Knutsen, J. H. J. *et al.* Cell-cycle analysis of fission yeast cells by flow cytometry. *PLoS ONE* **6,** e17175 (2011).
107. Egel, R. Fission yeast mating-type switching: programmed damage and repair. *DNA Repair (Amst.)* **4,** 525–536 (2005).
108. Singh, G. & Klar, A. J. S. Mutations in deoxyribonucleotide biosynthesis pathway cause spreading of silencing across heterochromatic barriers at the

mating-type region of the fission yeast. *Yeast* **25,** 117–128 (2008).
109. Partridge, J. F., Borgstrøm, B. & Allshire, R. C. Distinct protein interaction domains and protein spreading in a complex centromere. *Genes Dev.* **14,** 783–791 (2000).
110. Sugiyama, T., Cam, H., Verdel, A., Moazed, D. & Grewal, S. I. S. RNA-dependent RNA polymerase is an essential component of a self-enforcing loop coupling heterochromatin assembly to siRNA production. *Proc. Natl. Acad. Sci. U.S.A.* **102,** 152–157 (2005).
111. Yanagida, M. Basic mechanism of eukaryotic chromosome segregation. *Philos Trans R Soc Lond B Biol Sci* **360,** 609–621 (2005).
112. Alper, B. J., Lowe, B. R. & Partridge, J. F. Centromeric heterochromatin assembly in fission yeast--balancing transcription, RNA interference and chromatin modification. *Chromosome Res.* **20,** 521–534 (2012).
113. Wood, V., Gwilliam, R., Rajandream, M. A., Lyne, M. & Lyne, R. The genome sequence of Schizosaccharomyces pombe. *Nature* (2002).
114. Cam, H. P., Sugiyama, T., Chen, E. S. & Chen, X. Comprehensive analysis of heterochromatin-and RNAi-mediated epigenetic control of the fission yeast genome. *Nature* (2005).
115. Gaither, T. L., Merrett, S. L., Pun, M. J. & Scott, K. C. Centromeric barrier disruption leads to mitotic defects in Schizosaccharomyces pombe. *G3 (Bethesda)* **4,** 633–642 (2014).
116. Choi, E. S. *et al.* Identification of noncoding transcripts from within CENP-A chromatin at fission yeast centromeres. *J. Biol. Chem.* **286,** 23600–23607 (2011).
117. Lorenz, D. R., Meyer, L. F., Grady, P. J. R., Meyer, M. M. & Cam, H. P. Heterochromatin assembly and transcriptome repression by Set1 in coordination with a class II histone deacetylase. *Elife* **3,** e04506 (2014).
118. Grewal, S., Bonaduce, M. J. & Klar, A. Histone deacetylase homologs regulate epigenetic inheritance of transcriptional silencing and chromosome segregation in fission yeast. *Genetics* (1998).
119. Chan, F. L. & Wong, L. H. Transcription in the maintenance of centromere chromatin identity. *Nucleic Acids Res.* **40,** 11178–11188 (2012).
120. Cam, H. P., Noma, K.-I., Ebina, H., Levin, H. L. & Grewal, S. I. S. Host genome surveillance for retrotransposons by transposon-derived proteins. *Nature* **451,** 431–436 (2008).
121. Zaratiegui, M. *et al.* CENP-B preserves genome integrity at replication forks paused by retrotransposon LTR. *Nature* **469,** 112–115 (2011).
122. Casola, C., Hucks, D. & Feschotte, C. Convergent domestication of pogo-like transposases into centromere-binding proteins in fission yeast and mammals. *Mol. Biol. Evol.* **25,** 29–41 (2008).
123. Murakami, Y., Huberman, J. A. & Hurwitz, J. Identification, purification, and molecular cloning of autonomously replicating sequence-binding protein 1 from fission yeast Schizosaccharomyces pombe. *Proc. Natl. Acad. Sci. U.S.A.* **93,** 502–507 (1996).
124. Maundrell, K., Hutchison, A. & Shall, S. Sequence analysis of ARS elements in fission yeast. *EMBO J.* **7,** 2203–2209 (1988).

125. Halverson, D., Baum, M., Stryker, J., Carbon, J. & Clarke, L. A centromere DNA-binding protein from fission yeast affects chromosome segregation and has homology to human CENP-B. *J. Cell Biol.* **136,** 487–500 (1997).
126. Lander, E. S., Linton, L. M., Birren, B., Nusbaum, C. & Zody, M. C. Initial sequencing and analysis of the human genome. *Nature* (2001).
127. Chinwalla, A. T., Cook, L. L., Delehaunty, K. D. & Fewell, G. A. Initial sequencing and comparative analysis of the mouse genome. *Nature* (2002).
128. Jordan, I. K., Rogozin, I. B., Glazko, G. V. & Koonin, E. V. Origin of a substantial fraction of human regulatory sequences from transposable elements. *Trends Genet.* **19,** 68–72 (2003).
129. González, J. & Petrov, D. A. The adaptive role of transposable elements in the Drosophila genome. *Gene* **448,** 124–133 (2009).
130. Chan, S. W. L., Henderson, I. R. & Jacobsen, S. E. Gardening the genome: DNA methylation in Arabidopsis thaliana. *Nat. Rev. Genet.* **6,** 351–360 (2005).
131. Martens, J. & O'Sullivan, R. J. The profile of repeat-associated histone lysine methylation states in the mouse epigenome. *The EMBO ...* (2005).
132. Matzke, M. A. & Birchler, J. A. RNAi-mediated pathways in the nucleus. *Nat. Rev. Genet.* **6,** 24–35 (2005).
133. Bernstein, B. E., Meissner, A. & Lander, E. S. The mammalian epigenome. *Cell* **128,** 669–681 (2007).
134. Jones, J. M. & Gellert, M. The taming of a transposon: V(D)J recombination and the immune system. *Immunol. Rev.* **200,** 233–248 (2004).
135. Gao, X. & Voytas, D. F. A eukaryotic gene family related to retroelement integrases. *Trends Genet.* **21,** 133–137 (2005).
136. Volff, J.-N. Turning junk into gold: domestication of transposable elements and the creation of new genes in eukaryotes. *Bioessays* **28,** 913–922 (2006).
137. Tudor, M., Lobocka, M., Goodell, M., Pettitt, J. & O'Hare, K. The pogo transposable element family of Drosophila melanogaster. *Mol. Gen. Genet.* **232,** 126–134 (1992).
138. Smit, A. F. & Riggs, A. D. Tiggers and DNA transposon fossils in the human genome. *Proc. Natl. Acad. Sci. U.S.A.* **93,** 1443–1448 (1996).
139. Bowen, N. J., Jordan, I. K., Epstein, J. A., Wood, V. & Levin, H. L. Retrotransposons and their recognition of pol II promoters: a comprehensive survey of the transposable elements from the complete genome sequence of Schizosaccharomyces pombe. *Genome Res.* **13,** 1984–1997 (2003).
140. Bjerling, P. *et al.* Functional divergence between histone deacetylases in fission yeast by distinct cellular localization and in vivo specificity. *Mol. Cell. Biol.* **22,** 2170–2181 (2002).
141. Nicolas, E. *et al.* Distinct roles of HDAC complexes in promoter silencing, antisense suppression and DNA damage protection. *Nat. Struct. Mol. Biol.* **14,** 372–380 (2007).
142. Sugiyama, T. *et al.* SHREC, an effector complex for heterochromatic transcriptional silencing. *Cell* **128,** 491–504 (2007).
143. Yamanaka, S. *et al.* RNAi triggered by specialized machinery silences developmental genes and retrotransposons. *Nature* **493,** 557–560 (2013).

144. Esnault, C. & Levin, H. L. The Long Terminal Repeat Retrotransposons Tf1 and Tf2 of Schizosaccharomyces pombe. *Microbiol Spectr* **3,** (2015).
145. Mourier, T. & Willerslev, E. Large-scale transcriptome data reveals transcriptional activity of fission yeast LTR retrotransposons. *BMC Genomics* **11,** 167 (2010).
146. Scott, K. C. & Sullivan, B. A. Neocentromeres: a place for everything and everything in its place. *Trends Genet.* **30,** 66–74 (2014).
147. Hayashi, T., Fujita, Y., Iwasaki, O., Adachi, Y. & Takahashi, K. Mis16 and Mis18 are required for CENP-A loading and histone deacetylation at centromeres. *Cell* (2004).
148. Furuyama, T., Dalal, Y. & Henikoff, S. Chaperone-mediated assembly of centromeric chromatin in vitro. *Proc. Natl. Acad. Sci. U.S.A.* **103,** 6172–6177 (2006).
149. Choi, E. S. *et al.* Factors that promote H3 chromatin integrity during transcription prevent promiscuous deposition of CENP-A(Cnp1) in fission yeast. *PLoS Genet.* **8,** e1002985 (2012).
150. Gonzalez, M., He, H., Dong, Q., Sun, S. & Li, F. Ectopic Centromere Nucleation by CENP-A in Fission Yeast. *Genetics* (2014).
151. Gonzalez, M., He, H., Dong, Q., Sun, S. & Li, F. Ectopic centromere nucleation by CENP--a in fission yeast. *Genetics* **198,** 1433–1446 (2014).
152. Nakagawa, H. *et al.* Fission yeast CENP-B homologs nucleate centromeric heterochromatin by promoting heterochromatin-specific histone tail modifications. *Genes Dev.* **16,** 1766–1778 (2002).
153. Schubert, V., Lermontova, I. & Schubert, I. Loading of the centromeric histone H3 variant during meiosis-how does it differ from mitosis? *Chromosoma* **123,** 491–497 (2014).
154. Lermontova, I., Koroleva, O., Rutten, T. & Fuchs, J. Knockdown of CENH3 in Arabidopsis reduces mitotic divisions and causes sterility by disturbed meiotic chromosome segregation. *The Plant ...* (2011).
155. Ravi, M. *et al.* Meiosis-specific loading of the centromere-specific histone CENH3 in Arabidopsis thaliana. *PLoS Genet.* **7,** e1002121 (2011).
156. Grewal, S. I. S. & Jia, S. Heterochromatin revisited. *Nat. Rev. Genet.* **8,** 35–46 (2007).
157. Hahn, M., Dambacher, S. & Schotta, G. Heterochromatin dysregulation in human diseases. *J. Appl. Physiol.* **109,** 232–242 (2010).
158. Bannister, A. J. *et al.* Selective recognition of methylated lysine 9 on histone H3 by the HP1 chromo domain. *Nature* **410,** 120–124 (2001).
159. Nakayama, J., Rice, J. C., Strahl, B. D., Allis, C. D. & Grewal, S. I. Role of histone H3 lysine 9 methylation in epigenetic control of heterochromatin assembly. *Science* **292,** 110–113 (2001).
160. Folco, H. D., Pidoux, A. L., Urano, T. & Allshire, R. C. Heterochromatin and RNAi are required to establish CENP-A chromatin at centromeres. *Science* **319,** 94–97 (2008).
161. Kagansky, A. *et al.* Synthetic heterochromatin bypasses RNAi and centromeric repeats to establish functional centromeres. *Science* **324,** 1716–1719 (2009).

162. Kato, H. *et al.* RNA polymerase II is required for RNAi-dependent heterochromatin assembly. *Science* **309,** 467–469 (2005).
163. Kloc, A., Zaratiegui, M., Nora, E. & Martienssen, R. RNA interference guides histone modification during the S phase of chromosomal replication. *Curr. Biol.* **18,** 490–495 (2008).
164. Volpe, T. A. *et al.* Regulation of heterochromatic silencing and histone H3 lysine-9 methylation by RNAi. *Science* **297,** 1833–1837 (2002).
165. Grewal, S. I. RNAi-dependent formation of heterochromatin and its diverse functions. *Curr. Opin. Genet. Dev.* **20,** 134–141 (2010).
166. Clarke, L. & Baum, M. P. Functional analysis of a centromere from fission yeast: a role for centromere-specific repeated DNA sequences. *Mol. Cell. Biol.* **10,** 1863–1872 (1990).
167. Moazed, D. Small RNAs in transcriptional gene silencing and genome defence. *Nature* **457,** 413–420 (2009).
168. Verdel, A. *et al.* RNAi-mediated targeting of heterochromatin by the RITS complex. *Science* **303,** 672–676 (2004).
169. Li, H. *et al.* An alpha motif at Tas3 C terminus mediates RITS cis spreading and promotes heterochromatic gene silencing. *Mol. Cell* **34,** 155–167 (2009).
170. Motamedi, M. R. *et al.* Two RNAi complexes, RITS and RDRC, physically interact and localize to noncoding centromeric RNAs. *Cell* **119,** 789–802 (2004).
171. Noma, K.-I. & Grewal, S. I. S. Histone H3 lysine 4 methylation is mediated by Set1 and promotes maintenance of active chromatin states in fission yeast. *Proc. Natl. Acad. Sci. U.S.A.* **99 Suppl 4,** 16438–16445 (2002).
172. Henikoff, S. & Shilatifard, A. Histone modification: cause or cog? *Trends Genet.* **27,** 389–396 (2011).
173. Grunstein, M. Yeast heterochromatin: regulation of its assembly and inheritance by histones. *Cell* **93,** 325–328 (1998).
174. Panchenko, T. *et al.* Replacement of histone H3 with CENP-A directs global nucleosome array condensation and loosening of nucleosome superhelical termini. *Proc. Natl. Acad. Sci. U.S.A.* **108,** 16588–16593 (2011).
175. French, B. T. & Straight, A. F. Swapping CENP-A at the centromere. *Nat Cell Biol* **15,** 1028–1030 (2013).
176. Duggan, N. M. & Tang, Z. I. The Formation of Heterochromatin. *Nature Education* (2010).
177. Lorenz, D. R. *et al.* CENP-B cooperates with Set1 in bidirectional transcriptional silencing and genome organization of retrotransposons. *Mol. Cell. Biol.* **32,** 4215–4225 (2012).
178. Moreno, S., Klar, A. & Nurse, P. [56] Molecular genetic analysis of fission yeast Schizosaccharomyces pombe. *Methods in enzymology* (1991).
179. Mata, J., Lyne, R., Burns, G. & Bähler, J. The transcriptional program of meiosis and sporulation in fission yeast. *Nat Genet* **32,** 143–147 (2002).
180. Chen, E. S. *et al.* Cell cycle control of centromeric repeat transcription and heterochromatin assembly. *Nature* **451,** 734–737 (2008).
181. Mitchison, J. M. & Nurse, P. Growth in cell length in the fission yeast Schizosaccharomyces pombe. *J. Cell. Sci.* **75,** 357–376 (1985).

182. Toedling, J. *et al.* Ringo--an R/Bioconductor package for analyzing ChIP-chip readouts. *BMC Bioinformatics* **8,** 221–221 (2007).
183. Aguilar-Arnal, L., Marsellach, F.-X. & Azorín, F. The fission yeast homologue of CENP-B, Abp1, regulates directionality of mating-type switching. *EMBO J.* **27,** 1029–1038 (2008).
184. Orthaus, S. *et al.* Assembly of the inner kinetochore proteins CENP-A and CENP-B in living human cells. *Chembiochem* **9,** 77–92 (2008).
185. Catania, S. & Allshire, R. C. Anarchic centromeres: deciphering order from apparent chaos. *Curr. Opin. Cell Biol.* **26,** 41–50 (2014).
186. Warburton, P. E. Epigenetic analysis of kinetochore assembly on variant human centromeres. *Trends Genet.* **17,** 243–247 (2001).
187. Earnshaw, W. C. *et al.* Molecular cloning of cDNA for CENP-B, the major human centromere autoantigen. *J. Cell Biol.* **104,** 817–829 (1987).
188. Okada, T., Ohzeki, J., Nakano, M., Yoda, K. & Brinkley, W. R. CENP-B controls centromere formation depending on the chromatin context. *Cell* (2007).
189. Sullivan, K. F. & Glass, C. A. CENP-B is a highly conserved mammalian centromere protein with homology to the helix-loop-helix family of proteins. *Chromosoma* **100,** 360–370 (1991).
190. Koenig, M., Dieudé, M. & Senécal, J.-L. Predictive value of antinuclear autoantibodies: the lessons of the systemic sclerosis autoantibodies. *Autoimmun Rev* **7,** 588–593 (2008).
191. Goldberg, I. G., Sawhney, H., Pluta, A. F., Warburton, P. E. & Earnshaw, W. C. Surprising deficiency of CENP-B binding sites in African green monkey alpha-satellite DNA: implications for CENP-B function at centromeres. *Mol. Cell. Biol.* **16,** 5156–5168 (1996).
192. Voullaire, L. E., Slater, H. R., Petrovic, V. & Choo, K. H. A functional marker centromere with no detectable alpha-satellite, satellite III, or CENP-B protein: activation of a latent centromere? *Am. J. Hum. Genet.* **52,** 1153–1163 (1993).
193. Sart, du, D. *et al.* A functional neo-centromere formed through activation of a latent human centromere and consisting of non-alpha-satellite DNA. *Nat Genet* **16,** 144–153 (1997).
194. Depinet, T. W. *et al.* Characterization of neo-centromeres in marker chromosomes lacking detectable alpha-satellite DNA. *Hum Mol Genet* **6,** 1195–1204 (1997).
195. Fowler, K. J. *et al.* Uterine dysfunction and genetic modifiers in centromere protein B-deficient mice. *Genome Res.* **10,** 30–41 (2000).
196. Kapoor, M. *et al.* The cenpB gene is not essential in mice. *Chromosoma* **107,** 570–576 (1998).
197. Rattner, J. B. The structure of the mammalian centromere. *Bioessays* (1991).
198. Hall, I. M., Noma, K.-I. & Grewal, S. I. S. RNA interference machinery regulates chromosome dynamics during mitosis and meiosis in fission yeast. *Proc. Natl. Acad. Sci. U.S.A.* **100,** 193–198 (2003).
199. Sato, H., Masuda, F., Takayama, Y., Takahashi, K. & Saitoh, S. Epigenetic inactivation and subsequent heterochromatinization of a centromere stabilize dicentric chromosomes. *Curr. Biol.* **22,** 658–667 (2012).

200. Ishii, K. *et al.* Heterochromatin integrity affects chromosome reorganization after centromere dysfunction. *Science* **321,** 1088–1091 (2008).
201. Ogiyama, Y., Ohno, Y., Kubota, Y. & Ishii, K. Epigenetically induced paucity of histone H2A.Z stabilizes fission-yeast ectopic centromeres. *Nat. Struct. Mol. Biol.* **20,** 1397–1406 (2013).
202. Guerra-Moreno, A., Alves-Rodrigues, I., Hidalgo, E. & Ayté, J. Chemical genetic induction of meiosis in Schizosaccharomyces pombe. *Cell Cycle* **11,** 1621–1625 (2012).
203. Rhind, N. *et al.* Comparative functional genomics of the fission yeasts. *Science* **332,** 930–936 (2011).
204. Chatterjee, A. G. *et al.* Serial number tagging reveals a prominent sequence preference of retrotransposon integration. *Nucleic Acids Res.* **42,** 8449–8460 (2014).